The Dissertation Committee for Youngmok Yun
certifies that this is the approved version of the following dissertation:

A Hand Exoskeleton for Study of Rehabilitation and Assistance of Spinal Cord Injury Patients

Committee:

Ashish D. Deshpande, Supervisor

Dragan Djurdjanovic

James S. Sulzer

Marcia K. O'Malley

A Hand Exoskeleton for Study of Rehabilitation and Assistance of Spinal Cord Injury Patients

by

Youngmok Yun, B.S., M.S.

DISSERTATION

Presented to the Faculty of the Graduate School of

The University of Texas at Austin

in Partial Fulfillment

of the Requirements

for the Degree of

DOCTOR OF PHILOSOPHY

THE UNIVERSITY OF TEXAS AT AUSTIN

May 2017

Dedicated to my wife, Sooeun.

Acknowledgments

I have looked back the time of my PhD program. I found that my PhD study could not have been accomplished without the supports of great advisers, collaborators, friends, and my family. The most valuable part in my PhD was to have opportunities to meet great people and work with them.

First, I met the greatest adviser, Dr. Ashish Deshpande. He gave me an opportunity to study in the University of Texas at Austin and advised my whole PhD program. He taught me how to write a high quality research paper and mentored me on how to communicate with research colleagues. The countless discussion with him made my research solid and heightened my standard.

It was my honor to finish my PhD degree with great committee members. Dr. Marcia O'Malley has actively supported our collaboration project to develop the hand-wrist exoskeleton. She has always kindly hosted our team in Rice University and encouraged the collaborations with researchers of MAHI lab. Dr. James Sulzer has given many helpful suggestions to improve my research. Because of his valuable suggestions, my research could be more focused. Dr. Dragan Djurdjanovic gave me many opinions not only for the hand exoskeleton project but also another study on a statistical model-based control.

I have enjoyed the collaboration with my research colleagues in ReNeu Robotics lab. Priyanshu Argarwal's endless passions always inspired me to advance our re-

search. We have discussed a number of topics and encouraged each other. Jonas Fox has led the design of our hand exosokeleton, Maestro. Dongyang Chen has conducted a considerable number of experiments to identify Bowden cable characterstics. Kaci Madden has the kindest heart and always brightens team's dynamics. Sarah Dancausse has been always energetic and initiated the reaserch on assisting spinal cord injury patients. Because of Paria Esmatloo's enthusiasm, we could accomplish the amazing research on assisting SCI patients. In addition to the people above, many research collegues, therapists and patient participants helped my PhD research. They gave me countless advises and their kind hearts rasied me up again when I was exhausted.

One of the greatest experience in my PhD program was the collaboration with Jonathan Ko. He was a super star from the first moment I met him. He was very smart but always humble about himself. He showed passion and commitment to research even in his last moments. It was my great honor to have worked with him on his last journal paper. I will never forget his attitude towards the world.

My family made all of my PhD achievements possible. Every morning I got a super power from the smiles of Chloe and Elin. They brightened my life during the PhD program. Without the devotion of my wife, I cannot imagine anything that I have achieved. I dedicate this dissertation to my wife.

A Hand Exoskeleton for Study of Rehabilitation and Assistance of Spinal Cord Injury Patients

Publication No. _____

Youngmok Yun, Ph.D.
The University of Texas at Austin, 2017

Supervisor: Ashish D. Deshpande

A large number of people experience neurological disorders in their life time, and these patients seek to regain their body functions with rehabilitation and assistive devices. In this dissertation, we present the development of a hand exoskeleton, called Maestro, which is designed to advance research in fields of hand rehabilitation and hand assistive devices. Maestro is mechanically and electrically robust, accurate in sensing and actuation, and compatible to various rehabilitation schemes, subjects, hardware/software, and different operators. As a result of these features, Maestro has led to research on adaptive control theories for diverse properties of hands, the development of a hand-wrist exoskeleton, the development of a novel rehabilitation framework, progress of hand muscle fatigues, and assistance for SCI patients. Particularly on the assistance for SCI patients, we present that the advantage of a compliant hand assistive device may result in high success ratios for grasping various objects required in activities of daily living (ADL) with surface EMG sensors. The hand functions of SCI subjects are evaluated with and without Maestro through a

standardized hand function test called Sollerman hand function test (SHFT). The results with six SCI subjects show that the hand functions of C6 and C7 SCI subjects improved with assistance from Maestro.

Table of Contents

List of Tables

List of Figures

Chapter 1

Introduction

A large number of people experience neurological disorders in life time. More than 790,000 stroke cases occur every year in the US [5]. Some patients are born with neurological disorders such as cerebral palsy. Some neurological disorders such as a spinal cord injury (SCI) occur regardless of age [6] and demand a huge amount of lifetime costs. For example, the estimated lifetime cost of a patient injured on the C5-C8 spinal cord at 25 years old is approximately 3.5 million dollars [6]. Neurological disorder patients also need continuous assistance from care givers to perform the activities of daily living (ADL).

After neurological disorders, patients seek to regain their body functions with rehabilitation and assistive devices. First, patients go through rehabilitation procedure. Doctors, physical therapists (PT), and occupational therapists (OT) help patients to obtain muscle strength, to enhance motor coordination, to stimulate neuroplasticity, to relieve spasticity, and other recoveries. However, in many cases, rehabilitation does not completely restore original body functions to the patients. After rehabilitation, patients obtain more abilities required in ADL with assistive devices. They learn how to use a device to assist their body functions. A wheelchair

This chapter includes a part of writing in [4]. Youngmok Yun made a contribution for developing the exoskeleton and conducting experiments with SCI subjects.

is one of the most common assistive devices to obtain mobility required in ADL. With rehabilitation and assistive devices, neurological disorder patients return to their lives with regained body functions.

Previous studies have shown potentials of robotics technology in rehabilitation of neurological disorders. Accurate, precise, and quickly responsive sensors along with fast, powerful, and fatigueless actuators in robotic systems have many advantages in the rehabilitation process. First, robotic systems have been used to study fundamental principles of human motor learning, which is critical for understanding the mechanisms of rehabilitation. One remarkable example is the use of two DoF robotic manipulandums in the study of motor learning and control strategies of the upper extremities [7–13]. Second, robotic systems are advantageous in the assessment of neurological disorders. Kinarm brought a reliable and quantitative assessment tool with a continuous scale to assess upper-extremity position sense following a stroke [14, 15]. Langs group showed a potential of wrist-worn sensors as an assessment tool following a stroke by examining the correlation between the acceleration acquired from the sensor and the score of Action Research Arm Test (ARAT) [16, 17]. Last, robotics technologies have introduced novel paradigms in rehabilitation therapy. Virtual reality and interactive games with robotics technology have emerged as new treatment approaches in stroke rehabilitation [18–21]. Virtual reality programs are often designed to be more interesting and enjoyable than traditional therapy tasks, thereby encouraging a higher numbers of repetitions. Recent studies with randomized clinical trials showed that rehabilitation with virtual reality have clinical effectiveness in motor recovery after stroke [18, 21]. Rehabilitation

robots introduced novel adaptive therapeutic motions with advanced control algorithms. Assist-as-needed (AAN) is one of the well-known robot control algorithms in rehabilitation robotics [22, 23], which encourage patient participation. Patton et al. recently have shown that an error-enhancing therapy, which is an opposite concept of AAN, could be more effective than AAN [24].

Robotics researchers also introduced novel forms of assistive devices for neurological disorder patients. Robotics autonomy has been integrated with wheelchairs (often called smart wheelchairs) to help with obstacle avoidance, navigation, route planning, and spatially constrained maneuvers [25, 26]. Recently, a wearable lower-body exoskeleton called Rewalk, which has motors at the hip and knee joints, enabled SCI patients to walk again [27]. The robotic movement is controlled by using subtle changes in his/her center of gravity; crutches are used to prevent falls and help operation of the robot. One key technology in assistive robotics is to recognize the intention of patients. Activating the robots with conventional control interfaces is challenging for people with neurological diseases. To address this challenge, considerable research has been conducted on intention recognition with electromyography (EMG) and electroencephalography (EEG) signals. Surface EMG sensors provide a convenient way to extract muscle activation commands by detecting electrical potentials on the skin above the muscles. EMG signals have been successfully applied in exoskeleton control in the past [28–31]. The crucial advantage of EMG-based methods is that, even if the subject is unable to produce sufficient joint torques, the intention of the user can still be read; consequently, the exoskeleton can be controlled. However, if the injury level is severe, the EMG signal is not sufficiently available.

For these cases, brain-machine interfaces have been developed to decode the signals of brain (EEG) to control assistive robotic devices [32]. This system allows users to send commands or instructions to robots or other external devices by using brain signals, which means the system can bypass conventional channels of communication such as through muscles, nerves, speech, etc.

In this dissertation, we present the development of a hand exoskeleton, called Maestro, which facilitates the study of hand rehabilitation and assistance of SCI patients with an EMG-based intention recognition method. The human hand is a vitally important part of our daily activities. Humans interact external environments with hands, which are capable of a wide variety of functions: touching, grasping, feeling, holding, manipulating, etc. The ultimate goal of this research is to help neurological disorder patients regain their hand functions with rehabilitation and assistive devices to better their lives.

Chapter III to Chapter V of this dissertation includes 1) mechanical design and manufacturing of Maestro; 2) sensing and actuation; and 3) control system. The hand exoskeleton is developed as a research platform to study hand rehabilitation and active hand assistive devices. To date, many rehabilitation robots have been developed for human motor learning studies, assessment of neurological disorders, therapeutic motions, and assistance of tetraplegic patients. However, many studies have focused on lower bodies or proximal upper limbs, including shoulders and elbows. Compared with studies of lower bodies and proximal upper limbs, the number of studies on the human hand is relatively small [33–35]. Moreover, the unique characteristics of the human hand, including a complex tendon structure, low inertia,

and significant role of passive stiffness on digit joints [36] make it difficult to directly accept the hypotheses validated in other body parts such as lower limbs and proximal upper extremities. Hence, we have developed a hand exoskeleton to facilitate the study of hand rehabilitation and assistive devices. The exoskeleton consists of thumb, index, and middle finger modules. Maestro is mechanically and electrically robust, accurate in sensing and torque-actuation, and compatible with various rehabilitation schemes, subjects, hardware/software, and different operators. As a result of these features, Maestro has led to research on adaptive control theories for diverse properties of hands, the development of a handwrist exoskeletons, the development of a novel rehabilitation frameworks, progress of hand muscle fatigue, and assistance for SCI patients.

Among the research paths driven by Maestro, we will present one particular research result with Maestro in Chapter VI, which is control of an assistive hand exoskeleton with sEMG sensors for SCI patients. As previously explained, the EMG-driven assistive devices have many advantages. A user does not require extensive training because the target muscles of EMG sensors are generally relevant with tasks. A user is able to perform a task without being disturbed by other body motions. If an assisive device is operated by other body motions such as the tongue [37], neck [38], or wrist motion [39], the user needs to stop some activities in order to operate the assistive device. Based on the advantages, researchers have developed EMG-driven active hand orthoses [40–42]. However, the operation of those devices has been performed only with a one-dimensional variable or a threshold for 1-DoF actuation, leading to the result that subjects with these devices were not capable of grasping

various objects required in ADL. One challenge in controlling an EMG-driven hand orthoses to grasp various objects is that the orthosis needs to generate many different hand poses depending on the target objects. It is difficult to generate many different hand poses required for the target object by recognizing the noisy EMG signals. Our solution is to take advantage of compliant actuators of Maestro. The compliance of actuator in Maestro enables subjects to grasp various object required in ADL with a small number of grasping modes, which are easily classifiable with sEMG signals. We evaluated the hand function of SCI subjects with and without Maestro through a standardized hand function test, and the results show that the proposed method improved the hand function of C6/C7 SCI patients.

The contributions presented in this dissertation includes the following:

- We have developed, for the first time, a hand exoskeleton that can control the torques of four individual joints (CMC flexion/extension, CMC abduction/adduction, MCP flexion/extension, IP flexion/extention) of thumb and two individual joints (MCP and PIP flexion/extension) of the index and middle fingers.

- We have designed, modeled, controlled, and tested a miniaturized Bowden cable-based series-elastic-actuator for a hand exoskeleton.

- We identified, for the first time, the minimal set of target hand poses of a hand assistive device that allows a subject to grasp a wide range of objects.

- We conducted, for the first time, a standardized hand function test for a robotic hand assistivie device with SCI patients.

- For the first time, experiment results with a hand function test report that the hand functions of C6 and C7 SCI patients improved with a robotic assistive device.

Chapter 2

Background Information and Previous Works

2.1 Background Information

Recent studies have shown that rehabilitation procedures for neural disorders can benefit from accurate actuation and sensing abilities of robotics [34]. Rehabilitation robots serve a precise therapeutic motion based on a prescription. Also, the robots assess the degree of impairment and recovery quantitatively without human subjective errors, which can be reliably used in different institutions, such as hospitals and insurance companies. Based on these advantages, a number of rehabilitation robots have been recently developed [34, 44], and several clinical trials have shown the effectiveness in the recovery of body functions [45–47].

Many rehabilitation researchers have explored various robot rehabilitation schemes to find efficient rehabilitation procedures. For example, [48, 49] showed that rehabilitation effect is higher when subjects learn individual joint motions for a task involving multi-joint movement rather than when subjects learn a complete task in one-go. Another study [50, 51] showed that assisting a therapeutic motion only when the assistance is needed with a force controlled robot improves the rehabilita-

This chapter includes a part of writing in [43]. Youngmok Yun made a contribution for designing the thumb exoskeleton.

tion effect. However, these explorations have been performed mostly for lower limb or arm/shoulder rehabilitation, and the study for hand rehabilitation is relatively rare [34, 52]. The rehabilitation effects validated by other body parts, including the above two examples, cannot be guaranteed for hand rehabilitation due to the unique features of hand anatomy. For example, the biomechanics of hand joints are strongly correlated with other hand joints due to a complex tendon structures [53], and the dynamics of hand is dominated by the joint stiffness rendered by tendon and ligament configurations, not by inertia which commonly dominates the dynamics of arm and lower limbs [36].

A number of hand assistive devices have been developed for SCI patients to help their essential hand tasks in activities of daily living (ADL). Most of the current commercial devices are passive devices that either help with passive extension/flexion or locate the fingers/thumb in a predetermined position [54]. Although these devices are economical and easy to use, they have several limitations. The passive stiffness or elasticity hinders finger movement when it is not needed. Moreover, they assume the subjects to be able to apply enough force in at least one direction. In order to address these limitations, active devices have been recently developed. These devices recognize the intention of subjects and assist the subjects to achieve a task by adding extra strength. Since the active device recognizes the intention, the assistive force is added only when a subject needs the force. In addition, because active devices add force, even the subjects with weak muscle forces can perform tasks. Although several researchers have developed active hand assistive devices [35, 41, 42], still the number of research on active hand assistive devices is relatively smaller than those

for lower body parts such as smart wheel chairs [25, 26] or Rewalk [27].

The goal of our project is to develop a research platform, called Maestro, capable of exploring various rehabilitation schemes and assistance methods for hand of neurological disorder patients. We hope that Maestro facilitates to find efficient hand rehabilitation procedures and assistance methods by conducting experiments with a large number of subjects. To achieve this goal, we developed three major requirements: robustness, accuracy, and compatibility. First, the exoskeleton needs to be robust mechanically and electrically under various loads and disturbances. Also, the exoskeleton must always be safely operated or terminated even under operator's mistake or machine errors. The robustness is the foremost requirement for conducting experiments with a large number of subjects, in order to ensure the safety of subjects and the consistent high-quality of experiment data. Second, the exoskeleton needs be accurate. The accuracy is a main advantage of rehabilitation robots superior to human abilities. The robot needs accurately measure the kinematics and dynamics of the subject's hand and need to apply the desired forces. Third, the exoskeleton needs to be compatible in various aspects. Many rehabilitation schemes need to be compatibly implemented into the robots. The exoskeleton needs to be fitted with diverse hand shape and size. The exoskeleton needs to be easily integrated with other hardware/software that may bring promising improvement in rehabilitation and assistive devices. The exoskeleton needs to be operated by different operators, including robot researchers, OT, and PT.

Table 2.1: System requirements and selected attributes for Maestro

Requirements	**Mechanical design and manufacturing**	**Sensing and actuation**	**Control system**
Robustness	Rigid metal structure	Embedded and covered electric parts, Dedicated electric enclosures	Multi-stage safety features
Accuracy	Rigid physical-human-robot-interface (pHRI), 3D printed Nylon parts for light weight	Calibration with redundant sensors, Embedded and covered electric parts, Series-elastic-actuator (SEA), Backlash compensation of Bowden cable, Optimal Bowden cable configuration	High-speed signal processing with FPGA, Real-time interrupt with RT-Linux
Compatibility	Eight active exoskeleton joints, Optimized fourbar mechanism with linear slider	Portability with Bowden cable	C/C++ programming on RT Linux, Modulized hardware components in cRIO, Object-oriented programs, Independent ethernet network

2.2 Previous Works

To date, a number of hand rehabilitation robots have been developed for different hand rehabilitation motions. Many robots provide a grasping motion by binding four fingers together [46, 47, 55, 56]. The exoskeletons provide one of the most essential motion of hand, or wrapping motion for grasping, with a simple structure and a small number of actuators. However, possible motions generated by the exoskeleton are limited, and the analysis of an individual finger is also challenging. On the other hand, several hand exoskeletons have been developed for actuating individual digits [57, 58]. However, in contrast, the actuation of individual digits requires a complex but compact design which is a major challenge of hand exoskeleton design. As a result, only few hand exoskeletons have been developed for multi digits including thumb. Most of them take advantages of underactuation mechanisms for actuating [59–62]. The multi-digit exoskeletons with underactuation is able to generate a coordinated motion for individual digit joints with a relatively small number of actuators. However, the underacuation mechanisms generate only a predefined motion, which is usually determined by a healthy hand. The underactuation mechanism is generally not robust to different hand sizes because the digits are a part of the mechanism. A multi-digit exoskeleton which independently actuates individual joints [63] has the biggest potential, but the trade-off is that a more complex system requires a higher cost in design and maintenance.

Hand exoskeleton researchers have adopted various mechanisms to resolve joint misalignment problems which are commonly critical issues in exoskeleton development. The mechanisms are mostly classified into three categories. The first

one is the direct matching method, locating exoskeleton joints coincident to digit joints. The direct matching method is advantageous for simple design and for direct measurement of digit joint angles. If the joint is well-matched, the mechanism is able to apply a pure torque on digit joints, that is only normal directional force on links (phalanges). However, the location of the digit joints is varying on a person and not easily visible, and the design space for direct matching is limited. As a result, the hand exoskeletons with this mechanism [46, 47] have a relatively smaller DoF and designed for simple tasks such as a one-pose grasping. Second, several hand exoskeletons uses a glove-tendon structure [64, 65]. The glove-tendon mechanism is like a skin-tendon structure of human hand so that the exoskeletons avoid the joint misalignment problems. A subject can easily wear the glove, and the large surface contact provides comfort in wearing. In addition, because the tendons are usually embedded, the design is compact. However, the tendon structure must be well-customized for a subject, otherwise a wrong tendon configuration may cause undesirable motion and force on digit joints. A small moment arm to the hand joints requires a large tension for actuation and may lead a large reaction forces to digit joints. Due to the flexible structure of the mechanism, the accurate kinematics estimation or torque control are also challenging. Lastly, various rigid link mechanisms were introduced for hand exoskeletons. The rigid link mechanism such as fourbar and six bar mechanisms uses phalanges as a part of the mechanism to avoid the needs of accurate joint matching [60, 61, 63]. Because of the rigidity of mechanism, the kinematics and the applied torque are deterministically modeled with the mechanism equation. However, because human phalanges are a part of the mechanism, the

accurate estimation and control require the accurate knowledge of hand kinematics. The rigid link mechanisms must be carefully designed not to apply a large amount of force on the finger joints and to obtain a large RoM for different hand sizes.

Several thumb exoskeletons have also been developed to date for rehabilitation, virtual reality or teleoperation applications that allow for active actuation of the thumb (Table 2.2). For this review, we consider the devices (total 15) that could actively actuate the thumb and are published in the literature with some experimental results. We compare the devices based on the following 8 criteria, which are important for a thumb exoskeleton for rehabilitation: (i) whether the device supports each thumb joint individually (exoskeletal type) or connects to the distal phalanx of the thumb (end-effector type), (ii) the number of active DOFs in the device, (iii) the type of actuators used, (iv) whether the actuators are situated locally or remotely, (v) the type of sensors in the device, (vi) weight of the device, (vii) what physical quantities could be controlled using the device and (viii) what are the peak achievable forces or torques on the device.

Exoskeletal type devices allow for controlling the position or torque applied at each joint explicitly as compared to end-effector type devices, which could only control the position or force at the distal phalanx. The number of active DOFs in a device determines the variety and complexity of assisted motions it could provide. Individual support of thumb joints is important to provide targeted therapy to a specific joint, which may be necessary for certain thumb pathologies (e.g. spasticity). Ensuring natural coordinated motion at pathological thumb joints require that the device be exoskeletal type with each DOF actuated individually. The type of

actuator and its placement determine whether the device would be bulky or light and therefore, whether it will allow for free movement of the hand while in operation. It is important for certain hand pathologies where the upper extremity could not be oriented in a certain manner. The type of sensors on the device determines what physical quantities the device could control. The weight of the device determines how easy or cumbersome it is for use. The controller on the device governs what physical quantities (position or force) the device could control, which in turn decides what robotic rehabilitation control paradigms (e.g. force-field control, assist-as-needed control [66]) the device is capable of rendering. Finally, the peak achievable forces or torques determine for what kind of impairments the device could be used. One of the limitations of the exoskeletons developed for virtual reality applications is that they only allow to apply unidirectional forces on the thumb. Rehabilitation exoskeletons, are however, required to apply bidirectional forces on the thumb based on the nature of the impairment. A comparison of the weight of the proposed thumb exoskeleton with the existing ones shows that it has the least weight for the number of degrees of freedom it offers. The weight per DOF for our device is about 34 g including the weight of the exoskeleton base on hand (Table 2.2).

There have been five main types of actuation mechanism used for thumb exoskeletons: (i) linkage-based actuation with locally situated motor [46, 67–69], (ii) tendon-based actuation with locally situated motor [70, 71], (iii) cable and sheath transmission with remotely located motor [60, 72–75], (iv) flexible shaft transmission with remotely located motor [76] and (v) pneumatic actuation [77, 78]. None of these mechanisms allow for accurate and stable torque control of the digit joints

individually. Furthermore, these mechanisms have poor backdrivability and results in high reflected inertia. In addition, the transmission and actuator gearing in some of these mechanisms suffer from nonlinear friction and stiction, which makes it difficult to control actuator force or torque accurately.

The actuator mechanism of our thumb exoskeleton lies in category (iii) and so we discuss the designs in that category in more detail. Commercially available system, CyberGrasp [74, 77], supports only 1 DOF motion of the thumb, control unidirectional phalanx force using motor current and cannot be used to control the position or forces of the thumb phalanges individually. iHandRehab [73] is another hand exoskeleton with a thumb module that supports 4 DOF of the thumb. However, experiments with their device showed that significant friction (percentage of friction torque accounting for the driving torque is up to 95%) was present in their transmission. In addition, no control experiments were presented with their device. [75] introduced a 2 DOF thumb exoskeleton, called IOTA (isolated orthosis for thumb actuation), for unidirectional actuation of the thumb. However, their device was designed to only control position of the joints. HX is another hand exoskeleton with a 2 DOF thumb module [60]. However, the flexion-extension motion at the MCP and IP joints is under-actuated in their design and their device is designed to be position controlled. Also, so far they have only presented the design of the thumb module. Recently, [79] designed a hand exoskeleton having a thumb module with a linear series elastic actuator (SEA) to control the grip force. However, their design has only 1 DOF for thumb with no allowable abduction-adduction motion at the CMC joint. Also, they have presented only preliminary testing of the SEA and no

experiment with human subjects have been conducted with the device so far.

Several important features such as physical human-robot interface (pHRI), manufacturing method, adaptation to different hand sizes, control hardware/software and safety features have been rarely presented or neglected in the previous literatures. However, after several pilot tests, it turned out that these practical problems crucially hinder smooth experiments with a number of human subjects. The previous works for these topics will be further explained in the next sections while presenting our strategies for these features.

Many upper-body rehabilitation robots have been developed for the last two decades. The robots have been experimented with human subjects, and results have showed the effectiveness to study human motor learning, to assess the impairment degree of neuromuscular system, and to provide therapeutic motions. For example, MIT-MANUS [8] facilitated many studies of human motor learning with 2D shoulder-elbow motions. KINARM [80] showed potential of rehabilitation robots as an advanced assessment tool for neural disorders. ARMin [81] and Armeo [82] showed their efficacy in stroke rehabilitation. One remarkable point is that most of clinical experiments have been focused on proximal parts of upper body. As shown in a recent review of robotic devices for upper-limb rehabilitation [34], the clinical experiments with human hands have been conducted with only few robots.

Table 2.2: A comparison of the characteristics and specifications of the actuated thumb exoskeletons.

	Physical Characteristics						Specifications		
Thumb Exoskeleton	**Type**	**Active Independent DOFs**	**Actuator Type**	**Actuation** [6]	**Sensors**	**Weight** (g)	**Control**[2]	**Peak Force/ Torque**	**Remarks**
Rutger's Master II [77]	End-effector	1[1] (CMC E, MCP E)	Pneumatic actuators with compressed air source	Remote, Pneumatic tubes	infrared reflective sensor for position, hall-effect angle sensor, pressure sensor	80[4]	Unidirectional phalanx force using pressure	16 N[5]	Designed for virtual reality applications
[78]	exoskeletal	1 (MCP F/E)	Air cylinder with compressed air source	Remote, Pneumatic tubes	Bend sensor, electric pressure regulator	-	Grasping on-off	-	Experimental evaluation with a wooden hand model is presented
CyberGrasp [74, 77]	End-effector	1[1] (CMC E, MCP E, IP E)	Servo motor	Remote, Cable + Sheath	position	539[4]	Unidirectional phalanx force using motor current	12 N[5]	Losses in the transmission are neglected

[1] coupled actuation of DOFs present in design [2] missing control represents that only mechanical design has been presented so far [3] combined weight of index finger and thumb exoskeleton [4] total weight of the hand exoskeleton [5] only allows for unidirectional force [6] actuation refers to whether the actuator was located at the joint (local) or remotely (remote) and the transmission mechanism

Table 2.2: Contd.

Thumb Exoskeleton	Physical Characteristics						Specifications		Remarks
	Type	**Active Independent DOFs**	**Actuator Type**	**Actuation** [6]	**Sensors**	**Weight** (g)	**Control**[2]	**Peak Force/ Torque**	
[71]	Exoskeletal	2[1]	DC motor + Gear drive	Local, Tendon	Potentiometer, Encoder, EMG	–	Position or Grasping on-off	–	Thumb opposition and IP + MP joint are each actuated by one actuator.
HEXORR [46]	End-effector	1 (CMC F/E)	AC servo motor + Harmonic drive (100:1)	Local, Linkage	Encoder, Torque sensor	–	–	–	Hand is fixed in the device. CMC A/A angle is adjustable
iHandRehab [73]	Exoskeletal	4 (CMC F/E, CMC A/A, MCP F/E, IP F/E)	DC motor + Capstan drive (8:1)	Remote, Cable + Sheath	Potentiometer, Force sensor	250[3]	–	–	Significant losses ($\sim$ 95 %) were observed in the transmission

[1] coupled actuation of DOFs present in design [2] missing control represents that only mechanical design has been presented so far [3] combined weight of index finger and thumb exoskeleton [4] total weight of the hand exoskeleton [5] only allows for unidirectional force [6] actuation refers to whether the actuator was located at the joint (local) or remotely (remote) and the transmission mechanism

Table 2.2: Contd.

Thumb Exoskeleton	Physical Characteristics						Specifications		Remarks
	Type	**Active Independent DOFs**	**Actuator Type**	**Actuation** [6]	**Sensors**	**Weight** (g)	**Control**[2]	**Peak Force/ Torque**	
[76]	Exoskeletal	5 (CMC F/E, CMC A/A, MCP F/E, MCP A/A, IP F/E)	RC servo motor	Remote, Flexible shafts	Potentiometer, strain gage	200	Position	±2.5 Nm	Significant losses were observed in the transmission
[67]	Exoskeletal	4 (CMC F/E, MCP F/E, IP F/E, Opposition)	DC servo motor	Local, Linkage	Encoders, 3-axis Force sensors	–	Position	±3.72 Nm	Hand is fixed in the device
[68, 70]	End-effector	3[1]	–	Local, Linkage	–	510	3D tip force	5 N	Distal and middle exoskeleton phalanx are coupled
[69]	Exoskeletal	1[1] (CMC A/A)	Linear servo motor	Local, Linkage	Single axis force sensor	126	Position	10 N[5]	

[1] coupled actuation of DOFs present in design [2] missing control represents that only mechanical design has been presented so far [3] combined weight of index finger and thumb exoskeleton [4] total weight of the hand exoskeleton [5] only allows for unidirectional force [6] actuation refers to whether the actuator was located at the joint (local) or remotely (remote) and the transmission mechanism

Table 2.2: Contd.

Thumb Exoskeleton	Physical Characteristics						Specifications		Remarks
	Type	**Active Independent DOFs**	**Actuator Type**	**Actuation**	**Sensors**	**Weight** (g)	**Control**[2]	**Peak Force/ Pressure**	
IOTA [75]	End-effector	2 (CMC A/A, MCP F/E)	Servo motor	Remote, Cable + Sheath	Encoder, Bend sensor	230	Position	±0.384 Nm	Pediatric disorders
[83]	Exoskeletal	1[1] (CMC F/E, MCP F/E, IP F/E)	Fluidic actuator + compressor	Remote, Pneumatic tubing	–	200	Grasping on-off	345 kPa	No CMC A/A motion is supported
[84]	End-effector	1[1]	–	Local, Linkage	–	–	Unidirectional force	3 N [3]	No experiments with thumb module are presented
[79]	Exoskeletal	1[1] (CMC F/E, MCP F/E, IP F/E)	Linear SEA with linear motor	Local, Linkage	Potentiometer	298[4]	Grip force (Only preliminary SEA testing presented so far)	9 N[3]	No CMC motion is supported

[1] coupled actuation of DOFs present in design [2] missing control represents that only mechanical design has been presented so far [3] only allows for unidirectional force [4] total weight of the hand exoskeleton [5] weight of the index finger and thumb exoskeleton (only moving parts) [6] force at thumb tip [7] includes the weight of the hand base which is 30 g

Table 2.2: Contd.

Thumb Exoskeleton	Physical Characteristics						Specifications		Remarks
	Type	**Active Independent DOFs**	**Actuator Type**	**Actuation**	**Sensors**	**Weight** (g)	**Control**[2]	**Peak Force/ Pressure**	
HX [60]	Exoskeletal	2[1] (MCP F/E, IP F/E, Opposition)	DC motor + Gear drive (14:1)	Remote, Cable + Sheath	–	270[6]	–	–	No experiments with thumb module are presented
BRAVO [85]	Exoskeletal	1[1] (MCP F/E, IP F/E)	DC motor + Gear drive	Local, Linkage	EMG, Sensorized object pressure	950[4]	Position	±30 N	Designed for grasping of cylindrical objects
Proposed	Exoskeletal	4 (CMC F/E, MCP F, IP F)	SEA with DC motor + Gear drive (14:1)	Remote, Cable + Sheath	Magneto-resistive angle sensor, Potentiometer, Encoder	136[7]	Torque	±0.3 Nm	Accurate torque control of individual thumb joint can be achieved

[1] coupled actuation of DOFs present in design [2] missing control represents that only mechanical design has been presented so far [3] only allows for unidirectional force [4] total weight of the hand exoskeleton [5] weight of the index finger and thumb exoskeleton (only moving parts) [6] force at thumb tip [7] includes the weight of the hand base which is 30 g

Force-controlled rehabilitation robots have additional advantages in rehabilitation and assistance of patients. Force-controlled robots encourage participation of subjects during therapy. For example, assist-as-needed (AAN) strategies prevent subjects from passively following a rehabilitation robot, and the effectiveness has been verified by clinical tests [22]. Accurately controlled force control is also advantageous for safe operation. Many subjects with neural disorders have spasticity on joints [86], which needs delicate care. Position control, without considering the stiffness of subject's joint, may cause a significant accident during rehabilitation. On the other hands, the treatment with a delicate force control can be safer. Nevertheless, the torque control of hand joints with an exoskeleton is challenging. The most intuitive method is to directly match the exoskeleton joint to the finger joints and to control the exoskeleton joint torque [46, 87]. However, the design of the direct matching method is difficult particularly for multiple finger exoskeletons because of space constraints. As a result, these exoskeletons control only the grasping force of whole hand or the torque of only index finger joints. As a solution some hand exoskeleton developers adopted a remote actuation method using Bowden cable transmission [60, 88]. However, due to the substantial friction between outer sheath and inner wire, accurate force control is challenging. For lower limb exoskeletons, a series-elastic-actuator (SEA) is combined with the Bowden cable for accurate torque control [89, 90]. However, the implementation of the SEA mechanisms, which were introduced in other studies, into a hand exoskeleton is not simple mainly due to the large sizes.

Most of hand exoskeleton research have been focused on the application of

rehabilitation rather than the application of assisting a neurological disease patient. As a result, the number of research for assistance is smaller than that for rehabilitation. Nevertheless, there are several important previous studies. The research on the active assistive hand exoskeleton was pioneered by Benjuya and Kenney [40]. In et al. [39] developed a soft hand exoskeleton to assist SCI patients and the robot recognized the intention with the wrist motion of patients. The exoskeleton is compact and comfortable, and one unique advantage is that the robot is washable, which is practically important. Soekadar et al. [91] developed a hybrid EEG/EOG-based brain/neural interface to operate a hand exoskeleton.Dicicco et al [41] developed a pinching device with a pnuematic actuator which has compliance in actuation, helping grasping multiple objects with one-DoF pinching motion.

Four years ago, we developed the first prototype exoskeleton for an index finger [92], and conducted pilot tests with the prototype to validate the concepts of design [3, 93, 94]. After the pilot tests, we were able to determine the most important requirements of a a hand exoskeleton (robustness, accuracy, and compatibility) to explore promising rehabilitation schemes and assistance methods with a large number of subjects. We have iterated the design process to meet the requirements and to resolve the problems found during pilot tests (Fig. 2.1). We have optimized the Bowden cable configurations to maximize the transmission efficiency and to minimize unpredictable effects [95], and tried multiple manufacturing methods to have compact design, light weight and robust structure simultaneously [96]. Based on the research on exoskeleton elements, we recently developed a thumb exoskeleton which supports a complex anatomy of thumb [43]. For accurate force control, we have

designed, modeled, and controlled a miniaturized series-elastic-actuator (SEA) [97] and investigated control algorithms for efficient interaction with subjects [93, 94].

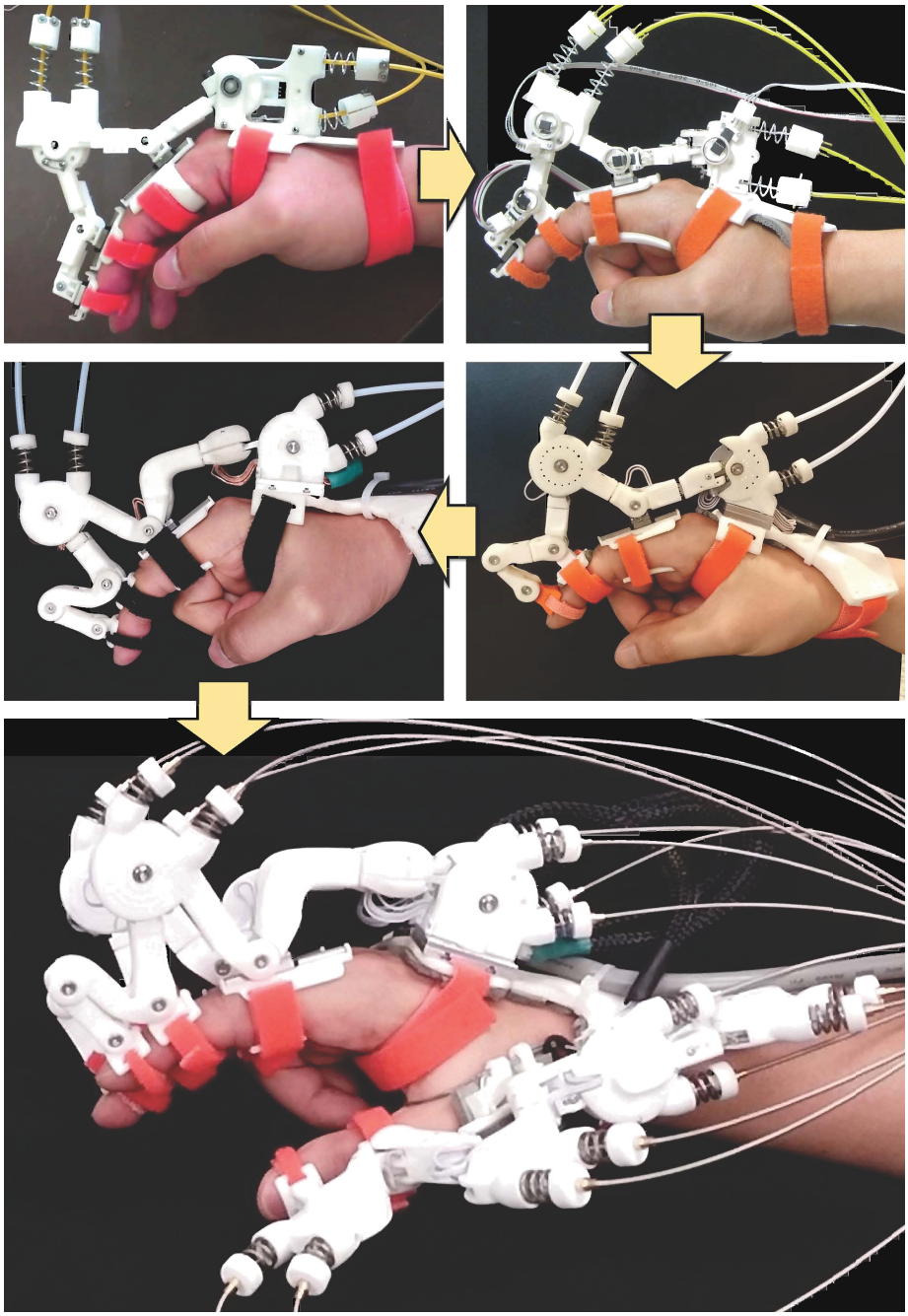

Figure 2.1: Iterative design process for the development of Maestro. We have iterated the design process to develop a robust, accurate, and compatible hand exoskeleton and to resolve technical challenges which were found in pilot tests.

Chapter 3

Mechanical Design and Manufacturing of Maestro

While designing Maestro, we have come across ironical problems. The mechanical structure of exoskeleton needs to be compact and light, but mechanically strong. The interface of hand exoskeleton needs to be fixed with hand rigidly for accurate force transmission and kinematics estimation, but softly for comfort in wearing. Introduction of a mechanism is required to avoid joint misalignment but simultaneously reluctant because it causes uncertainty in estimation of hand kinematics and actuation of forces. Lastly, actuating all DoF of hand may provide full freedom for designing therapy schemes, but also cause a high cost and complexity in maintenance. To resolve these issues, we needed to conduct research to make a number of decisions.

3.1 Degree of Freedom in Maestro

Determining which hand joints must be actuated was one of the most important decisions for hand exoskeleton development. Actuating all DoF of hand may bring full potential of hand exoskeleton, however which also increases the cost and complexity. To answer this question, we reviewed hand ergonomics and anatomy literatures. Several ergonomics studies [1, 98, 99] showed that thumb, index and middle

fingers contributes a significant portion of hand functions in our daily life. For example, a house maid and a professional machinist performed about 80% and 70% of grasping respectively without helps of ring finger and little finger (disc grasping and some other grasping motions need these fingers) [99]. In this regard, we decided to actuate thumb, index and middle fingers. Next, hand anatomy studies showed that most of finger motions for grasping and pinching are performed mainly by two flexors (FDS and FDP) with less contributions of the abduction/adduction tendons (LU,RI,UI) [100], and the DIP flexion is coupled with MCP and PIP flexion by the tendon configuration of FDS and FDP [101]. For thumb, not only the flexion/extension but also the abduction/adduction are critical for hand function [102, 103]. In contrast to fingers, thumb is capable to move all flexion/extension joints independently [102, 103]. As a result, we have determined to actuate four DoF of thumb, that are CMC abduction/adduction, CMC/MCP/IP flexion/extension, and two DoF of index and middle fingers, that are MCP/PIP flexion/extension, which are the most substantial joints for daily hand functions.

3.2 Hybrid Mechanism for Deterministic Kinematics and a Large RoM

We have introduced a hybrid mechanism involving direct matching mechanisms and four-bar mechanisms for avoiding joint misalignment and achieving accurate joint angle estimation and torque actuation (Fig. 3.1). The abduction/adduction motions of each digit were directly matched with the exoskeleton abduction/adduction joints (see yellow axes in Fig. 3.1 (a) and (b)). Theoretically, this direct match-

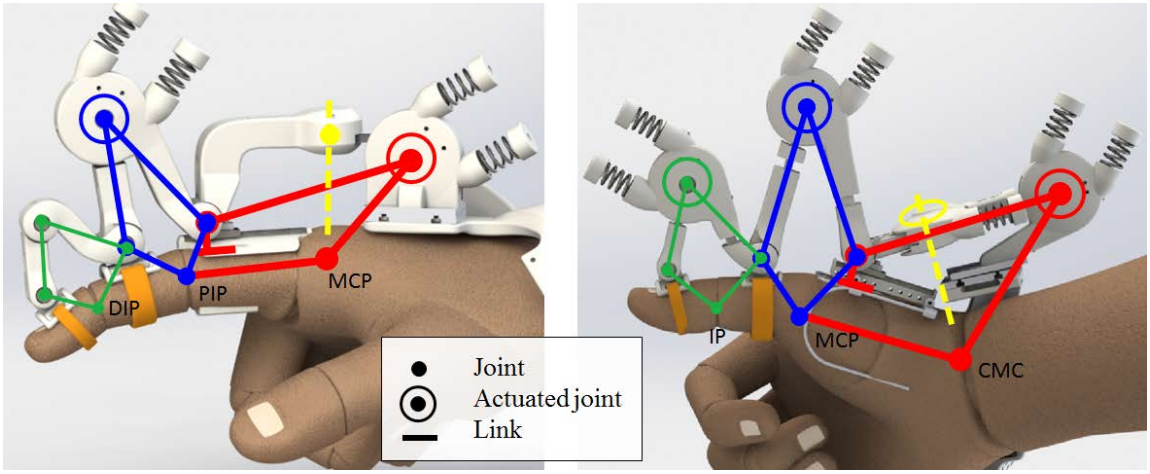

Figure 3.1: Maestro is actuated by four-bar mechanisms. The introduction of four-bar mechanisms fundamentally resolve the exoskeleton joint alignment problem because the digit joints are a part of the mechanism. The finger exoskeleton modules (left) and the thumb exoskeleton module (right) have the same configuration of mechanisms. The first mechanism including MCP flexion/extension (for thumb CMC flexion/extension) is an inverted-crank-slider mechanism which ensures a normal force on the proximal phalange. The second and third mechanisms for PIP and DIP flexion/extension (for thumb, MCP and IP flexion/extension) are basic four-bar mechanisms. All these four-bar mechanisms move along with the MCP abduction/adduction (for thumb CMC abduction/adduction). For fingers, MCP/PIP flexion/extension are actively actuated, and for thumb, CMC/MCP/IP flexion/extension and CMC abduction/adduction are actively actuated.

ing causes a joint misalignment problem depending on the flexion angle of finger MCP, but the hand anatomy allows a significant motion of finger MCP abduction/adduction only at a certain MCP flexion angle [104]. This anatomical effect is similar for thumb CMC as well. Therefore, we directly matched the exoskeleton abduction/adduction joint to finger MCP and thumb CMC where the abduction/adduction motion of finger MCP and thumb CMC is largest. As a result, the abduction/adduction joints move smoothly without the joint misalignment problem.

Multiple four-bar mechanisms were introduced for digit flexion/extension. The four-bar mechanisms fundamentally resolved the joint misalignment issue because the digts are a part of the mechanism. The flexion/extension mechanism incorporates one inverted-slider-crank mechanism for the first kinematic chain (red lines in Fig. 3.1) and two basic four-bar mechanisms for the second and third kinematic chains (blue and green lines in Fig. 3.1 respectively). These three mechanisms move along with the MCP abduction motion. The invert-crank mechanism includes a linear slider which ensures a normal force on a proximal phalange (for thumb, metacapal), so that the actuator does not apply an undesirable reaction force on MCP (for thumb, CMC). Because a required joint torque of PIP is generally lower than MCP [105], and the space for the interface on an intermediate phalange is limited, the PIP is actuated through a basic four-bar mechanism without a linear slider. For the thumb module, all kinematic chains contain actuators (Fig. 3.1). For the finger modules, the kinematic chains for DIP flexion and MCP abduction do not have an actuator, but the states are observed passively by angle sensors.

The disadvantage of the four-bar mechanisms is that the RoM is limited

depending on the link length configuration. Hence, we optimized the link lengths to obtain a wide RoM for various finger sizes. We developed a computer simulator calculating the available RoM for given mechanism link lengths. The simulator calculated the RoM for a wide range of finger sizes (phalange lengths and thickness) based on the statistics [2], and found the optimized exoskeleton link lengths. The shape of mechanism parts were optimized to avoid all interferences with other links and phalanges (Fig. 3.2). The lengths of exoskeleton links were adjusted depending on a size of finger. As a result, Maestro provides a high compatibility to different sizes of hand. We evaluated the RoM with two different subjects whose index fingers are small and large. Statistically their index finger lengths are located on 9% and 94% of the distribution of adult index finger lengths [2]. Fig. 3.2 shows experimental results. Both two subjects were able to reach full active RoM of flexion and extension of index fingers. For thumb exoskeleton, we carried out tests on four subjects to evaluate its workspace and kinematic transparency using a motion capture system. Results show that the device allows for a large workspace with the thumb, is kinematically transparent to natural thumb motion to a high degree (86%). For the detail analysis, refer [43].

3.3 Hybrid Manufacturing to Minimize Weight, Reduce Size, and Enhance Strength

To date, most of hand exoskeletons have been fabricated with conventional metal machining [34, 44]. Additive manufacturing technologies, which are influencing many engineering fields as of late, have brought various advantages to the hand

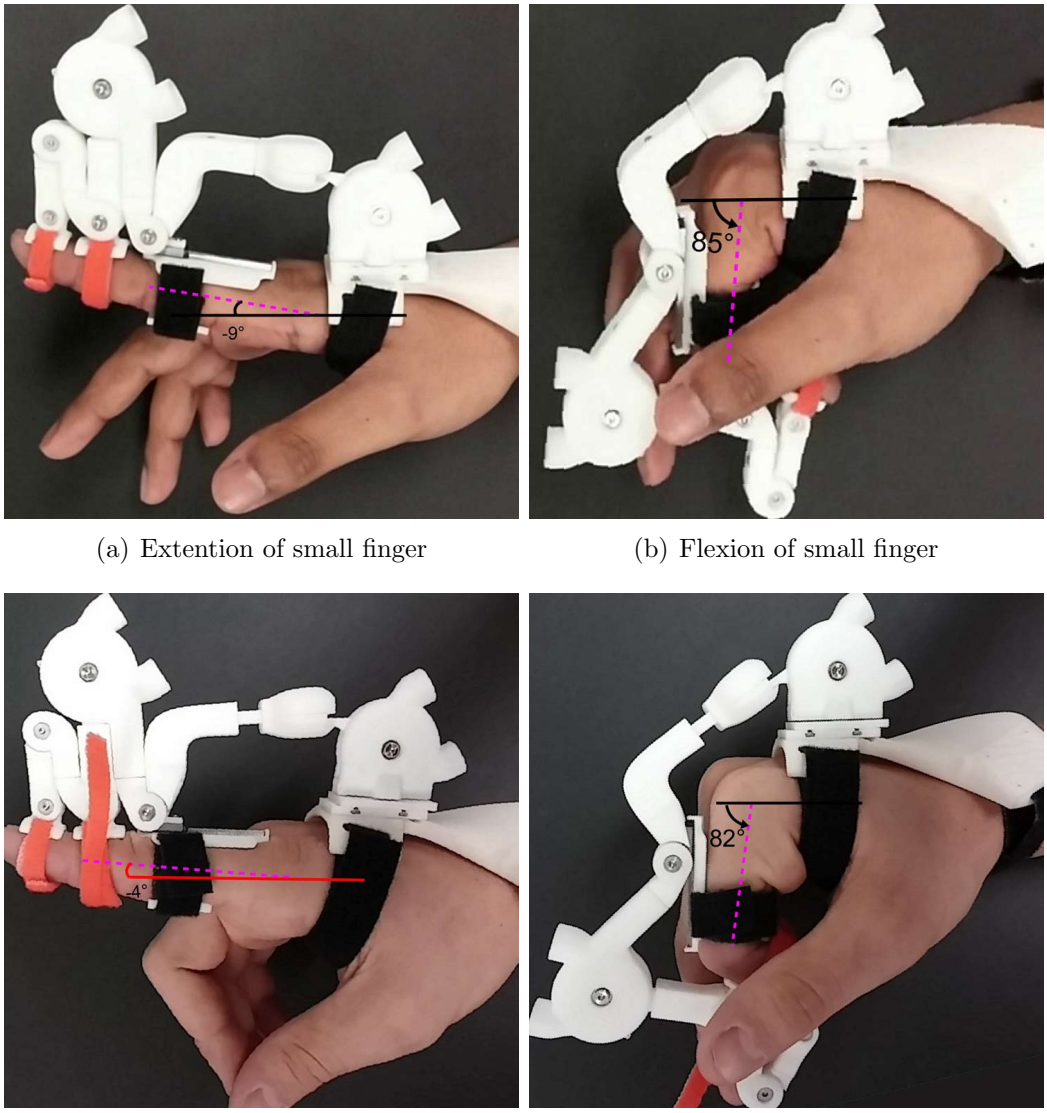

(a) Extention of small finger

(b) Flexion of small finger

(c) Extention of large finger

(d) Flexion of large finger

Figure 3.2: The range of motion of Maestro. To validate the RoM, we have conducted experiments with two subjects whose index finger is short and long. Their index finger lengths are statistically located on 9% and 94% of the distribution of adult index finger lengths. They could achieve full active RoM as shown in the figures [2].

exoskeleton development as well [96]. Some hand exoskeletons [106] include a light and compact finger exoskeleton only with a 3D printing technology, and another hand exoskeletons [107] introduced a parameterized design idea into the development of hand exoskeletons.

We have actively taken advantage of various additive manufacturing technologies during the development of the Maestro. The Maestro is primarily fabricated out of Nylon-12 material using selective-laser-sintering (SLS) technology. Comparing to the most common 3D printing technology, that is fused deposition modeling (FDM), which uses ABS or PLA plastic as its material (e.g., Makerbot 3D printing), SLS machines can fabricate more complex structures with a high resolution (0.17mm). By harnessing the capabilities of SLS based additive manufacturing, we were able to strategically design our hand exoskeleton in the following ways.

First, using SLS we designed a compact hand exoskeleton. By combining the design of multiple parts into a single complex part, we were able to both reduce the number of hand exoskeleton components and simplify the assembly process (Fig. 3.3(a)). Second, since Nylon is about three times lighter than aluminum in terms of density, our device is significantly reduced in weight compared to exoskeletons fabricated by conventional metal machining. Third, the use of additive manufacturing allows for the fabrication of complex 3D surfaces, an inherent design requirement of ergonomic interfaces (Upper-left of Fig. 3.4). Lastly, since the greatest determinant of additive manufacturing cost is part volume, not complexity, it is a cost-effective means of fabricating our small volume hand exoskeleton.

A critical problem of SLS fabricated Nylon parts is that the fracture strength

(a) Complex structure in a plastic part

(b) Failure of part

(c) Example of hybrid structure

Figure 3.3: Maestro is fabricated by a selective-laser-sintering (SLS) technology. With SLS, we were able to design components with complex structure (a), reducing the size, number, and weight of parts. A critical disadvantage of a nylon part fabricated by SLS is the low fracture strength. An example is shown in (b). Hence, we introduced a hybrid structure consisting of machined aluminum parts for a simple-shape inner parts and SLS-printed nylon parts for outer complex parts (c).

is considerably weaker than metal parts. Robustness issues were presented during pilot testing of a Maestro version made completely out of Nylon (Fig. 3.3(b)). As a result, we updated the design such that load bearing components were machined out of metal to enhance the strength of the hand exoskeleton during actuation. By fabricating the majority of the hand exoskeleton out of Nylon and enhancing the strength with metal parts (Fig. 3.3(c)), we achieved a compact design, a light weight (finger module: 57g, thumb module: 91g) and robustness to high loads.

3.4 Design of Physical Human-Robot Interface

The pHRI, or attachment between robot and human, is an important feature for all rehabilitation exoskeletons [108]. The pHRI must be comfortable [109] and

ensure the proper transfer of forces between device and human hand. However, these two requirements are especially challenging when designing hand exoskeletons. First, the amount of space available to attach a device to the hand is limited by the small size of each digit segment and the need to locate the device on the back side of the hand to preserve the user's dexterity [110]. Second, the pHRI must conform to the complex topography of the hand to increase the contact area between device and human, and therefore, decrease localized pressure [108] during exoskeleton force transmission [88].

Many soft robotic gloves are used as pHRI's in pneumatic driven hand exoskeletons [65, 111] and tendon driven systems [64, 112]. Gloves are inherently comfortable and easy to don and doff, however, they stretch during actuation causing imprecise torque control and require different sizes to accommodate varying hand anthropometry. Another popular method of pHRI attachment uses Velcro straps [59, 63, 113]. Velcro straps accommodates the majority of hand sizes and provide a much tighter fit to the fingers and hand resulting in accurate torque control. However, the presence of Velcro straps adds bulk and makes donning and doffing more cumbersome.

The Maestro uses a combination of 3D contoured Nylon saddles secured with Velcro straps and a wireform structure to attach to the thumb (Fig. 3.4). The dorsal saddle, which rests on the back of the hand and serves as a grounding point for the finger modules, is 3D contoured to match the shape of the hand and is secured to the palm and wrist using Velcro straps. The finger saddles are C-shaped shells that hug each finger segment and are secured using Velcro. Both the dorsal and finger

saddles are padded with medical foam for added comfort. The thumb is the most difficult phalange to interface with, however, due to the dynamically changing size of its muscle group on the palmar side of the hand [96]. To address this, we developed a wireform attachment that forms a ring around the MCP joint and consists of four struts that protrude downward to rest snugly against the metacarpal. The struts are strategically placed to allow the bellies of the thumb muscles to protrude through the windows of the struts during contraction. The wire framework provides structural stability to transfer and distribute the exoskeletal loads onto the metacarpal segment.

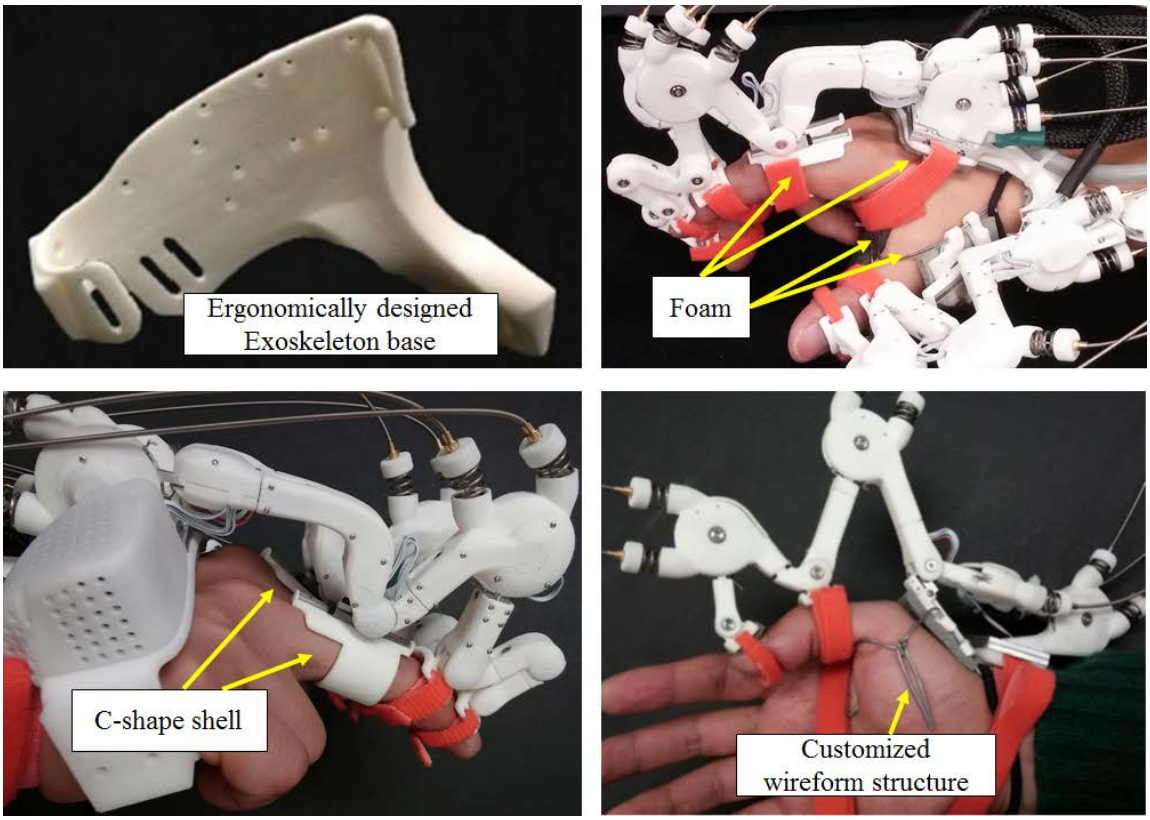

Figure 3.4: The physical human robot interface (pHRI) of Maestro. Maestro uses a 3D contoured saddles secured with Velcro straps and a customized wireform structure to attach to the thumb. Many foams are attached on the interfaces to soften the contact points

Chapter 4

Sensing and Actuation of Maestro

In this chapter, we present the sensing and actuation system of Maestro. The advantages of robotic actuation and sensing abilities in rehabilitation are obtained only when the hardware and algorithm of the system are designed in accord with human biomechanical system. We developed mechatronic systems robust to various disturbances, sensor configuration taking into account the mechanical structure, and actuators capable to generate accurate torques on hand joints.

4.1 Robust Electric Connection and Sensing

Maestro has 16 analog angle sensors, 8 optical incremental encoders, 8 DC motors, and many other electric components for safety and general operation. All these electric components are critical for safe operation and high quality control and estimation. However, while conducting experiments with previous versions of Maestro, a number of robustness issues occurred from these electric components. Unstable connections between components were the most common, exposed electric wires were pulled out by a subject or an operator, unintended load on sensors changed the calibration parameters, electric wires were worn out by repetitive actuations, and an operators connected wrong wires while changing experiment settings. As the

system got more complex, the maintenance time has been also increased. Merely a cautious operation could not be a solution for these robustness issues.

We developed systematic solutions to resolve these issues. First, we installed angle sensors not to be exposed to an external disturbance, created channels for wire routing in the exoskeleton links, and secured rooms for extra wires required for for link length adjustment and joint rotation (Fig. 4.1 (a)). Second, we covered all these items by thin plastic covers by screws (Fig. 4.1 (a) and (b)). All components are securely fixed by pressure of covers, and thus a subject cannot touch the inside. Third, we introduced a precise calibration feature for angular sensors. We added small holes on actuated pulley and pulley cover, informing specific angles. By inserting a small dowel pin into two holes, actual positions of sensor values were acquired. Fourth, we fabricated a PCB for rearrangement of electric connections. Thus we reduced the size of electric circuits and obtained stable connections. Fifth, standard connectors were used for frequently disconnected electric components. Sixth, we developed dedicated electric enclosures called Actuator box and Control box including actuators and control systems respectively (Fig. 4.1 (b)). With the dedicated enclosures and connectors, the system is easily moved to experiment locations and reassembled while keeping the high quality of robustness. Seventh, in the enclosure, the all wires are cleanly organized by breakout board, wire duct, terminal block, and labels.

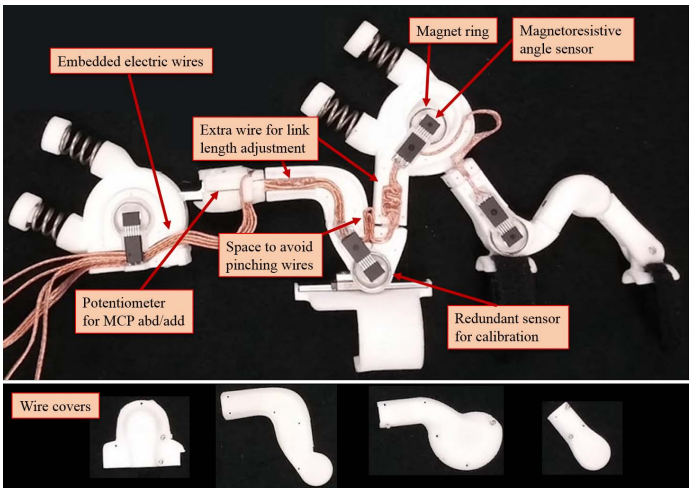

(a) Inside of Maestro

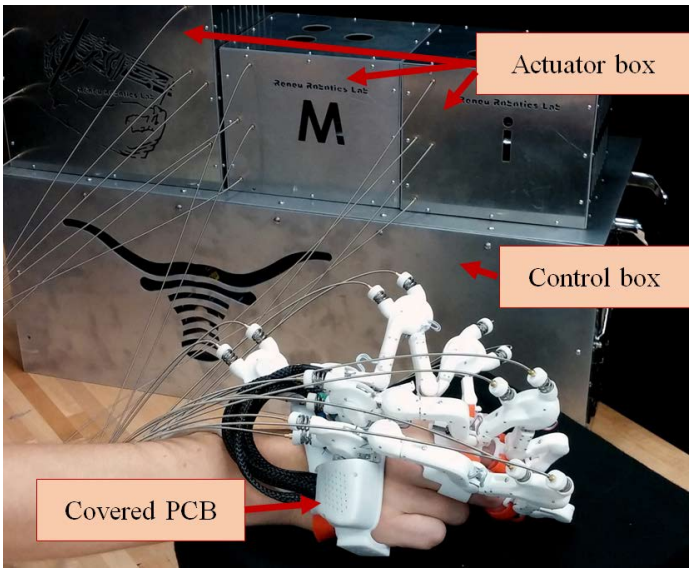

(b) Full system of Maestro

Figure 4.1: The robust electric connections and sensing have been achieved by embedding and covering electric components as shown in (a) and (b). The flexions of all joints are measured by magnetoresistive sensors, and the abductions are measured by a potentiometer-type sensor due to the interference of magnetic field. We developed dedicated electric enclosures shown in (b) for portability and modularization. All of electric wires are cleanly arraged by breakout board, wire duct, terminal block, and labels.

4.2 Automatic Calibration of Kinematic Parameters and Joint Angle Estimation

The introduction of four-bar mechanisms resolved the design problem in a limited space and the joint misalignment problem. However, the four-bar mechanisms also caused uncertainty in kinematics estimation because digit bones and joints are a part of the mechanism. To resolve this issue, we introduced a redundant sensor configuration that aids in accurate calibration and estimation of hand kinematics. The basic idea is to conduct calibration and estimation seamlessly while wearing the hand exoskeleton with extra sensors. Theoretically, four joint angles in a digit are observable by four angle sensors which are located in each kinematic loop. Introduction of an extra sensor installed on the exoskeleton joint whose angle is correlated with both the first and second mechanism loops (Fig. 4.1 (a) and 4.2) helps in reducing the uncertainty by estimating the kinematic parameters of a hand. The abduction joint of exoskeleton is directly matched with the MCP joint of finger (CMC for thumb), thus the abduction angle is directly measured. The DIP flexion is observed by angle sensor, but its function is less significant than MCP or PIP joint [100]. Therefore we decided not to introduce an extra sensor for the third loop. For thumb, because the third loop is also important as explained in III-1, we introduced one more sensor. In this subsection, we will explain only the joint angle estimation of finger MCP and PIP, which are essential for torque control. The development of a joint angle estimation algorithm for thumb, considering the complex anatomy, is our ongoing work and a preliminary study is shown in [43].

For calibration, first the exoskeleton is actuated to sweep the RoM of MCP

and PIP flexion while collecting sensor data ($\mathbf{q} = [q_1 \quad q_2], \quad z$) where q_1 and q_2 are the angles of actuated joints, and z is the angle for the extra sensor introduced for calibration (Fig. 4.2). Then N samples of sensor data are randomly selected from the collected dataset for calibration. Lastly, the uncertain kinematic parameters, $\mathbf{p}$, are optimized where $\mathbf{p}$ is the six link lengths that contain parts of finger kinematic parameters. More specifically, they are lengths of green solid lines in Fig. 4.2. In the optimization, the errors between the measured and estimated redundant sensor values, $\Delta\mathbf{z}$, are minimized as:

$$\begin{aligned} &\underset{\mathbf{p}}{\operatorname{argmin}}\, C = (\Delta\mathbf{z}^\top \Delta\mathbf{z}) \\ &\Delta\mathbf{z} = \begin{bmatrix} \hat{z}_1 - z_1 \\ \vdots \\ \hat{z}_N - z_N \end{bmatrix} = \begin{bmatrix} h(\mathbf{p}, \mathbf{q}_1) - z_1 \\ \vdots \\ h(\mathbf{p}, \mathbf{q}_N) - z_N \end{bmatrix} \end{aligned} \tag{4.1}$$

where $\mathbf{q}_i$ and z_i are the i-th sampled data set among N data sets. h is the estimator of z obtained from the analytical solution of four-bar mechanisms [114]. Because the measurement model is nonlinear and the number of elements in $\mathbf{p}$ is six, the optimization problem is not a simple convex optimization problem. However, since we are able to provide a good initial values of the optimization by measuring the link lengths with a ruler, which is close to the actual value, the optimization is normally successful.

After calibration, the joint angles of digits are estimated with two angle sensors on the actuated joints, that are q_1 and q_2 as:

$$\theta = \mathbf{f}(\mathbf{q}, \mathbf{p}) \tag{4.2}$$

where $\theta = [\theta_1 \quad \theta_2]^\top$, θ_1 and θ_2 are joint angle of MCP and PIP respectively (Fig. 4.2). $\mathbf{f}$ is the kinematics function for finger joint angles, determined by the inverted-crank-slider mechanism and four-bar mechanisms equations [114]. Because the calibration is conducted just before the kinematics estimation, the kinematics estimation is performed with an reliable kinematics model.

We developed a testbed finger for validating the performance of Maestro. The validation of a hand exoskeleton is tricky because the measurement of kinematic parameters are not easy even with a motion capture system due to occlusion [115] and the direct measurement of the torque of finger joints are more challenging with a human subject. In this regard, we have developed the testbed finger which contains magnetoresistive angle sensors with magnets and torsion springs on MCP and PIP flexion joints. The physical interface for a human finger was replaced for the assembly with the testbed finger. From the CAD model, we could obtain the exact kinematic parameters of the testbed finger and exoskeleton. The angle sensors are calibrated independently and the stiffness curve of the joints were experimentally obtained. With the testbed finger, we evaluated the performance of kinematics estimator (in this subsection) and torque actuator (in the next subsection).

We evaluated the calibration algorithm and joint angle estimation algorithm. In the calibration step, we added Gaussian random noise to the true values of $\mathbf{p}$ obtained from CAD model of the testbed finger and exoskeleton, and input them as an initial guess for the optimization of (4.1). The standard deviations of the Gaussian random noises were 5mm - 10mm depending on the difficulty of measuring the values (e.g., the measurement of phalange length is easier than the measurement

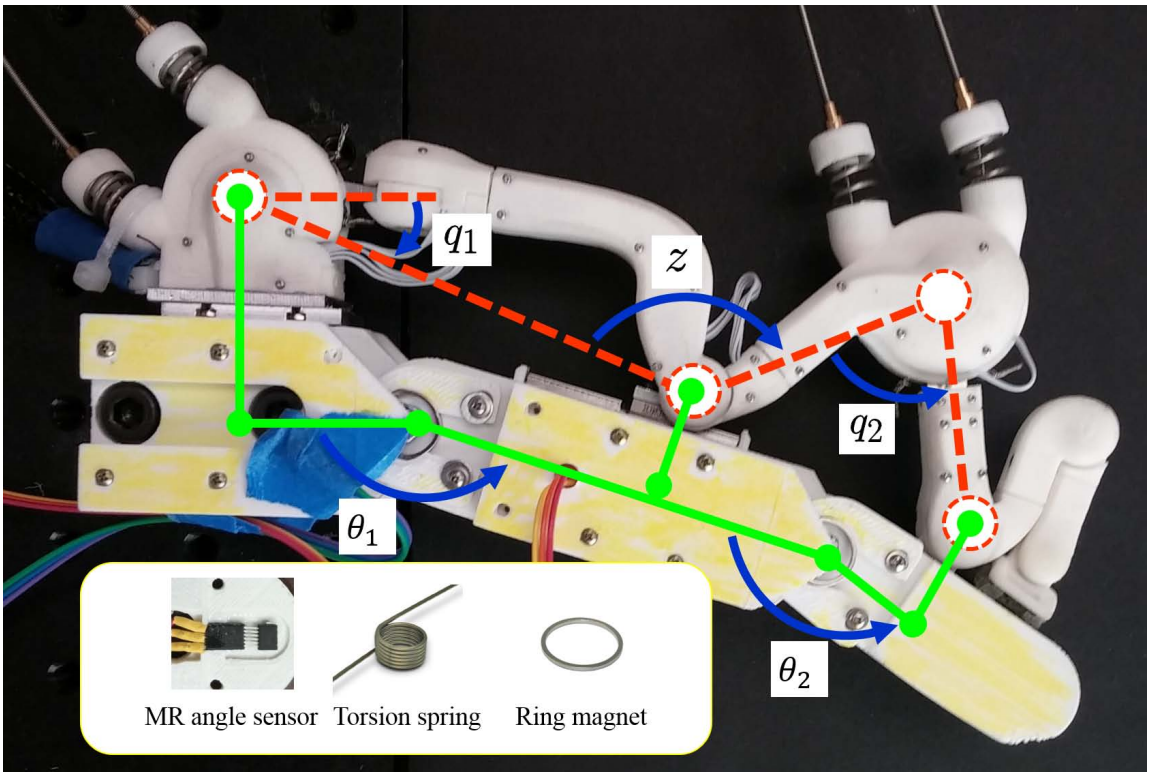

Figure 4.2: Maestro with a testbed finger. A testbed finger has been developed for validation of Maestro. The testbed finger has two DoF joints corresponding to MCP and PIP flexion of human finger. Each joint includes a magnetoresistive angle sensor and torsion spring. Thus, all joint angles are directly measurable, and the stiffness of joint rendered by torsion spring were experimentally obtained. Because the connection with Maestro is rigid, all kinematic parameters are fully known which are not possible for human finger. With the measured joint angle and stiffness, the validation of kinematics estimation and torque control performance was possible.

of the MCP location relative to the exoskeleton joint). Then, optimization (4.1) was conducted. We repeated the optimization 100 times, and the Fig. 4.3 (a) shows the results that most of optimized values converged to the true values with reasonably low variance. After calibration, the joint angles of testbed finger were estimated with a calibrated kinematic parameter set. For the first 20 seconds the SEAs moved the testged finger, and for the next 20 seconds a researcher applied a random disturbance to simulate the torque generated by a subject. One experiment result is shown in Fig. 4.3 (b) and the RMSE were 2.32 deg and 2.86 deg for MCP and PIP respectively. Existing estimation errors might be caused by residual calibration error and sensor noise.

4.3 Bowden Cable Series Elastic Actuator

Maestro is actuated through Bowden cable consisting of outer sheath and inner wire (commonly seen in bicycle brakes). The pulley of exoskeleton joint is connected to the pulley of motor shaft with a pull-pull mechanism (like a timing belt connection through Bowden cable. See Fig. 4.5). The pulley of the motor shaft is position-controlled by a servo motor system (Maxon DC motor + Maxon EPOS2 driver).

The introduction of Bowden cable as a transmission system resolved many challenges in the hand exoskeleton development. First, the Bowden cable allows for a compact design of exoskeleton. Actuating 8 DoF (2 for index finger + 2 for middle finger + 4 for thumb) in a limited space needs a compact design of actuator. By locating the electric motors in a remote place, the design could be compact. Second,

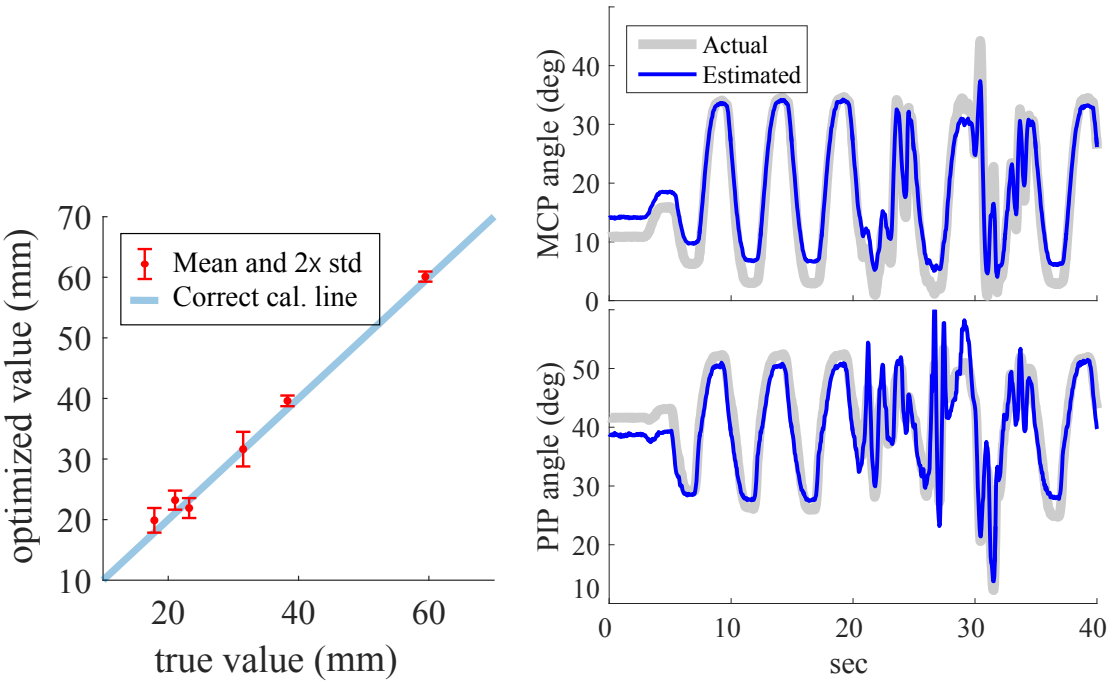

(a) Calibration result

(b) Joint angle estimation

Figure 4.3: Results of calibration and estimation of the exoskeleton kinematics with a testbed finger. (a) shows the distribution of optimized kinematic values after 100 iterations of optimization with random initial inputs. As the optimized values are close to the correct calibration line, the optimization is successful. (b) plots the MCP and PIP angles obtained from the testbed finger (gray lines) and estimated from exoskeleton sensors (blue lines).

the Bowden cable allows for a light weight of the exoskeleton, which is important for dynamic transparency. Generally, the weight of actuators such as electric motor is substantial. The remote actuation reduced the weight significantly, so that the inertia effect for force control is ignorable. Third, the exoskeleton does not need to be grounded. Because the outer sheath generates a pushing force while the inner wire generates a pulling force, the sum of reaction forces in the exoskeleton is zero. Due to this unique characteristics, the exoskeleton can be easily combined with other systems such as a wrist exoskeleton [3].

However, the Bowden cable transmission also introduced additional problems. The first problem is a low efficiency of power transmission. The friction between the inner wire and outer sheath significantly deteriorates the efficiency of power transmission. The second problem is that the friction of Bowden cable is not predictable. The friction is correlated with many factors including material property, routing path, and even time [95, 116]. One unique feature of the Bowden cable is the backlash-like effect [116, 117]. That is, the tension of inner wire in Bowden cable transmits to the other side after some displacement. The sources that cause the backlash are guessed as the elongation of inner wire due to large friction, the play between outer sheath and inner wire, and motor gear head.

Our first solution for these challenges was to find the best configuration of Bowden cable which has a high transmission efficiency and low nonlinearity. We have conducted experimental analysis with various combinations of different materials [95], and finally, we selected a steel sheath and a braided stainless steel cable. This combination provides a reasonably high efficiency due to its high stiffness, and does

not have time-dependent properties. Polymer-based material such as PTFE provides a higher transmission efficiency than metal but the friction with the polymer-based material changes as operation time goes by [116]. In addition, the durability of polymer-coating is generally low, so that the coated surface on metal gets damaged during operation, deteriorating the transmission efficiency. Strong pre-tension also helped to eliminate an undesirable nonlinear effect such as slackening.

Next, we modeled the backlash effect for the selected Bowden cable configuration. The exoskeleton joint angle q was measured while the corresponding motor generated sinusoidal motions without load on the exoskeleton joint. The backlash effect was observed as shown in the blue lines of Fig. 4.4. The observed backlash is modeled as (4.3) and shown in the red line of Fig. 4.4.

$$\tilde{q}(t) = BL(\phi(t)) \tag{4.3}$$

where ϕ is the pulley rotation angle on the motor shaft, $\tilde{q}$ is the modeled angle change of the pulley on the exoskeleton joint through the backlash model (4.3).

With the Bowden cable model (4.3), the pulley rotation on the exoskeleton joint is estimated, but the force control is still challenging due to substantial friction. For the torque actuation, we introduced two compression springs before the exoskeleton joint pulleys (Fig. 4.5). With these elastic components, we built a miniaturized SEA. The basic idea of our SEA is to estimate the joint torque by measuring the deflection of springs. The deflection is calculated from the motor angle, the SEA joint angle, and the compensation of the backlash-effect. The SEA torque is expressed by

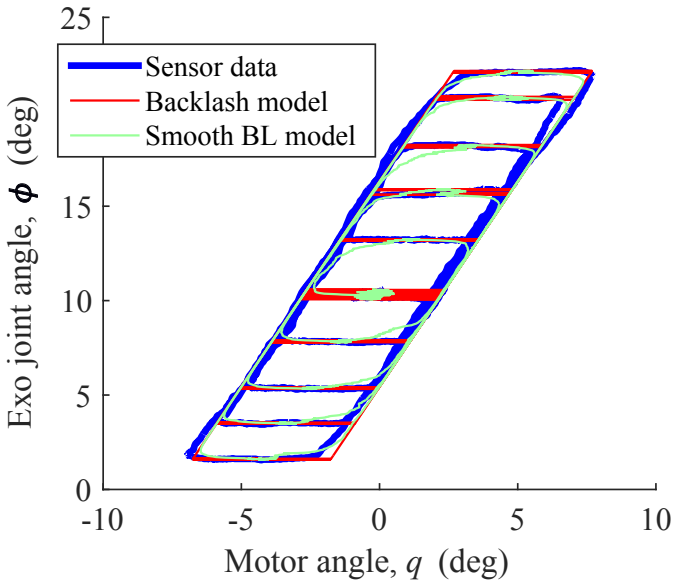

Figure 4.4: Backlash-like effect was observed in Bowden cable transmission as shown in the blue line. For control with the Bowden cable, the backlash model is obtained as shown in the red line. To avoid a jerky motion of actuator in control, the model is smoothed with a sigmoid function as shown in the green line.

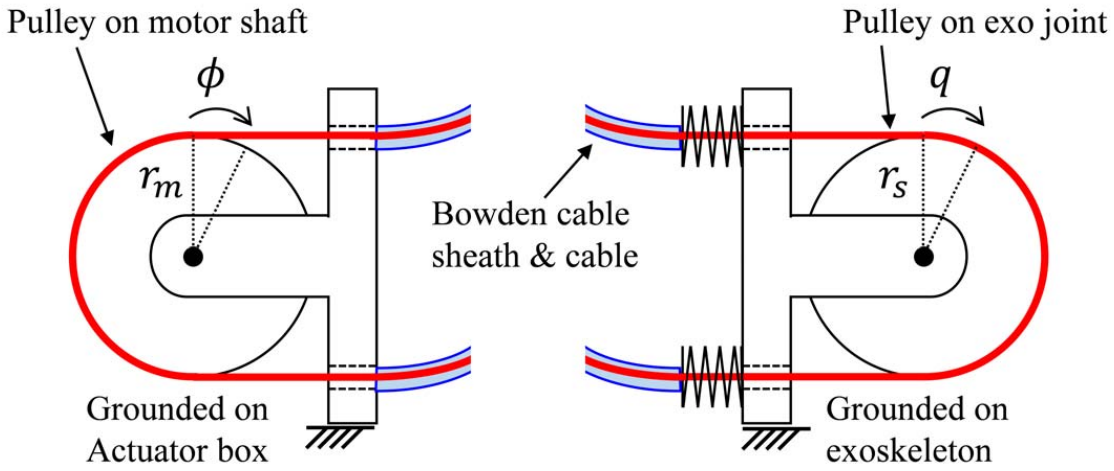

Figure 4.5: Bownden cable actuation with a miniature SEA. The pulley on exoskeleton joint is actuated by the pulley on motor shaft through Bowden cables. By introducing two compression springs before the the exoskeleton joint pulley, we built a miniaturized SEA which converts a displacement into a torque

(4.4):

$$\begin{aligned} \tau_s &= r_s(2k\Delta d) \\ &= 2kr_s^2(\tilde{q} - q) \end{aligned} \tag{4.4}$$

where τ_s is the torque of the SEA, k is the stiffness of the compression spring, r_s is the pulley radius of SEA joint, Δd is the deflection of the compression springs representing $r_s(\tilde{q} - q)$. q is the SEA angle and $\tilde{q}$ is obtained from (4.3).

For controlling the SEA torque, τ_s, we needed a inverse of the backlash model. However, the inverse of backlash model includes discontinuity which is unrealistic in real applications. Thus, we developed a smoothed version of backlash model shown in the green line of Fig. 4.4, and the smoothed backlash inverse model was used for

torque control of SEA. Since the weight of exoskeleton is light and the operation speed is slow in rehabilitation, we assume a quasi-static condition for torque control of exoskeleton. The SEA torque for the desired finger joint torque is obtained with the virtual work principle as:

$$\tau_s = \mathbf{J}^\top \tau_f \tag{4.5}$$

where $\mathbf{J}$ is the Jacobian of $\mathbf{f}$ of (4.2) with respect to $\mathbf{q}$, defined as $\mathbf{J} = \frac{\partial \mathbf{f}}{\partial \mathbf{q}}$. For evaluation, the SEA generated torques to follow a given desired trajectory. Fig. 4.6 shows the result, and the RMSEs for MCP and PIP joints were 7.66 mNm and 6.35 mNm respectively in the experiment. For the detail of experiments and equations, refer to [95, 97, 118].

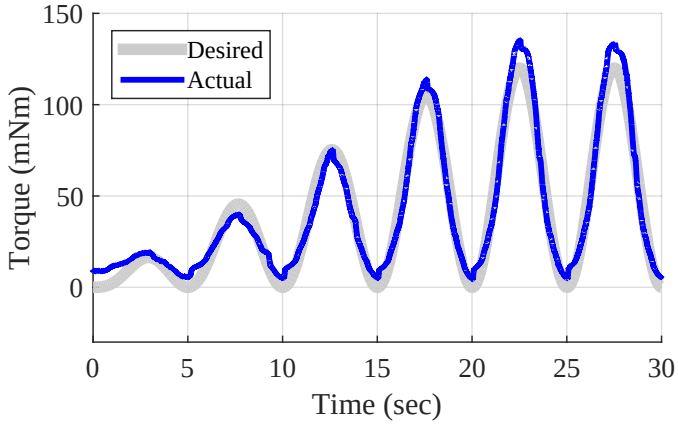

(a) Torque control of MCP joint

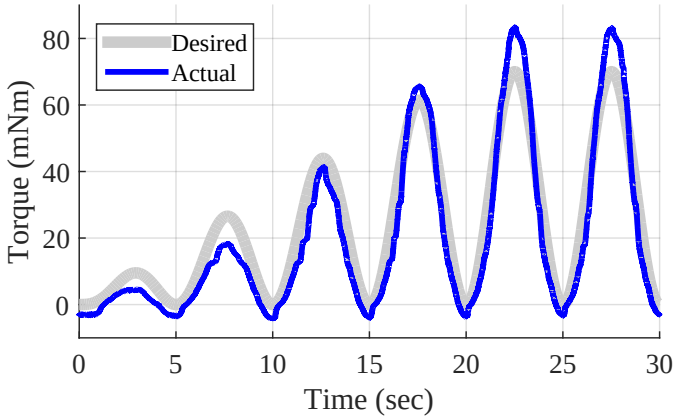

(b) Torque control of PIP joint

Figure 4.6: Torque control of finger joints with Maestro. Using the calibrated kinematic model and the smooth backlash model, the finger joint is controlled by two SEAs. The SEAs tracked the desired torque trajectories of finger joints. The actual torques were measured from the testbed finger.

Chapter 5

Control System of Maestro

In this section, we will present how we developed a control system including hardware and software architecture. The development of hardware and software structure for a control system has been often neglected in research papers because it is not a theoretical problem. However, in a practical aspect, the development of a high quality control system needs a significant amount of time and efforts because it is difficult to know the pros and cons of the systems before having extensive experience of them. We also spent considerable amount of time to find a good combination of hardware, operation system (OS), and program structure for Maestro. We surveyed robotics engineers, had consultation from hardware and software suppliers, and tried multiple systems.

5.1 Two-layer control system including FGPA and RT-Linux achieves both powerful capability and flexibility

When selecting hardware and operation system (OS), we considered several important points. The control system needs to have a powerful signal processing performance to process various control algorithms. Most of precise force control algorithms generally require a high frequency control loop (greater than 1kHz) and a small jitter (less than 1ms). Lower-level signal processing such as high/low-pass

filtering or current control of motors needs even faster sampling rate. Implementation of a complicated control algorithm such as a neural-network based algorithm needs a high speed microprocessor and sufficient RAM. The system also needs to receive and process many signal inputs and outputs simultaneously. The exoskeleton has total 8 actuators, and 16 analog-voltage-output sensors, 8 incremental encoders, and extra signal lines for other purposes (e.g., emergency switches).

The control system also must be flexible in terms of hardware and software. The goal of our exoskeleton is to investigate various promising rehabilitation strategies studied in neuroscience research. In this regard, the exoskeleton needs to be integrated with other hardware such as motion capture system, EMG and other body exoskeletons, and also with other software including hardware drivers and math libraries. In the current status, C/C++ programming environment provides the largest compatibility to hardware and software of robotics applications.

Based on the requirements, we have explored four different options of hardware and OS combinations and compared them by data sheet and by our experience. The result is shown in Table 5.1, and we finally selected NI-cRIO and RT-Linux combination. The combination has a strong real-time (RT) performance by RT-preempt Linux, a reasonably strong computational power by Intel Atom processor, a convenient FPGA programming environment by Labview and a flexible C/C++ programming environment by GCC in Linux. The hardware package of cRIO is robust and validated in many industry applications such as automotive field tests. The modularized system of cRIO makes the system compatible to extra mechatronic parts.

After the selection of the main control hardware and OS, we developed a system in an enclosure, called Control box (Fig. 5.1), which is dedicated for processing the information of Maestro. In addition to cRIO, we established an independent ethernet network for general purpose communication by installing an ethernet hub in Control box. Control box communicates through the hardware interface of FPGA if a strict RT-communication is required, or for the hand exoskeleton sensing, actuation and safety features. Control box communicates through the ethernet if the communication does not require a strict RT performance, e.g., the communication with user interface and visualizer. The overview of the signal flow in Maestro is shown in Fig. 6.11.

5.2 Object-oriented program in C++, Labview for FPGA, and UDP communication provide flexibility, easiness of programming, and compatibility

The control system of Maestro is programmed by two programming languages: Labview for FPGA and C/C++ for RT-Linux.

5.2.1 FPGA programming by Labview

Field-programmable gate array (FPGA) is an integrated circuit (IC) developed to be configured after manufacturing. The advantage of FPGA in robotics application is at its fast response (almost same as an analog logic) so that many robotic applications introduced the FPGA when they needs a high-speed signal pro-

Table 5.1: Comparison of control system options

Control System	Hardware	Desktop + DAQ	Desktop + DAQ	NI cRIO	NI cRIO
	OS	RTAI (RT Linux)	xPC Target (Matlab)	VxWorks	RT-preempt Linux (RT Linux)
RT Performance[a]		Strong	Strong	Strong	Strong
Computational power at high level[b]		Strong	Strong	Medium	Medium
Integrated FPGA		N/A	N/A	Strong	Strong
Support of C/C++		Strong	Weak[c]	Weak[c]	Strong
hardware driver support by OS		Weak[d]	Strong	Strong	Strong

[a] VxWorks has the best RT performance in general, but all four OS shows great performances for the rehabilitation robot control application [119].
[b] NI cRIO devices generally have lower hardware specs than the state-of-art desktops in terms of CPU, RAM, and etc. However, cRIO can calculate the inverse of a 500x500 double-precision matrix within 1ms.
[c] Labview and Matlab/Simulink supports C/C++ partially. For integration, they requires several procedures of converting existing codes to fit with their systems.
[d] The hardware driver of RTAI is supported by Comedi (http://www.comedi.org). However, the support is limited and outdated.

Figure 5.1: The inside of Control box. Control box consists of NI cRIO, ethernet hub, power supply, safety devices, and others. For the connections in Control box, screw-type breakout boards were used for convenient maintenance, and for the connection to the other peripherals, standard connector housings (D-sub 25/37, HDMI A-type) were used for quick and robust connections. The wires in Control box were cleanly arranged by Din rail, wire duct, terminal block, and label.

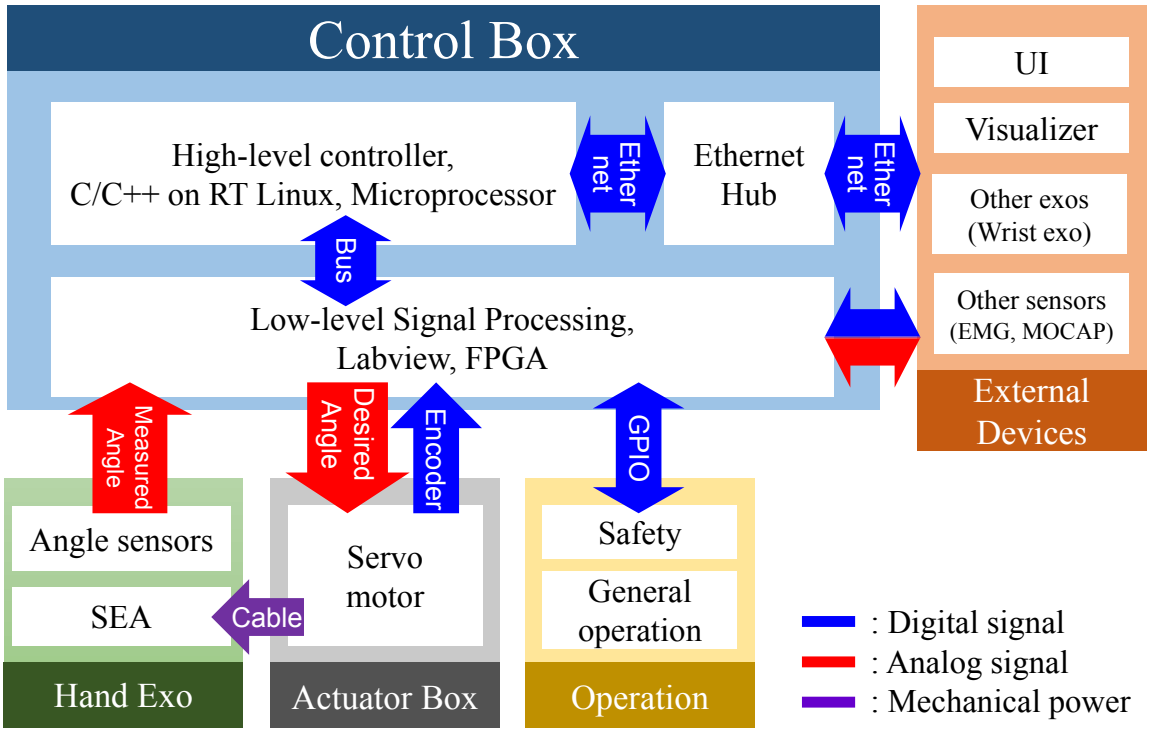

Figure 5.2: Overview of signal flow in Maestro system. All major signal processing occurs in Control box. The cRIO in Control box consists of two parts: C/C++ program on RT-Linux and Labview program on FPGA. The high-level controller is running on the C/C++ program, and the low-level signal processing is performed in FPGA. FPGA communicates with peripheral devices with GPIO, analog signals, etc. In Control box, an independent ethernet network is established. Through User-datagram-protocol (UDP) through the network, various general-purpose communications are performed for visualization, user-interface, connection with another exoskeleton.

cessing. The disadvantage of FPGA is that the development of FGPA is not convenient for frequent program changes and its programmable capacity is limited. FPGA programming requires low-level hardware knowledge, and the compilation and hardware synthesis time is significantly longer than a simple C/C++ compilation and linking time. Programming a FPGA by NI Labview saves the development time of FPGA significantly by using GUI-based programming tool and pre-built libraries. In addition to the easiness of programming, NI provides an C/C++ libraries which interfaces with the FPGA. As a result, the C/C++ programmer does not need to worry about NI hardware drivers.

In Maestro, the FPGA is used for hardware management, low-level signal processing, and safety features. The FGPA has multiple analog I/O and digital I/O. The FPGA manages those signal I/O for interfacing with C/C++ program (Fig. 6.11). Maestro has 16 analog sensors and the quality of the sensor values are improved by low-pass filters running at 20kHz. In addition, various bio-signals such as EMG can be postprocessed with a high-speed signal processing. The status of all electric components are monitored by the FPGA and if any abnormal status is found, the operation is safely terminated. The FPGA program is separated from the C/C++ program, thus any mistakes of C/C++ program do not affect the FPGA safety features.

5.2.2 C/C++ programming with GNU GCC/G++ for RT Linux

Although the Labview provides a convenient programming environment for FPGA, C/C++ with GNU GCC/G++ has several advantages for programming

high-level software. First, if a program is considerably large, the GUI-based programming is not anymore intuitive. Second, the connections with existing C/C++ codes are not simple. So far the most compatible programming language in robotic applications is C/C++. Most of hardware and software developers support C/C++ libraries essentially but Labview optionally. Lastly, some engineering schools have the license of Labview software, but many other institutions do not have Labview software which is expensive. Otherwise, GNU GCC/G++ in Linux provides a license-free programming environment.

In the C/C++ programming environment, we developed hand exoskeleton control program with a object-oriented-programming (OOP) concept. The OOP provides several advantages for Maestro. First, the end-user can program a rehabilitation scheme easily. We built a low-level software for managing RT interrupter and FPGA interface and the high-level software for the controller for rehabilitation. By dividing the program into two parts, an end-user does not need to know the knowledge of hardware or OS. Simply, an end-user needs to write a code to modify the controller existing in the high-level software. Second, the system can be safer by encapsulation. The low-level software is encapsulated, and thus an end-user does not need to touch the low level software which is critical for basic operation. Lastly, the maintenance is handy. The high level programs are modularized so that the development of those modules can be parallelized. We have developed many different types of high-level modules such as various controllers, user-interfaces, and communication tools. These modules will be upgraded and more parts will be added. The modularized structures supports sustainable upgrades of the software.

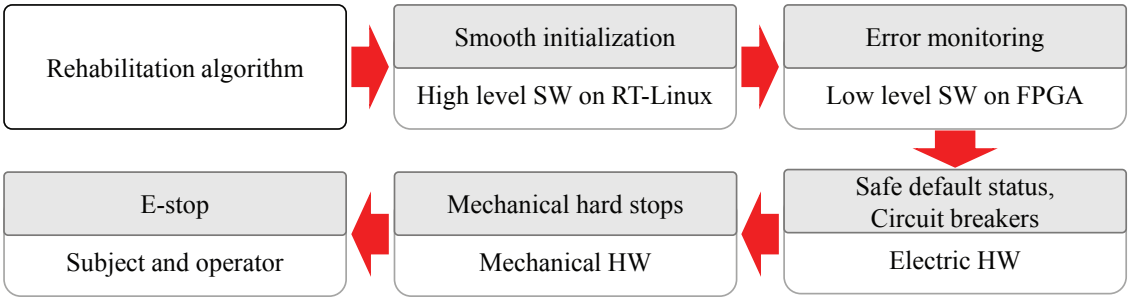

Figure 5.3: Multi-stage safety features prevent human mistakes or unexpected machine problems.

5.3 Multi-stage safety features ensure the safety of subjects

Since the mission of Maestro is to explore various rehabilitation strategies, the high level software will be modified frequently by different end-users. The high-level algorithm developers first have to do his/her best to build a stable algorithm, but many control schemes, particularly interacting with an unknown environment, have a risk of unstability. to prevent all possible accidents, we introduced multi-stage safety features (Fig. 5.3).

The first safety device is on the high level software running in C++ program on RT-Linux. The final output of the controller is transmitted to the low level software with a gain whose shape is a sigmoid function (smoothly increasing function). Because the sigmoid function begins from zero and reaches to one, the initial output of actuator is very small, and as time goes, the output becomes same with the actual control outputs. The basic motivation of this safety feature is to provide a time to press an emergency stop button if an unexpected problem occurs.

The second safety feature is on the low level software running in FPGA. The

FPGA keep monitoring hardware behaviors, and if hardware shows an unexpected behaviors such an impulsive motion or a significant difference between a desired and actual behavior, the FPGA safely halts the system operation.

The third and fourth safety features are on electrical and mechanical hardware. The default status of all electric circuits are set to be safe, and users need to activate each electric component manually after checking the safe status. Also, circuit breakers halt all system if electric hardware detects overcurrent or communication error. All exoskeleton joints have mechanical stops, thus an exoskeleton motion exceeding a safe region is blocked. Finally, the system is always safely terminated by pressing emergency stop buttons if a subject or an operator detects a danger. Since we introduced all these safety features, any safety accidents have not yet occurred to date while conducting many pilot tests.

Chapter 6

Control of a Hand Assistive Device with Surface EMG Sensors for Spinal Cord Injury Patients

For the last three chapters, we have presented the development of research platform to study hand rehabilitation and assistance for neurological disorder patients. The development of Maestro has led to research on adaptive control theories with human motion, development of a hand-wrist exoskeleton, fatigue progress of hand muscles, systematic rehabilitation framework and assistance for SCI patients. Among those, in this chapter, we will present our study on the hand assistive orthoses with sEMG sensors and with Maestro.

6.1 Background Information of Active Hand Assistive Orthoses

The number of spinal-cord-injury (SCI) patients is estimated to be 282,000 in the United States in 2016 [6]. Approximately 45% of SCI patients have residual function in their arms and shoulders [6], but have difficulty performing activities of daily living (ADL) due to insufficient hand function. An ultimate goal of the research in this chapter is to improve their hand function in ADL with an active

This chapter includes a part of writing in [4]. Youngmok Yun made a contribution for developing the exoskeleton and conducting experiments with SCI subjects.

assistive orthosis.

Most current commercial assistive orthoses are passive devices that either help with passive extension/flexion or locate the fingers/thumb in a predetermined position [54]. Although these orthoses are economical and easy to use, they have several limitations. The passive stiffness or elasticity hinders hand movement when it is not needed. Moreover, they assume the subjects are able to apply enough force in at least one direction. In order to address these limitations, active orthoses have been recently developed [37–42, 120]. Since the devices assist them in achieving a task by adding extra strength, even a subject with weak muscles is able to perform the tasks. A key challenge to achieve this advantage is to reliably recognize the intention of users. If the device fails to recognize the intention of the user, the orthoses "actively" hinder achieving tasks.

EMG-based operation of assistive orthoses has many advantages. First, the operation is intuitive because the target muscles of EMG sensors are generally selected to be relevant with desired tasks. Thus, users do not need to be trained for long time. Second, the operation of the assistive device is not disturbed by the motions of other body parts. Several user interfaces of active assistive devices sense the motion of other body parts such as tongue [37], neck [38], or wrist motion [39], or recognize voice commands [120]. In order to use these interfaces, a user must stop speech or nodding to operate the assistive device. In addition, using the motion of other body parts may restrict the scope of available tasks with the orthosis. For example, if a hand orthosis is operated by a wrist motion [39], a user may not achieve a task that needs both hand and wrist motions (e.g, jar opening).

Based on the advantages, researchers have developed EMG-driven active hand orthoses. However, the operation of those devices have been performed only with an one-dimensional variable or a threshold for 1-DoF actuation. Benjuya and Kenney [40] pioneered the research on an active hand orthosis with 1-DoF finger exoskeleton. The device is tested with two C6 SCI patients and one brachial plexus patient. The paper reported the enthusiasm of patients while using the orthosis, but did not report a quantitative result. DiCicco et al. [41] developed a 1-DoF orthosis assisting pinching motion of a SCI patient. The paper reported that a C5/C7 SCI subject with the orthosis was able to grasp a roll of tape, rubber ball, hockey puck, and not able to grasp a tooth brush, and deck of cards. Zhao et al. [42] recently presented a soft hand orthosis which is capable of increasing grasping force proportional to one-dimensional EMG-related variable. The paper showed a potential of soft actuators in a hand orthosis but did not show experimental results with a neurological disorder patient. A healthy subject with the soft orthosis grasped an apple [42]. A critical problem of the previous devices is that a subject with an 1-DoF orthosis is able to grasp only a limited number of objects.

Grasping various objects required in ADL with an EMG-driven orthosis is challenging. In order to grasp various objects required in ADL, a hand orthosis needs to generate many different hand poses depending on the objects. Bullock et al. [99] reported that humans use 34 different hand poses for grasping objects, and Sollerman [1] selected the eight most frequent hand grips for grasping objects required in ADL. What even more challenging part is that the many desired hand poses for a specific object needs to be determined by noisy EMG signals. EMG sig-

nals are inherently noisy because the action potential of motor neurons is very low, and particularly, sEMG sensors cannot monitor individual muscle activities. Moreover, similar patterns of EMG signals are measured while grasping different objects requiring different hand poses, which makes the EMG-based operation difficult.

One promising solution is to take an advantage of compliant actuators in operation of a hand orthosis. Actually, humans actively use the advantages of compliance in digit joints. While grasping an object, the hand poses are determined not only by the kinematics control of digit joints, but also by the stiffness of digit joints and the shape of objects in tasks [121]. Because of this strategy, humans are capable of grasping various objects even under uncertain environments (e.g, with insufficient visual information of an object). If a hand orthosis has compliance in actuation, a subject with the orthosis may grasp many different objects without generating specific hand poses for the objects. Furthermore, this idea may bring an advantage in the classification of EMG signals because the classification algorithm does not need to classify the noisy EMG signals into many different grasping modes.

A naturally following question after the above idea is "what is the minimal set of hand poses with a compliant hand orthosis to grasp various objects required in ADL?" We found that four different hand poses generated by a compliant hand orthosis are sufficient to enable subjects to grasp various objects required in ADL; the four hand poses are transverse volar grip, lateral pinch, extension grip, and extension. We will present the detailed procedure of answering this question in Section 6.2.

Next, we present the optimal locations of sEMG sensors for SCI patients to generate the command for the four hand poses. When selecting the location of sEMG

sensors, several points need to be considered. First, the muscles monitored by EMG sensors need to be relevant with the target hand poses. Second, the innervation of muscles from spinal cord needs to be considered because the assistive device is for SCI patients. The muscles innervated by an upper part of spinal cord is more desired. Third, the target muscles need to be located close to skin. Otherwise, the signals from the target muscle would be polluted by external electric noise and interfered by other muscle signals. Based on these considerations, we found three optimal locations of sEMG sensors, which are capable of efficiently classifying the EMG signals into one among the four hand poses.

Lastly, we present the evaluation of the hand function for 6 SCI subjects with and without Maestro. The ultimate goal of the assistive device is to improve the hand function of SCI patients in ADL. Thus, we evalutated their hand functions with a standardized hand function test, called Sollerman hand function test (SHFT). Three sEMG sensors were attached on the optimal locations, and then a classification algorithm classified the EMG signals into one of the four hand poses. Maestro generated the target hand pose based on the command. The results of SHFT shows that the hand functions of C6 and C7 SCI subjects were improved with the proposed method.

6.2 Target Hand Poses of a Compliant Hand Orthosis

In this section, we present how the target hand poses of a compliant hand orthsis were determined. The target hand pose is defined as a hand pose generated by a hand orthosis when the hand is relaxed and does not interact with an external

object. If a subject use a compliant hand exoskeleton, the hand pose would be different with the given target hand pose when interacting with an object or when the user generates strengths on their digits. Before explaining the detailed process of answering the question, we first present the background information that will be used in the next subsections, including the modification of Maestro and the definition of ADL based on the study of Sollermand and Ejeskr [1].

6.2.1 Modification of Maestro

The requirements of our active assistive hand orthosis is a light weight, comfort in wearing, compliance in actuation, and capability of generating diverse essential hand poses. We conducted experiments with Maestro because it has already many advantages required as an active hand orthosis. However, the assistive device needs several different factors, thus some modification of Maestro were performed. Except the explanation of the below, other properties are same with those of Maetro.

A major change is the interface of the exoskeleton. In the original design of Maestro, we intentionally used a rigid interface with a velcro, providing a transparent force transmission but simultaneously being less comfortable. For the experiment of assistive devices, we introduced a glove-type interface to provide more comfort than the original Maestro while sacrificing some transparency of force transmission because users need to wear an assistive device for long time and the exoskeleton does not need to measure the exact kinematic and dynamic properties of hands. We developed three sizes of gloves including small, medium and large sizes as shown in Fig. 6.1. Three different sizes of gloves provide comforts in wearing for a wide range of subjects.

We sewed rigid interfaces on to the dorsal sides of the glove to prevent undesired tilting motion of the rigid structure as shown in Fig 6.1. Leather also avoids direct contact of rigid structure with skin, preventing irritation. After wearing the glove, tightening velcro straps minimizes the play between the exoskeleton mechanism and the hand (Fig. 6.2 (a)). The fingertip parts of the glove were cut to preserve sensation (Fig. 6.2 (a)). For many SCI subjects, it is challenging to wear a glove because they have disability in moving and sensing their fingers and thumb. To resolve this issue, we cut the palmar side of glove and sewed velcro straps for SCI subjects to facilitate in wearing the glove (Fig. 6.2 (b)). Once a researcher find the correct size of glove for a subject, the rigid interface on the glove is connected with the rigid link mechanisms of Maestro by screws as shown in Fig. 6.3. In addition, we removed passive joints from the original Maestro because the passive joints were designed only for observing the angles of DIP joints, which is not required in an assisitve device.

6.2.2 Definition of Activities of Daily Living

A goal of this research is to assist SCI subjects with an assistive hand exoskeleton to perform hand functions in "ADL". By defining ADL systematically, we would be able to develop an assistive device in a systematic method. The hand functions of ADL is studied by several researchers [1, 99, 122]. Among those, the study conducted by Sollermand and Ejeskr [1] is one of the most extensive studies and focused on the essential hand functions of tetraplegic patients in ADL. Also the study provides a systematic evaluation method of hand functions for SCI subjects. Therefore, the control method of Maestro for assisting SCI patients is developed

Figure 6.1: We developed a customized glove to interface hands with a rigid link mechanism of exoskeleton. Depending on the size of a subject's hand, one among three different sizes of gloves is selected.

based on the study of [1].

Sollermand and Ejeskr selected the most frequently used eight grips in ADL; those are transverse volar grip, spherical volar grip, lateral pinch, diagonal volar grip, extension grip, tripod grip, five finger pinch, and pulp pinch as shown in Fig. 6.4. Based on the selected grips, they selected 17 objects which need to be grasped by the eight grips; those are a key, coin, wooden block, iron, screw driver, nut, jar lid, knife, socks, pen, paper, paper clip, telephone, door handle, pure-pak, and cup. The hand function is evaluated by how a subject correctly perform tasks with these objects with a correct grip. The detailed explanation of Sollerman hand function test will be described in the later sections.

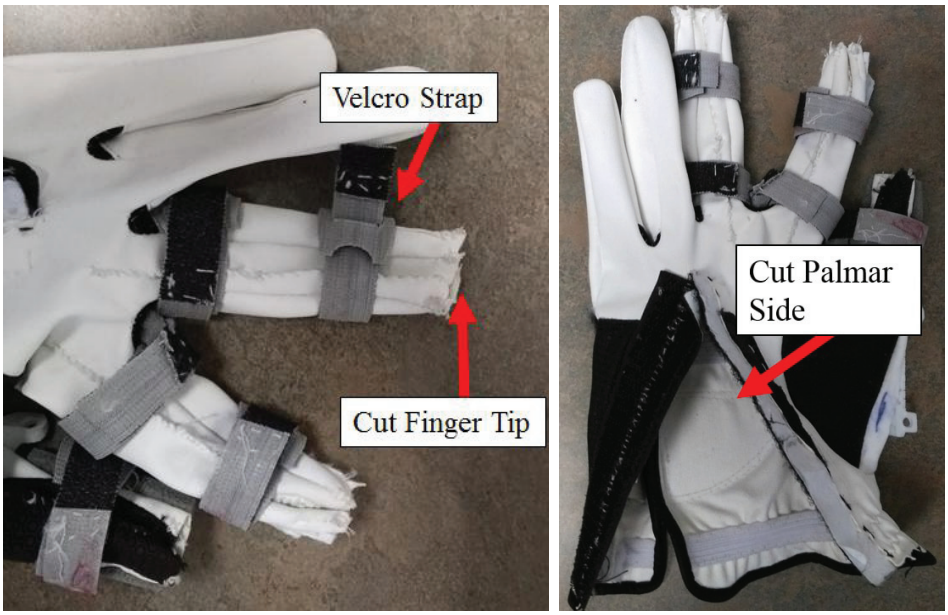

(a) (b)

Figure 6.2: (a) The finger tip and thump tip of gloves were cut to preserve sensation of SCI subjects. Velcro straps were attached on the side of glove digits to remove the stretch effect of the leather glove. (b) SCI subjects usually have difficulties in wearing a glove. Thus, we cut the palmar side of glove for SCI subjects to to facilitate in wearing the glove.

6.2.3 Experiments and Results

In this subsection, we will find a minimal set of target hand poses of Maestro which is capable of grasping the 15 objects listed in [1]. We excluded the grasp of a coin and a water-jug because grasping a coin and a water jug uses exactly same hand grips for a paper clip and an iron respectively. The basic idea of the experiment is that a researcher increase the number of a target hand pose or replace a target hand pose with another until a subject is able to grasp all 15 objects.

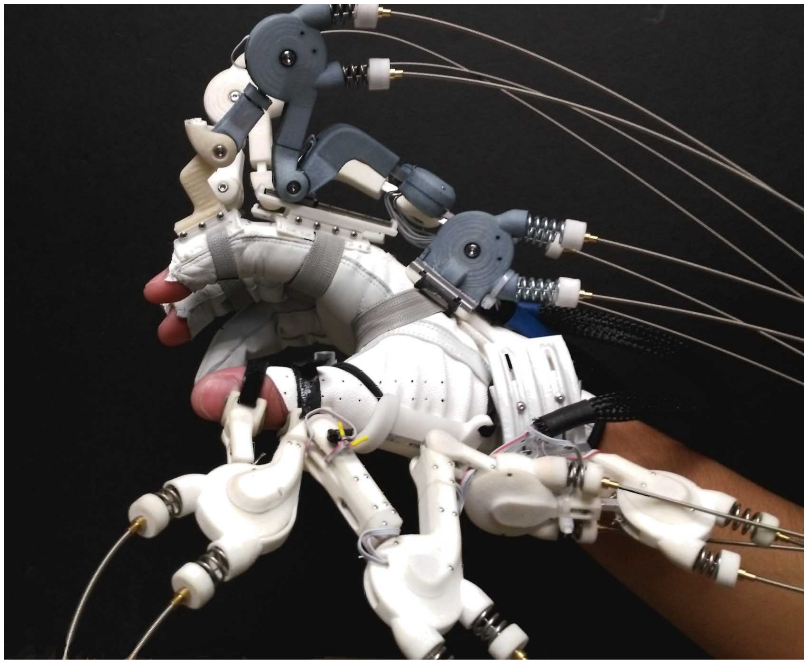

Figure 6.3: Maestro is modified from the original design of Maestro for experiments to study assistive devices. A novel interface is introduced and passive joints were removed.

The experiment was conducted through the following protocol. First a subject wears Maestro. All mechanical settings are tunned by a researcher to be optimal for the subject to obtain the maximum range of motion and comfort in wearing. Second, the subject is asked to relax his hand. This ensures that grasping an object is performed by Maestro. Third, a researcher places an object at the best location to be grasped by the subject. This eliminates effects from external environments. Fourth, a researcher generates a target hand pose which is desired for the object. Fifth, the subject with Maestro grasps the object. The subject is allowed to move their arm and shoulder to help his hand grasp the object. Sixth, a researcher judges

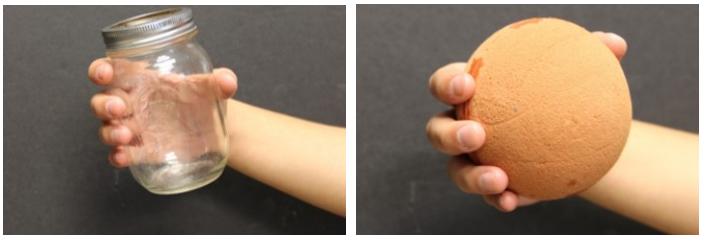

(a) Transverse volar grip

(b) Spherical volar grip

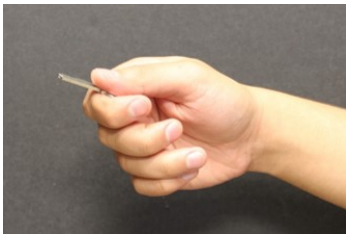

(c) Lateral pinch

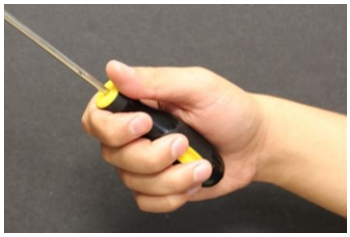

(d) Diagonal volar grip

(e) Extension grip

(f) Tripod grip

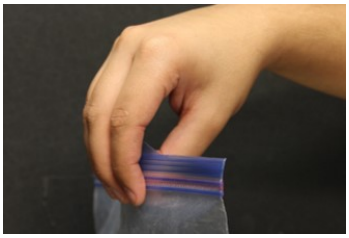

(g) Five finger pinch

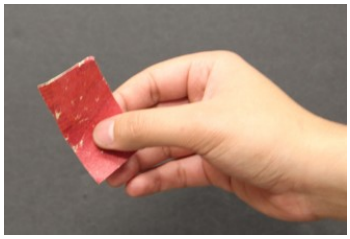

(h) Pulp pinch

Figure 6.4: Sollermand and Ejeskr selected the most frequently used eight grips in ADL [1].

if the subject grasps the object with a correct grip described in [1]. The compliance of Maestro was passively determined by the stiffness of compresseion springs located at the exoskeleton SEA. In other words, the motors in Actuator box was controlled in a position mode. The stiffness of springs was selected by a researcher in the range which provides reasonable comfort to a subject and simultaneously sufficient grasping strength. The selection of the stiffness was practically not difficult.

Two healthy subjects and one SCI subject participated in the experiment, and the experiment results were consistent through all subjects. As a first trial, we tried two target hand poses including transversal volar grip and extension. As shown in [41], results show that subjects could not make all hand grips which require thumb adduction (e.g., key pinching). In the second trial, we added lateral pinch into transversal volar grip and extension. This addition enabled subjects to grasp many objects requiring thumb adduction such as a key and screw driver, but subjects still could not grasp objects which are flat or small objects such as a nut, paper clip, and paper. Lastly, we added extension grip into the previous set, and subjects were able to grasp all 15 objects listed in [1]. Fig. 6.5 shows an experiment result with a C5/C7 incomplete SCI subject who is barely able to generate flexion force on his index and middle fingers.

The experiment results show that a subject with a compliant hand orthosis is able to grasp with only four hand poses including transverse volar grip, lateral pinch, extension grip, and extension, which are significant smaller than the number of hand grips reported in [1, 99, 122]. This significant reduction may bring an advantage in the EMG signal classification problem because a smaller number of classification

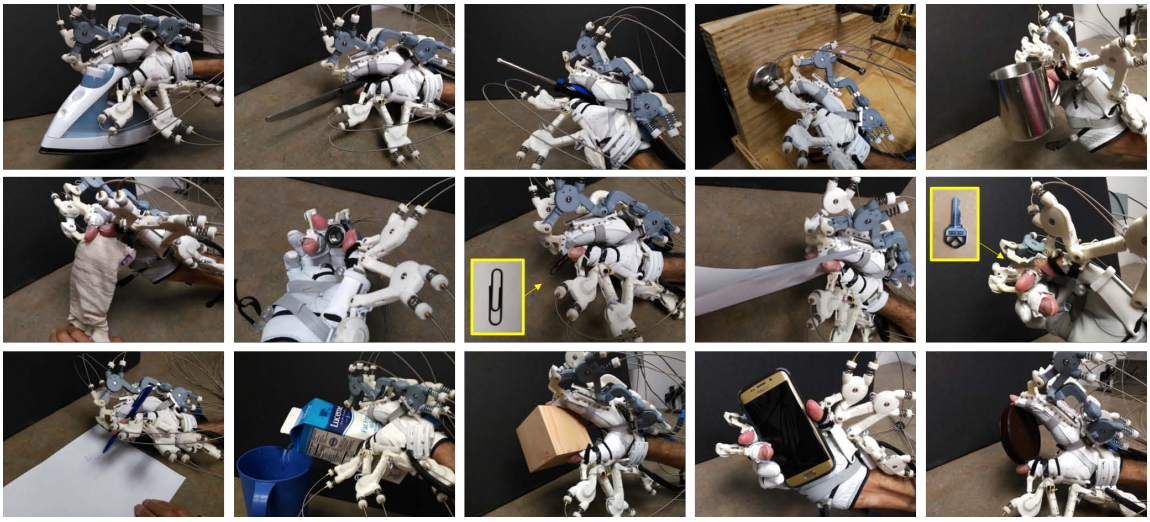

Figure 6.5: A C5/C7 incomplete SCI subject who is barely able to generate flexion of index and middle fingers was able to grasp 15 objects listed in Sollerman hand function test. In the experiment, only four target hand poses of Maestro were used.

generally leads to a higher success ratio of a classification algorithm.

There are several discussion points. The first one is the uniqueness of the target hand poses. During the experiments, we found that the compliance of actuation allowed for high flexibility in selecting the target hand poses that are capable of grasping various objects. As a result, the selected four target hand poses were not a unique solution. A variation of the selected target hand poses can be also a set of target hand poses of Maestro. However, the number of target hand poses would not be reduced because as shown in [99], there are clear requirement of thumb adduction and abduction motion depending on objects. The shape of fingers also determines the available shape of objects for grasping, which justifies two different target finger poses at thumb abduction, those are extension and flexion of fingers.

Another important point is that the difference between grasping an object and performing a task with the object. In the experiment of this section, we only conducted a grasping test, which means if a subject was able to hold an object with a correct grip, then a researcher determined the grasping was successful. Although subjects with Maestro were able to grasp all 15 objects listed in [1] with the four target hand poses, showing the advantages of Maestro over other hand orthoses, the success of grasping does not mean that the subject is able to perform a task with the object. Indeed, the performance of a task can be successfully conducted only when many complex components meet sufficient conditions including dexterous shoulder and arm functions, adequate grasping force, creativity in the task, and psychological effects like a motivation. Therefore, it must be clear that grasping the 15 objects required in ADL does not directly mean that a subject with Maestro is able to perform all tasks. The hand function of SCI subjects in task performance with Maestro will be evaluated in the later sections with Sollerman hand function test.

6.3 Location of Surface EMG Sensors

To develop a successful EMG-driven active hand orthoses, the intention recognition with EMG sensors is crucial. In the previous section, we found a minimal set of target hand poses of a compliant hand exoskeleton, which is capable of grasping various objects required in ADL. The small number of the target hand poses, that is four, has advantages in an EMG-based classification algorithm because an EMG-based classification algorithm would be less confused. The other important factor

for the EMG-based classification algorithm is to find the optimal locations of EMG sensors. This section will present an optimal set of locations for sEMG sensors to operate Maestro for SCI subjects.

6.3.1 Candidates of Surface EMG Sensor Locations

For determining the locations of sEMG sensors, several points need to be considered. First, the muscles monitored by EMG sensors need to be relevant with the four target hand poses. This reduces the training time and makes operation of the device more intuitive. Second, the innervation of muscles from spinal cord need to be considered. For instance, the muscles innervated by upper parts of spinal cord are more suitable because, SCI patients have less function in muscles innervated from lower parts of spinal cord. Third, the target muscles need to be located close to the skin. Otherwise, the signals would be polluted by external electric noise and interfered by signals from other muscles. Fourth, the number of EMG sensors need to be minimized. Using numerous sensors may provide a considerable amount of information, but simultaneously the application with the many sensors is not feasible in reality. For example, Liu et al [123] performed a successful EMG-signal classification with 57 sEMG sensors for SCI subjects. The study showed potential of using sEMG sensors to understand the intention of SCI patients. However, it is difficult to directly implement this sensor configuration in ADL due to high cost and long setting and calibration time. We also consulted with an occupational therapist to understand common muscle patterns of incomplete SCI and available muscles of SCI patients with limited hand function.

Based on the above factors, we selected six candidates of sensor locations to be monitored. We picked target muscles based on relevance to task and muscle innervation. Then we tested the pattern recognition algorithm with different combinations of located sensors to find out the minimal number and location of EMG sensors for achieving reliable control.

The muscles are listed in Table. 6.1. Flexor digitorum superficialis and Flexor carpi ulnaris are selected mainly for detecting the finger motion. Extensor digitorum and Extensor carpi ulnaris are selected mainly for finger and thumb extension. Flexor pollicis brevis and Flexor pollicis longus are selected to detect thumb abduction and flexion. Because the muscle and tendon configuration is correlated with multiple digit joint motions, it is difficult to build a one-to-one match between a joint motion and a muscle. Also due to the characteristics of sEMG sensors, each sensor measures not only a targeted muscle activity but also the activities of other muscles located around that muscle.

Based on these six muscles, we selected six candidate locations for sEMG sensors as shown in Fig. 6.6. The numbers in the figure correspond to the muscle numbers of Table. 6.1. The quality of the measured EMG signals is crucially dependent on choosing the correct location of sEMG sensors. The occupational therapist assisted us in locating the selected muscle bellies by palpating patient's forearm and palm. Multiple small muscles exist together in the small region of the third sensor (palm), so the third sensor measures activities of Abductor pollicis brevis in addition to the target muscle, Flexor pollicis brevis. However, this was not a problem in the experiment since our goal was to determine user's intent, not to monitor the single

Table 6.1: Six muscle candidates to be monitored by sEMG sensors

Muscle No.	Muscle Name	Innervation
1	Flexor Digitorum Superficialis	Median nerve (C7, C8 and T1)
2	Extensor Digitorum	Posterior interosseous nerve (C7 and C8)
3	Flexor Pollicis Brevis	Recurrent branch of median nerve (C8 and T1)
4	Flexor Carpi Ulnaris	Ulnar nerve (C7 and C8)
5	Extensor Carpi Ulnaris	Posterior interosseous nerve (C7 and C8)
6	Flexor Pollicis Longus	Anterior interosseous nerve from median nerve (C8 and T1)

muscle activities.

Based on the six muscles, we selected six candidates of locations for sEMG sensors on a subject's forearm and palm as shown in Fig. 6.6. The numbers in the figure corresponds to the muscle number of Table 6.1. The occupational therapist assisted to find the best location of a EMG sensor to monitor a specific muscle. Every muscle has different shapes and there is a "sweet spot" of each muscle for EMG sensors. Depending on the selection of the sensor location, the quality of measurement crucially changes. Because of his assistance, we were able to eliminate undesired factors caused by selecting incorrect locations. One remarkable point is that multiple small muscles exist together in the small region of the third sensor (palm). Therefore, it was not possible to measure the signals of the single target muscle, Flexor pollicis brevis. The third sensor measured the activities of not only

Flexor pollicis brevis but also Abductor pollicis brevis. This measurement was not a substantial problem in our experiment because the our goal only need to read the intention of users.

6.3.2 Experiment to Select an Optimal Set of Sensor Locations

In this subsection, we present an experiment method designed to find an optimal set of sEMG sensor locations from the six candidates of locations found in the previous subsection. The basic procedure of the experiment is to find a set of sensor locations that can provide a sufficient success ratio of an EMG classification algorithm.

In the experiment, first six sEMG sensors are attached on a subject's right forearm and palm. The precise locations are identified by palpating the subjects right forearm and palm. Delsys Trigno Wireless EMG sensors were used for recording EMG signals.

Second, the subject's hand is placed and secured in a hand splint to measure maximum voluntary isometric contraction (MVIC) of each muscle. A custom-made splint is used to measure the MVIC of hand muscles for SCI subject as shown in Fig. 6.7. The subject is asked to perform maximum finger flexion, finger extension and thumb flexion respectively, while the muscle activity is being displayed to the subject on a computer screen. The MVICs measured in this part are used to normalize EMG data in the post-processing of EMG signals.

Third, in order to train a EMG-classification algorithm, subjects are asked to perform 3 trials including 5 different tasks interacting with real objects while the

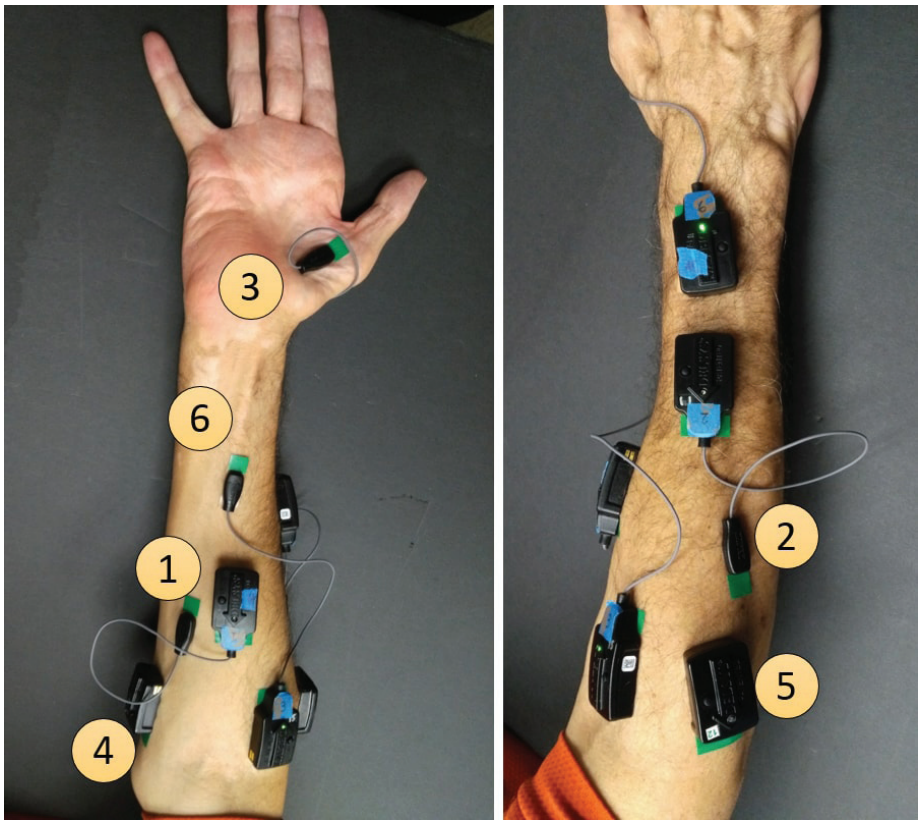

Figure 6.6: Six sEMG sensors were attached on a subject's forearm and palm to measure the muscle signals of 1) Flexor digitorum superficialis, 2) Extensor digitorum, 3) Flexor pollicis brevis, 4) Flexor carpi ulnaris, 5) Extensor carpi ulnaris, and 6) Flexor pollicis longus.

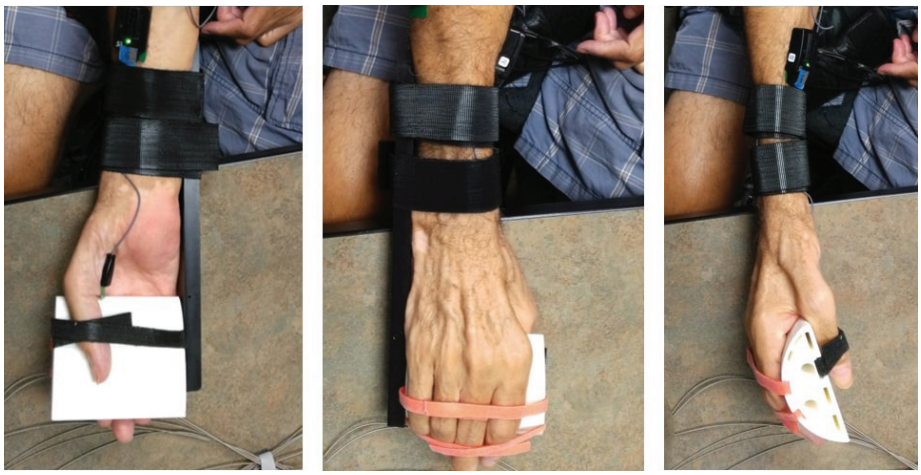

Figure 6.7: Maximum voluntary isometric contraction of muscles is measured with a custom made splint. Because SCI patients are not capable of moving their hands, we developed a custom splint to facilitate the measurement.

muscle activities were being recorded. The tasks included holding a jar (transverse volar grip), holding a key (lateral pinch), holding a plate (extension grip) (Fig. 6.4), relaxing the hand, and extending the fingers and thumb. If a subject is not able to complete a task due to his SCI, he is asked to perform the task as best as he can. Each task is asked for 10 seconds and after finishing a task, relaxation of muscles is asked for 10 seconds. In order to preserve the accuracy of recorded EMG data and eliminate the effects of transitioning between different grasp modes on EMG data, the 2 seconds in the beginning and at the end of each grasp were disregarded and only the midmost 6 seconds were used to train the classification algorithm.

During the training, the EMG signals are measured and post-processed. The basic post-process of EMG signal is same with [41]. First, the offset of signal is removed. Next, the signal is rectified to obtain the magnitude values. Then, the third

order Butterworth low-pass filter (cutoff frequency at 4 Hz) is performed to produce a linear envelope representation of the signal. Lastly, the signal is normalized with the MVIC of the muscle. The post-processed EMG signals are classified into five classes by an artificial neural network (ANN) algorithm. The five classes consist of the four target hand poses stated above, and relaxation. We selected a two-layer feed-forward network with sigmoid hidden and softmax output neurons [124]. The network model is trained with a scaled conjugate gradient back-propagation. For evaluating the success ratio of the classification algorithm, 70% of data is used for training, 15% of data is used for validation, and 15% data is used for test.

For the analysis of the classification performance versus a set of EMG sensor location, we generated all possible sets, those are all possible combinations of EMG sensor locations, of which the total number is 60. Then, we trained all individual ANN for 60 training data sets. Lastly, we compare the success ratio of the classification results with a given training data set.

6.3.3 Results and Discussion

Two healthy subjects and one C5/C7 incomplete SCI subject participated in the experiment. Fig. 6.8, Fig. 6.9, and Fig. 6.10 show the experiment results with the subjects. The results were sorted by the success ratios in descending order. Each subfigure in the first six bar graphs shows the success ratios of a classification algorithm with training data sets whose number of sensors is same. For example, when the number of selected sensors is 3, the number of possible combination of sensor configurations is 20 ($=_6 \mathbf{C}_3$). Thus, we compared 20 success ratios of the

sensor configurations. Then, we picked the highest success ratios from the first six subfigures and drew the seventh bar graph. This bar graph shows the best success ratios with the given number of EMG sensors.

When the number of sensor is only one (see (a) of Fig. 6.8, Fig. 6.9, and Fig. 6.10), the highest success ratios were obtained when measuring EMG signals from the location 1 of Fig. 6.6 for two healthy subjects and the location 2 of Fig. 6.6 for a SCI subject respectively. When the number of sensor is two, the highest success ratios were obtained when measuring EMG signals from location 1 and 2 for two healthy subjects and from location 2 and 3 for a SCI subject respectively. When the number of sensor is three, the highest success ratios were obtained when measuring EMG signals from location 1, 2 and 6 for the first healthy subject and from the location 1, 2, and 3 for the second healthy and a SCI subject. One remarkable point is that the second highest success ratio of the first subject, which is similar to the highest success ratio, was obtained from the same sensor configuration of the others, those are the location 1, 2, and 3. When the number of sensor is four, the highest success ratios were obtained when measuring EMG signals from the location 2,4,5, and 6 for the first subject, the location 1,2,3, and 6 for the second subject, and the location of 2,3,4, and 5. For the five sensors, the success ratios are almost similar to all others, the comparison does not have a significant meaning. Due to some randomness of initial values for the training of ANN, the results slightly changed when the trainings are repeated but the major trends were not substantially changed.

From Fig. 6.8 (g), Fig. 6.9 (g), and Fig. 6.10 (g), we found that the success ratios of classification result are settled from the three EMG sensors. This result was

expected because we intentionally selected two redundant muscles for each one joint motion. The highest success ratios for the three sensors were also from a consistent sensor configuration, those are the sensor location 1, 2, and 3. Although the result for the first subject was slightly different from the others, the sensor configuration for the second highest success ratio showed consistency. In addition, locating a "sweet spot" for the sixth EMG sensor location was practically difficult due to high variance among people. Based on these experiment results, we decided to use the EMG sensor location 1, 2, and 3 for the operation of Maestro.

6.4 Hand Function of SCI Subjects with Maestro

In the previous sections, we have developed an efficient method for operating an active hand orthoses by taking an advantage of compliance of exoskeleton. The compliance in actuation enabled a subject with Maestro to grasp various object required in ADL with only four target hand poses of Maestro. Then, we found three locations for sEMG sensors to command Maestro to generate one target hand poses among the four. The selected locations of EMG sensors are capable of providing high success ratio of a EMG-classification algorithm. The final goal of these works is to improve the hand function of SCI patients in ADL. In this section, we evaluate the hand fuction of SCI patients with and without Maestro through a standardized hand function test.

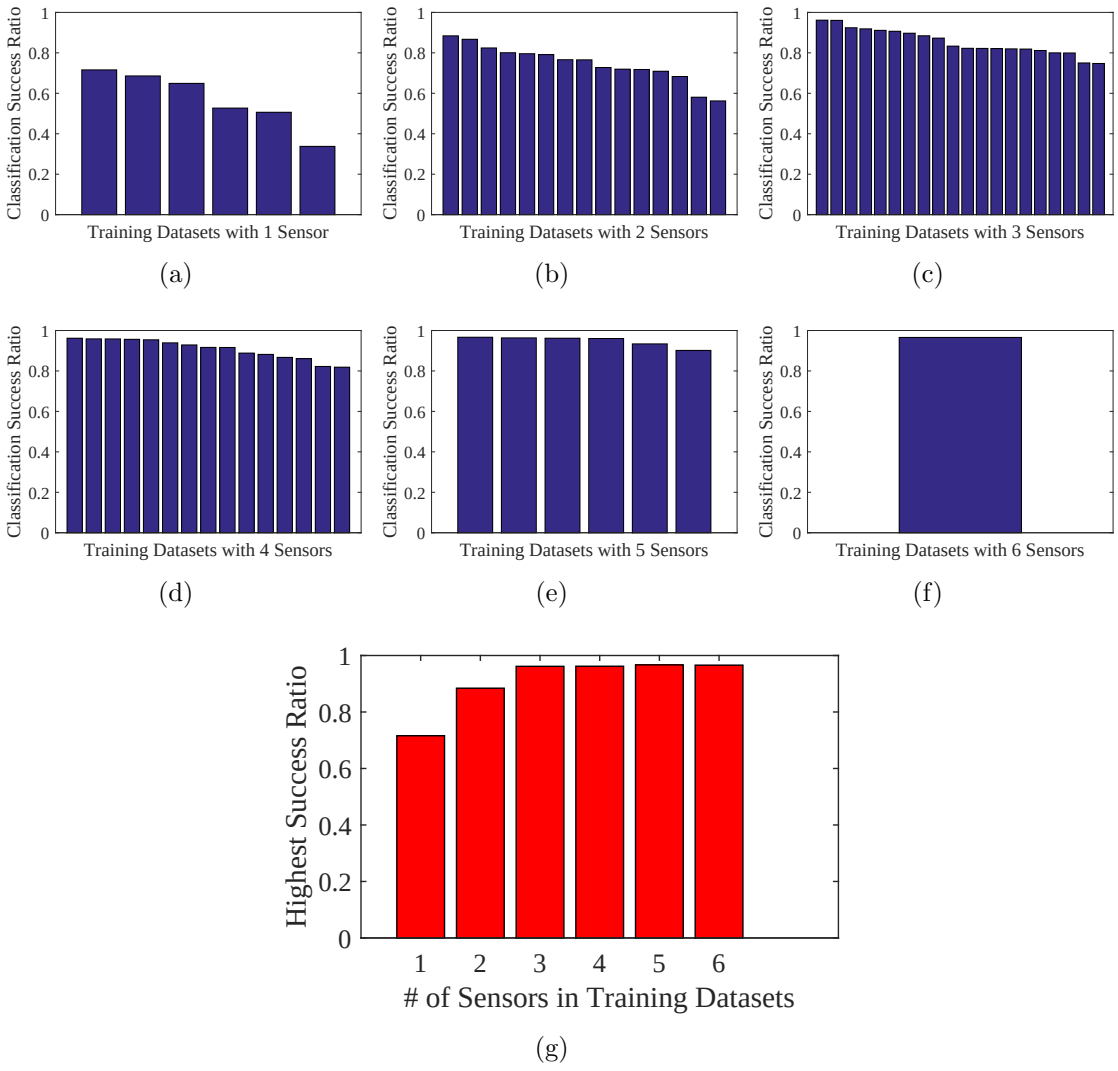

Figure 6.8: Experiment results with the first healthy subject. Each subfigure in the first six bar graphs (a)-(f) shows the success ratios of the classification algorithm with training data sets whose number of sensors is same. Then, we picked the highest success ratios from (a)-(f) and drew (g). The bar graph in (g) shows the best success ratio with the given number of EMG sensors.

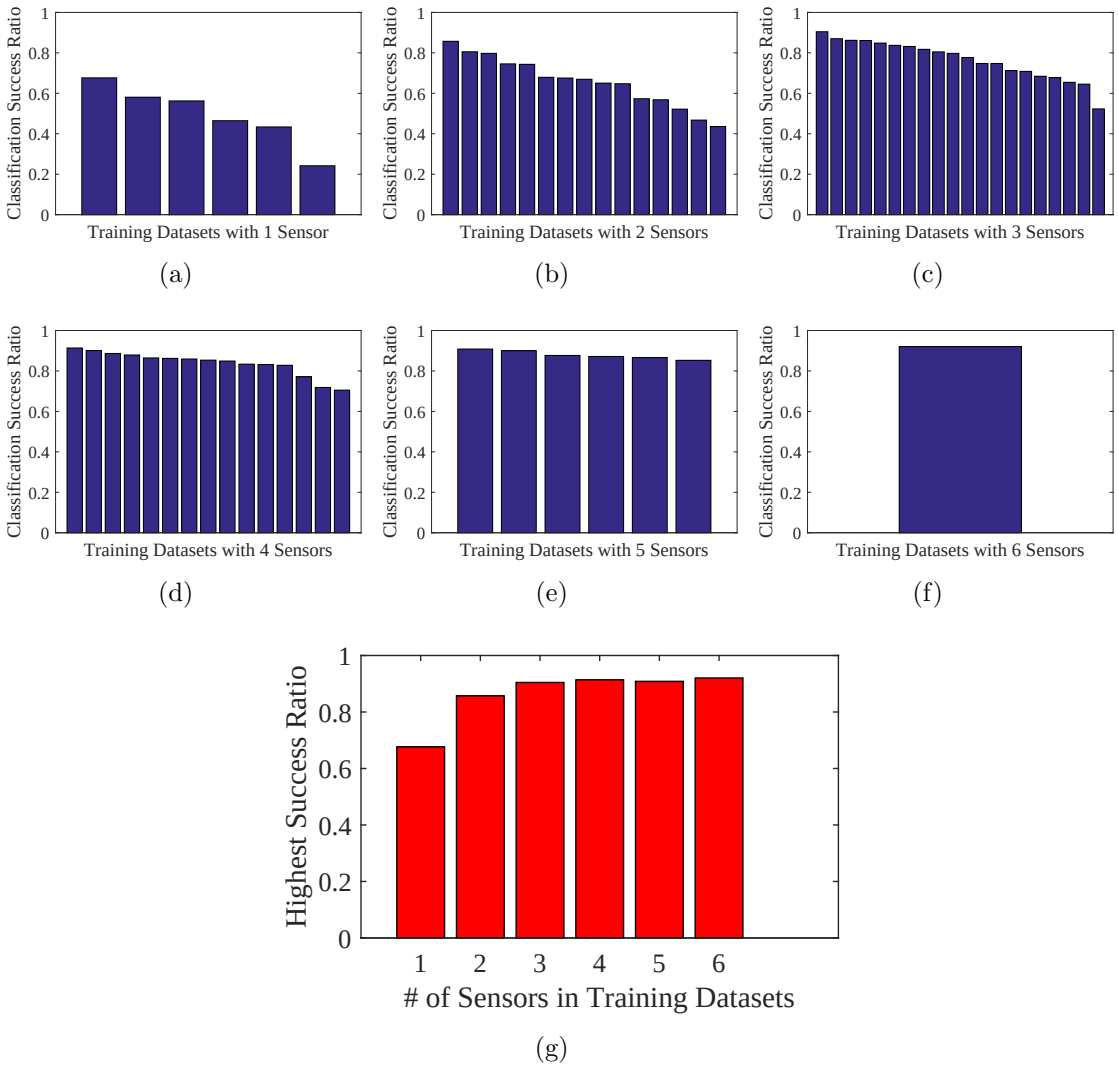

Figure 6.9: Experiment results with the second healthy subject. Each subfigure in the first six bar graphs (a)-(f) shows the success ratios of the classification algorithm with training data sets whose number of sensors is same. Then, we picked the highest success ratios from (a)-(f) and drew (g). The bar graph in (g) shows the best success ratio with the given number of EMG sensors.

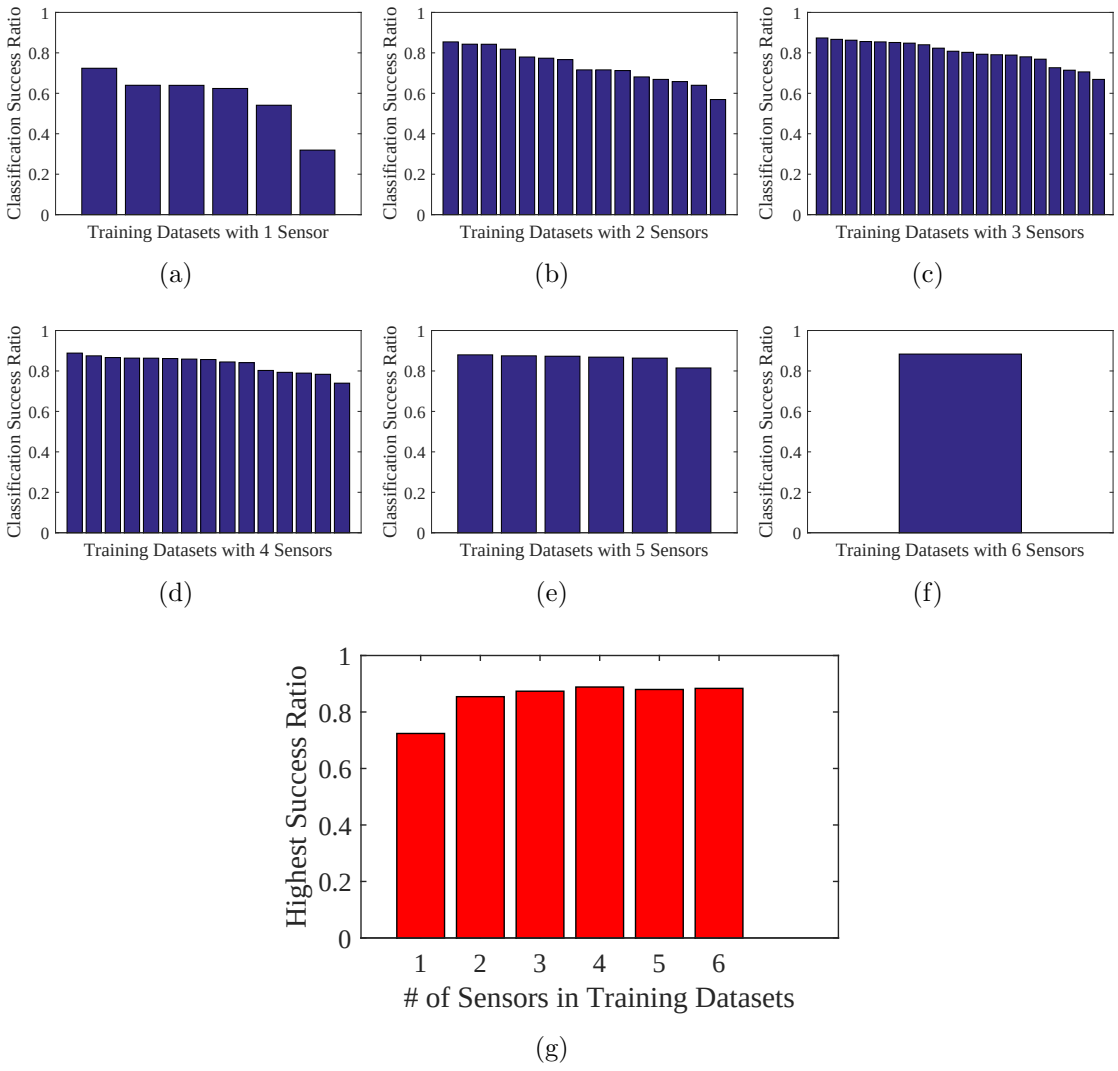

Figure 6.10: Experiment results with a SCI subject. Each subfigure in the first six bar graphs (a)-(f) shows the success ratios of the classification algorithm with training data sets whose number of sensors is same. Then, we picked the highest success ratios from (a)-(f) and drew (g). The bar graph in (g) shows the best success ratio with the given number of EMG sensors.

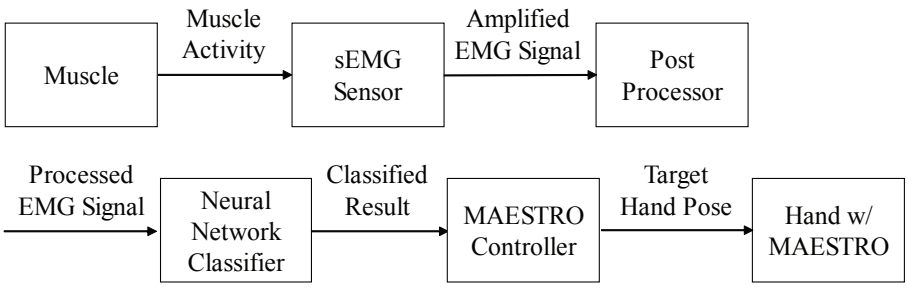

Figure 6.11: Signal flow of the muscle activities to the target hand poses of Maestro. The EMG of muscles are measured and amplified by sEMG sensors, the amplified signal is post-processed with several filters and classified into a target hand pose of Maestro with an Artificial neural network classifier.

6.4.1 Operation of Maestro

This subsection presents how we developed the operation method of Maestro to be suitable for performing tasks. The overview of the signal flow from the muscles activities to the target pose of Maestro is shown in Fig. 6.11. The goal is to generate commands for Maestro, that are the target hand poses, to perform various tasks in ADL reliably with the EMG signal of SCI subjects.

One essential feature for operating an active hand orthosis is stability based on a robust EMG classification algorithm. Although we have introduced a minimal set of target hand poses and an optimal set of EMG sensor locations to secure a successful user-intention algorithm through sEMG sensors, operating Maestro with the EMG-classification algorithm is still challenging. Because 95% of successful classification results also means that 5% of result is wrong, and this wrong classification results may lead to oscillation between misclassified hand poses. Hence, we introduce two more additional methods to make the operation of Maestro stable.

The first method is to take an advantage of the relaxation class while operating Maestro. The basic idea of this method is similar to that of [40]. The relaxation class plays a significant role for stable operation of Maestro. The relaxation class is selected when a subject relaxes all muscles that are monitored by EMG sensors. Compared to other classes, the relaxation class is classified without confusion because the muscle activations are all low so that the EMG pattern is clearly distinguishable from other EMG patterns. We use this distinguishing property of relaxation class to maintain the selected target hand pose consistently. That is, if the classification result of ANN is the relaxation class, Maestro does not change the target hand pose and maintains the current pose. Since the subject does not need to keep generating the EMG signal for the specific pose, subjects can comfortably maintain the desired hand pose with a low-rate of classification failure.

As the second method, we introduced a probabilistic approach for stable operation of Maestro. Although we reduced the number of target hand poses and introduced the relaxation mode, the noise in EMG signals and the movement of arms and wrist caused problems in the classification and lead to frequent fluctuation between hand poses of Maestro. For the operation of an active device in contrast to gesture recognition, we needed a higher success rate of EMG classification. To enhance the success ratio, the Maestro controller adopted a probabilistic approach. The Maestro controller records the classification results for a certain time duration. Then, classification results are counted for the time window. Lastly, only when the count of a classification result exceeds a certain threshold, the Maestro controller changes the target hand pose. This probabilistic approach filters out wrong classi-

fication results occurred by EMG noise or transition of muscle states. One scenario of operation is shown in Fig. 6.12 to help understanding of readers.

6.4.2 Experiments

In this section, we validate the effectiveness of Maestro for the improvement of hand function of SCI patients. The hand performance of six SCI subjects with and without Maestro was evaluated by a standardized hand function test, called Sollerman Hand Function Test (SHFT) [1].

6.4.2.1 Sollerman Hand Function Test (SHFT)

SHFT is developed to evaluate the hand functions of tetraplegic patients in ADL. Comparing to other evaluation methods such as GRASSP [125] or Toronto rehabilitation institutehand function test (TRI-HFT) [126], SHFT is more focused on the evaluation of the hand functions in daily activities with objects used in daily tasks rather than evaluating individual components of hand functions such as strength of muscles, sensibility, and motor coordination, which are main factors of GRASSP and TRI-HFT. Since we want to evaluate the hand functions in ADL of SCI patients, we selected SHFT for the experiments.

SHFT evaluates the hand function of subjects based on 20 tasks inspired by ADL. Each subtest is scored on a scale of 0 to 4 based on scoring criteria including time to complete the task, successful completion of task, use of the normal hand grip and number of drops. The maximum score of SHFT is 80. Tasks to be performed include closing and opening zippers, picking up coins, using a screw driver, writing

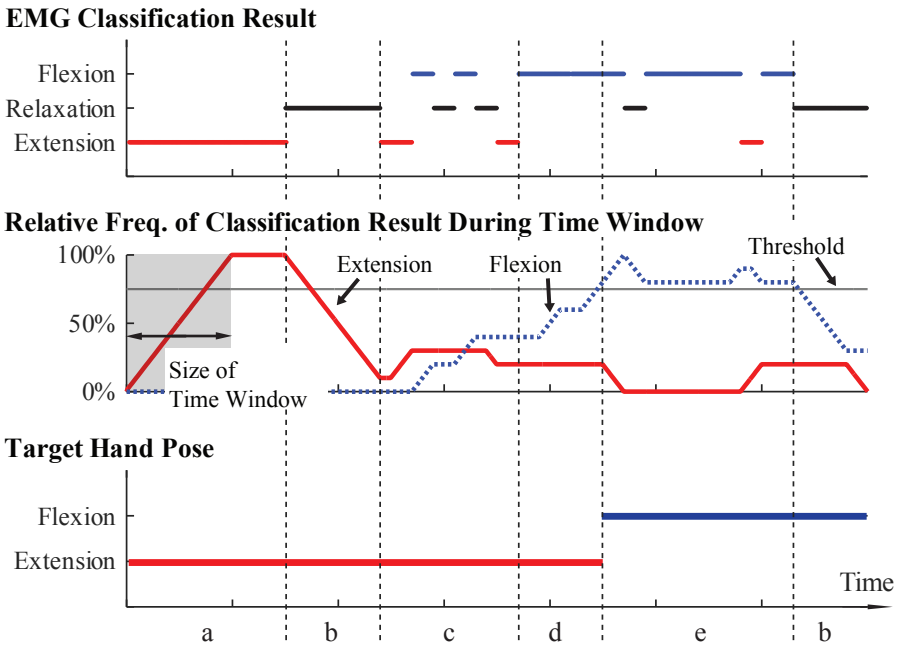

Figure 6.12: Control mode change of Maestro with EMG classification results. A virtual classification result, flexion, is introduced instead of transverse volar grip, lateral pinch, and extension grip to effectively illustrate the algorithm. The basic principle for full classification results is the same without loss of generality. We created a virtual scenario to show how a subject changes the target hand pose from extension to flexion. The top plot shows the EMG classification results obtained by ANN. The middle plot shows the relative frequency of classification results. The frequency is counted during a pre-determined time window. The bottom plot shows the target hand poses of Maestro controller. The change of target hand pose is made when the relative frequency of a classification result exceeds a threshold. (a) the frequency of extension crosses the threshold but the target hand pose does not change because it is already extension. (b) the subject relaxes the muscles but Maestro maintains the current target hand pose. (c) the subject changes the muscle activities. During the transition, the classification results are noisy, but the target hand pose is not changed. (d) The classification results are consistent, but the target hand pose is not changed yet due to the delay of a time-window approach. (e) The frequency of the flexion crosses the threshold, and the target hand pose is changed to flexion. Due to the probabilistic approach, the decision is robust to occasional fault of classification.

with a pen, pouring water from a jug, lifting an iron, etc. The brief description of tasks is listed in Table 6.4. For detailed task descriptions, refer to [1].

6.4.2.2 Recruitment of SCI Subjects

We included a SCI patient as a subject if 1) they provide written informed consent prior to any study related procedures, 2) his/her age is between 18-75 years, 3) he/she got diagnosis of complete or incomplete (C5-C8) spinal cord injury as defined by the American Spinal Injury Association (ASIA) impairment scale classification, and 4) they do not have "no conditions" (e.g., severe arthritis, extreme shoulder pain) that would interfere with valid administration of the measures or with interpreting motor testing. All experiments were conducted with an approval of the institutional internal review board (IRB). Based on the above conditions, we have recruited six SCI subjects to evaluate the assistance performance of Maestro. The detailed information of subjects is listed in Table 6.2.

6.4.2.3 Experiment Protocol of SHFT with Maestro

All experiments will take place in the ReNeu Robotics Lab, which is located in rooms 3.130 and 3.104 the ETC building on The University of Texas at Austin campus. The lab is part of the Department of Mechanical Engineering.

For evaluation of the hand functions of SCI patients in ADL with Maestro, researchers conducted experiments with the following protocol. Before the SHFT, the EMG system was set up and data were collected to train the ANN program. First, we attached EMG sensors on the forearm and palm of each subject. Three

Table 6.2: SCI patients who participated in the experiment

Subject No.	Gender	Hand Dominance		Age	Age at Injury	Injury Level
		Pre-injury	Post-injury			
1	M	R	R	57	53	C5/C7 Incomplete
2	M	R	R	34	29	C6 Incomplete
3	F	L	L	20	19	C5
4	M	R	L	41	24	C6
5	M	R	R	59	52	C6
6	M	R	R	51	33	C5

Delsys Trigno Wireless EMG sensors were used for recording EMG signals. Muscle locations were identified by palpating the subjects right forearm and palm. The EMG sensor locations for the experiment is shown in Fig. 6.13. After the EMG sensors are correctly attached, the EMG sensors are securely protected by wrapping the forearm with fabric strips and by covering with a tubular bandage (Fig. 6.14). Second, the MVIC of subjects hand is measured. The method of MVIC measurement is same as that in the previous Subsection 6.3.2. Third, the EMG-classification algorithm with ANN is trained. The method is same with that in Subsection 6.3.2.

Next, subjects wore Maestro. Researchers opened the palmar side of the leather glove (Fig. 6.2) and helped a subject to put their fingers and thumb in the glove. After a subject wear the glove, a researcher close the opened palmar side of the glove and tighten Velcros of digits. Then, we allowed them to get familiar

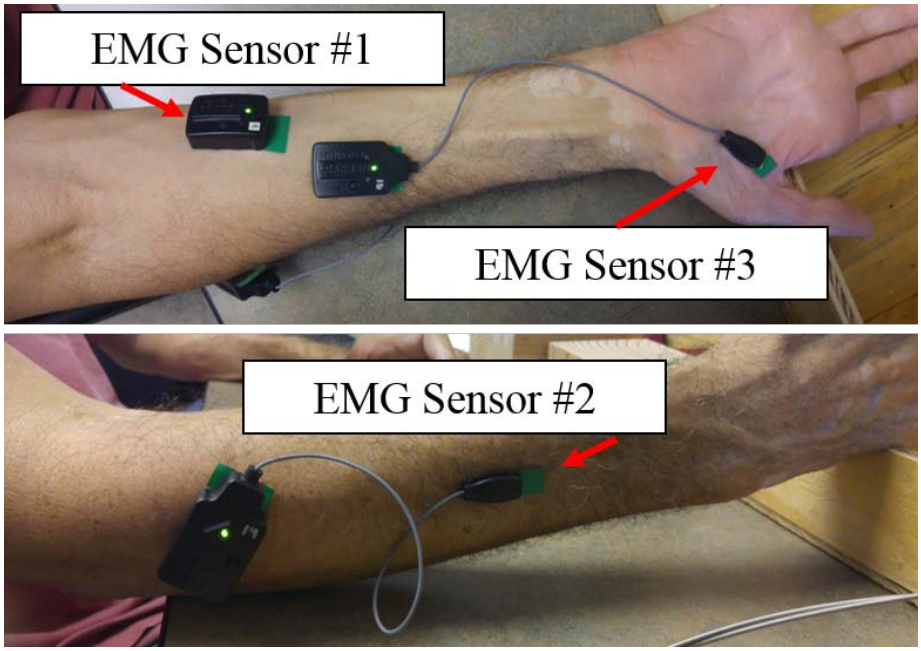

Figure 6.13: Three wireless EMG sensors are used to identify the intention of SCI subjects. The first sensor detects the flexion of fingers, the second detects the extension of fingers, and the third sensor detects the thumb flexion and abduction.

with the system. We adjusted the link lengths of the exoskeleton to fit the subjects hand size and ensure comfort. In addition, we customized the target hand poses of the Maestro controller, including transverse volar grip, lateral pinch, extension grip, and extension. After the customization of Maestro, the EMG-driven controller was turned on, and the subjects had 20 minutes to practice controlling Maestro with their muscle activities and interacting with objects.

After the practice, subjects performed SHFT with Maestro. A researcher introduced the SHFT and its scoring criteria (Table 6.3) to subjects. They sat at a table whose height had been adjusted for their wheelchair and the SHFT kit was

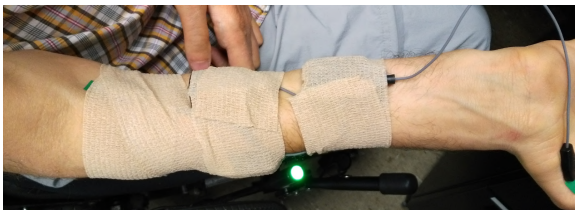

(a) Forearm with fabric strips

(b) Forearm with a tubular bandage

Figure 6.14: After conforming the locations of EMG sensors, the EMG sensors are protected by fabric strips (a) and a tubular bandage (b).

placed on the table. A researcher performed and demonstrated each task of the SHFT using the normal grasp mode and asked the subject to try to do the same task. An occupational therapist observed and timed each task and scored the task on a scale of 0-4 based on the scoring guide provided by SHFT (Table. 6.3).

After the SHFT with Maestro, we removed Maestro and the EMG sensors, and subjects had a break for 10 minutes. Then, subjects performed SHFT with their bare hands. Before every task, a researcher again performed and demonstrated each one using the normal grasp mode and asked the subject to try to do the same.

After the two SHFTs, subjects were asked about the comfort and difficulty of the session and tasks, and the effectiveness of Maestro in accomplishing ADL. Some questions were answered on a scale of 0-10 and others required short answers.

Table 6.3: SHFT Scoring Guide [1]

Criteria	**Score**
The task is completed without any difficulty within 20 seconds and with the prescribed hand-grip of normal quality	4
The task is completed, but with slight difficulty, or the task is not completed within 20 seconds, but within 40 seconds, or the task is completed with the prescribed hand-grip with slight divergence from normal	3
The task is completed, but with great difficulty, or the task is not completed within 40 seconds, but within 60 seconds, or the task is not performed with the prescribed hand-grip	2
The task is only partially performed within 60 seconds.	1
The task cannot be performed at all.	0

During the experiments, all subjects were asked to inform researchers when they feel uncomfortable. Anytime when subjects feel too uncomfortable to continue the experiment, we halted the experiments.

6.4.2.4 Results of SHFT

Among the six SCI subjects (Table 6.2), four SCI subjects accomplished the above protocol. Subject 1 volunteered to participate in the experiment one more. Thus, Subject 1 accomplished the experiment protocol two times. Two SCI subjects expressed uncomfort while performing the experiments, and the tests were immediately stopped. Subject 3, a SCI subject who gave up the experiment, had low functionality in shoulders and arms due to C5 SCI. Because the injury occurred recently (less than 1 year ago), the rehabilitation of the body functions were not fully

performed, and the emotional status was unstable. Subject 4, the other subject who gave up the experiment, also did not have sufficient shoulder and arm functions to perform tasks in SHFT. His injury was less severe than Subject 3, but his dominant hand was changed after the injury from the right to left hand. Hence, he has not used his right hand in daily activities, resulting in substantial weakness of all muscles and motor coordination of right upper extremity. Because Maestro was designed only for a right-hand user, he was asked to use the non-dominant hand, that is his right hand, for SHFT.

The scores of the SHFT in Table 6.4 and Table 6.5 show that the hand functions of Subject 1, 2 and 5 are improved with Maestro and the hand function of Subject 4 is overall not changed. For Subject 1, the SHFT without the exoskeleton was 41, the first SHFT score with the exoskeleton was 47 and the second SHFT score were 50. The improvement between the first trial and second trial was mainly because he learned how to use the exoskeleton for the tasks. SCI subjects spent long time with their bare hands to perform tasks. However, the subjects had a short time with Maestro before performing SHFT. Therefore, experiencing the exoskeleton longer resulted in better performance in SHFT tasks. Subject 1 had difficulty with active flexion of the fingers and abduction/adduction of the thumb. Maestro helped him to generate flexion of the fingers and abduction of thumb. He performed tasks with the correct hand grip and generated enough hand strength required in ADL. For instance, his scores were improved in lifting the iron, pouring water from a pure-pak, and writing with a pen. Subject 1 had limited sensory feedback on his fingertips, which made it difficult to perform delicate tasks, especially without visual feedback,

including picking up coins from a purse mounted on a wall and picking up nuts and putting them on bolts.

For Subject 2, the score went from 45 to 49 by wearing the exoskeleton. Subject 2 had stiff flexed fingers and difficulty in finger extension. He usually wrapped around an object by pushing his fingers, and opened his hand by using the other hand or by contacting with an object. When he used Maestro, he could extend his fingers more easily and got a higher score in lifting the iron and pouring water from a jug, cup, and pure-pak. On the other hand, he got lower scores in tasks that included pinching of small objects, such as unlocking a Yale-lock with a key and writing with a pen.

For Subject 5, the score went from 40 to 41 by wearing the exoskeleton. Subject 5 had a severer SCI injury than Subject 1 and Subject 2, and thus the available EMG signals were fewer than Subject 1 and Subject 2. The less available EMG signals resulted in difficulties in operating exoskeleton in a precise timing, and consequently the SHFT score was low. Nonetheless, the exoskeleton increased his grasping strength, thus he was able to lift heavy objects such as an iron and pure-pack with water.

For Subject 6, the scores were same with and without the exoskeleton. His injury was the most severe injury among the subjects who participated in the experiments. His EMG signals were barely available for operating the exoskeleton. He was able to generate signals only for the extension grip, and the control between the target hand poses were very unstable due to the low EMG signals. Nonetheless, the most remarkable part was that Subject 6 showed the most significant satisfaction

Table 6.4: Sollerman Hand Function Test Scores, Part 1

Task Description	Subject 1			Subject 2	
	w/o Exo	w/ Exo 1	w/ Exo 2	w/o Exo	w/ Exo
Pick up key, put into Yale-lock and turn 90.	1	1	1	3	2
Pick up the coins from flat surface, put into purses mounted on the wall.	2	2	2	2	3
Close and open zips.	2	1	1	2	2
Pick up coins from purses.	1	0	1	2	1
Pick up wooden blocks, lift over edge.	3	2	3	2	3
Lift iron over edge.	2	4	4	2	4
Turn screw with screwdriver.	2	2	3	3	3
Pick up nuts and put on bolts.	1	1	1	2	1
Unscrew lid of jars.	2	3	2	2	2
Do up buttons.	2	1	1	1	1
Cut Play-Doh (plasticine).	2	2	1	2	2
Put elasticated tubular bandage on the other hand.	2	3	3	2	1
Writing the word "name" on paper	2	4	4	4	3
Fold paper, put into envelope.	2	1	2	2	1
Put paper-clip on envelope.	2	3	3	2	3
Pick up telephone-receiver and put it to the ear.	3	3	4	3	3
Turn door-handle 30.	4	3	4	3	3
Pour water from one litre paper milk or juice package (pure-pak).	2	4	2	2	3
Pour water from jug.	2	3	4	2	4
Pour water from cup.	2	4	4	2	4
Total Score	41	47	50	45	49

Table 6.5: Sollerman Hand Function Test Scores, Part 2

Task Description	Subject 5		Subject 6	
	w/o Exo	w/ Exo	w/o Exo	w/ Exo
Pick up key, put into Yale-lock and turn 90.	1	1	1	1
Pick up the coins from flat surface, put into purses mounted on the wall.	3	1	1	1
Close and open zips.	2	1	1	1
Pick up coins from purses.	1	1	1	1
Pick up wooden blocks, lift over edge.	3	3	2	1
Lift iron over edge.	3	4	3	4
Turn screw with screwdriver.	2	3	1	1
Pick up nuts and put on bolts.	1	1	1	1
Unscrew lid of jars.	2	3	2	2
Do up buttons.	1	1	1	1
Cut Play-Doh (plasticine).	2	1	2	1
Put elasticated tubular bandage on the other hand.	1	1	1	1
Writing the word ”name” on paper	2	3	3	4
Fold paper, put into envelope.	1	1	3	1
Put paper-clip on envelope.	3	1	1	3
Pick up telephone-receiver and put it to the ear.	3	2	3	2
Turn door-handle 30.	3	4	3	4
Pour water from one litre paper milk or juice package (pure-pak).	2	4	1	1
Pour water from jug.	2	2	1	1
Pour water from cup.	2	3	1	1
Total Score	40	41	33	33

among subjects with achieving the movement of hand by his intention although the control was not stable. Another remarkable point is that the injury time of his case is the longest among all subjects. Thus, he had a wide range of knowledge how to use his SCI hands for tasks. He knew about compensated motions to achieve a certain task well. Therefore, his SHFT score with bare hands was higher than our expectation, and thus he was able to accomplish the tasks although Subject 3 and Subject 4 whose injury level is less severe or similar gave up the tests.

According to the feedback form completed by the subjects, most of subjects believed Maestro is comfortable to wear and reasonably weighed (Table. 6.6). Subject 1 thinks direct skin contact is better to grasp objects, whereas Subject 2 and 6 confirm that the glove interface helps significantly in grasps. All subjects believe the tasks performed in the session are representative of ADL. All subjects prefer the exoskeleton to be smaller and to have bigger workspace. Actually, the biggest challenge while performing task was the interference of the exoskeleton with a working space.

There are more remarkable points in the experiment results. First, the exoskeleton enabled subjects to perform tasks using the correct hand grip. Without the hand exoskeleton, although some subjects were able to accomplish many tasks, they used various compensating motions and help from other hand and body parts. Second, the time to achieve tasks was overall longer with exoskeleton than without exoskeleton. This is due to the delay of the system and implementation of probabilistic approach introduced in Section III that ensures stable operation of Maestro. Third, although most of subjects answered that SHFT represents ADL well, we were

Table 6.6: Feedback from SCI Subjects

Question	Subject			
	S1	S2	S5	S6
Is the hand exoskeleton comfortable to wear?	7	7	6	3
Is the weight of the exoskeleton reasonable?	10	9	6	9
Is the glove comfortable?	9	8	6	8
Does the glove help to grasp objects?	5	9	7	9
Are the tasks representative of daily activities?	8	10	7	10
Were the tasks difficult to achieve without the exoskeleton?	6	3	7	5
Were the tasks difficult to achieve with the exoskeleton?	6	3	8	3

able to find several disadvantages. SHFT tends to set low points for compensated motions. We agree that some compensated motions are not stable and may cause another problem in ADL, but we also observed that some compensated motions are able to perform ADL tasks without serious problems.

Chapter 7

Conclusion

We have developed a robust, accurate, and compatible hand exoskeleton, Maestro, by integrating multiple novel design attributes (Table 2.1). First, the exoskeleton is robust. The hybrid fabrication method allows for a strong mechanical structure while keeping the exoskeleton light and compact. The embedded and covered electric systems consistently perform a high quality of sensing and actuation even under various disturbance. The multistage safety features protect subjects and exoskeleton systems from human and machine errors.

Second, Maestro is accurate. The rigid attachment of pHRI allows for accurate kinematics measurement and force actuation. Dynamic transparency during force control was achieved by the light weight of the exoskeleton. The redundant sensor configuration reduced the uncertainty caused by the diversity of hand sizes. The optimal configuration and modeling of Bowden cable and miniaturized SEA allowed accurate control of the finger joint torque. The high-speed signal processing with FPGA and the strict real-time performance with RT-Linux made the sensing and actuation precise.

Last, Maestro is compatible. The exoskeleton actuates the most essential 8-DoF of the hand, which is compatible with many rehabilitation schemes and as-

sistance methods with independent joint motion or coordinated joint motion. The fourbar mechanisms resolved the joint misalignment problem, commonly occuring when subjects have different hand sizes. The automatic calibration with the redundant sensors made the kinematics estimation algorithm compatible with different hand sizes. The Bowden cable transmission freed the exoskeleton from grounding; thus, the exoskeleton can be integrated with other devices such as a wrist or upper-body exoskeleton. C/C++ on Linux and NI-cRIO combinatoin are compatible with many hardware and software. Different users can easily change the program due to the OOP-based structures.

There are a number of avenues for making improvements to Maestro. The Bowden cable-based actuation offers many advantages for Maestro, but neatly arranging the wires is an issue. The total of 16 Bowden cables actuate 8 SEA through a pull-pull mechanism. The hanging cables sometimes get tangled with each other, which is not aesthetically appealing. Developing a Bowden cable holder may be a solution. Development of a comfortable and transparently force-transmitting pHRI is a challenging and important problem to resolve. Based on a number of discussions with occupational therapists and stroke and SCI subjects, we are developing an improved version of pHRI that would migrate away from the use of Velcro straps, a cumbersome method that requires a long don-doff time, commonly interferes with muscle contractions, and would also allow for an intimate fit between the subject and device. Another ongoing direction is to develop a customized glove, which is seamlessly connected with rigid structures of the hand exoskeleton. A network of string or elastic will be carefully routed throughout the glove such that it will wrap

around the finger and hand in locations where creases in the human skin naturally occur, ultimately avoiding any muscle bellies. The wire will secure the glove to the hand using adjustable loop knots that tighten under tension and lengthen to accommodate all hand sizes. The overall shape would be similar to a complicated version of shoe-lace tightening. The estimation and control of thumb joint angle and torque are part of our ongoing work. Although we developed a thumb exoskeleton whose workspace is close to the workspace of the bare thumb, accurate estimation and actuation of thumb are still challenging because accurate modeling of thumb anatomy is challenging. According to the literature [102, 103], the thumb anatomy is more diverse among people than fingers and cannot be easily represented by mechanical joints. The challenge may be resolved with a statistical model-based approach instead of a mechanical joint-based approach. The statistical mapping between the thumb pose and the exoskeleton joints would be a model representing the complex joint anatomy of the thumb.

The development of Maestro has led to a number of research avenues for rehabilitation and assistive devices for the hand. First, a subject-specific assist-as-needed controller has been developed with Maestro for effective rehabilitation of patients with neurological disorders [93, 94]. The force-field is learned for a subject with a neural-network model, and then the controller builds a force-field to assist the subjects finger joint motion. Second, we have conducted experiments to develop an optimal rehabilitatioini framework by studying human motor learning and re-learning abilities. In the experiments, the challenges in robotic rehabilitation are modulated in multidimensional space (task, assistance, and feedback), and the degree of motor

learning and re-learning are evaluated during the experiments. Third, we are developing an advanced assessment tool with Maestro. Recent research has demonstrated that robotic devices, especially robotic exoskeletons, have the potential to be used in the assessment of stroke recovery. However, the works thus far have focused on the assessment of arm function, leaving the use of robotic devices in assessing recovery of hands unexplored. We are developing a new assessment metric, which can provide highly repeatable, real-time, and automated feedback to the therapist and patient, thus reducing assessment time. Last, another ongoing project is to integrate Maestro with a wrist exoskeleton from Rice University [3] (Fig. 7.1). The biomechanics of the hand are significantly coupled with that of the wrist because of the location of muscles and tendon structure. The study on the coupled biomechanics between the hand and wrist may reveal significant factors on rehabilitation of coupled body parts.

We have presented a detailed research result with Maestro on the control of an assistive hand orthosis with the surface of EMG sensors for SCI patients. In previous works, the active hand orthoses with EMG sensors actuated the hands of SCI patients with only 1-DoF motion. However, the orthoses with 1-DoF motion are capable of grasping only a limited number of objects required in ADL. To enable an SCI subject to grasp various objects required in ADL, we developed a novel control method for sEMG sensors with Maestro. First, we took advantage of compliant actuation of Maestro. With this advantage, a subject with Maestro-alpha was able to grasp various objects required in ADL with only four target hand poses. Second, we found an optimal set of sEMG sensor locations to generate a target hand pose among the four. Only with three sEMG sensors, an EMG-classification algorithm classified

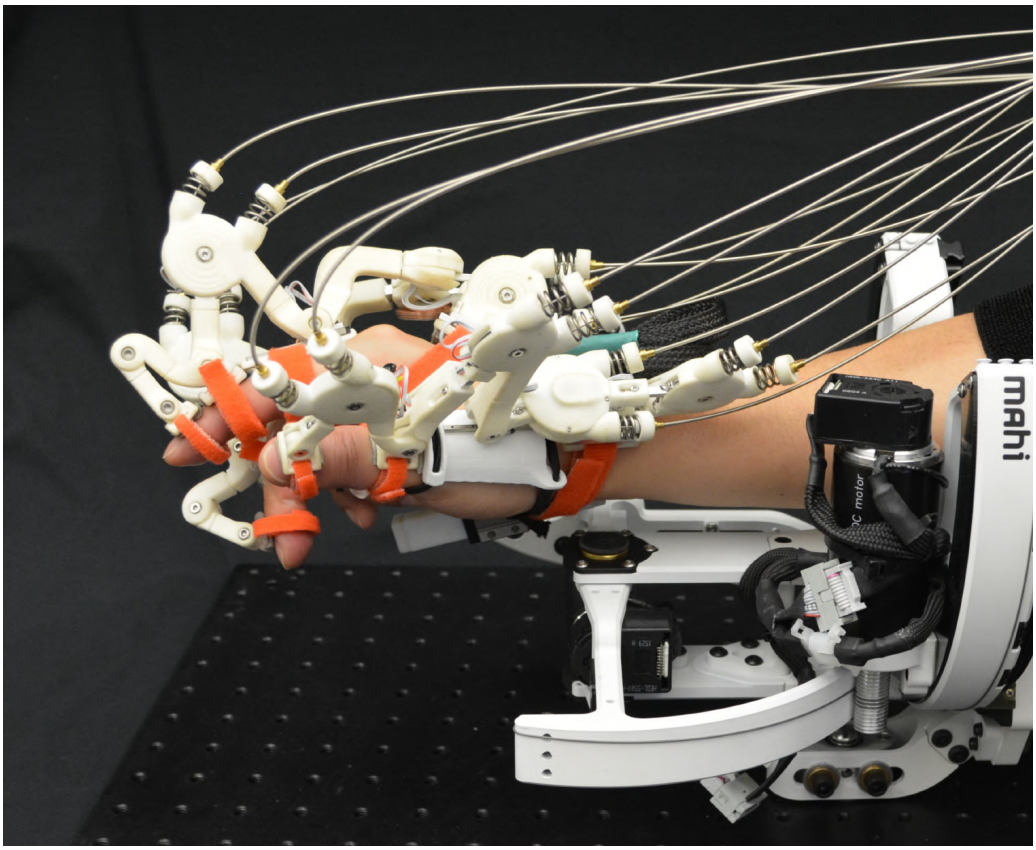

Figure 7.1: We are developing a hand-wrist exoskeleton by integrating Maestro with a wrist exoskeleton from Rice University [3].

noisy sEMG signals into one among the four target hand poses with high success ratios. Last, we evaluated the hand functions of SCI patients with a standardized hand function test (the Sollerman hand function test). The results show that the hand functions of C6 and C7 SCI patients were improved with the proposed control method and with Maestro.

The results showed several benefits of the proposed method. First, the selected four target hand poses and three sEMG sensor locations would be beneficial to other researchers for designing an active hand orthosis driven by EMG sensors. The results, as shown in Sections 6.2 and Sectiion 6.3, can be applied not only to Maestro but also to other hand orthoses whose actuation is compliant. Selecting a small number of target hand poses may help to reduce failure rate of their classification algorithm, and the optimal locations of EMG sensors may not reduce the success ratio, although the number of EMG sensors is small, which is critical in practical applications. Also, the small number of target hand poses suggests a potential design of a mechanical system of hand orthsis with a small number of actuators. Last, the experimental results in Section 6.4 show the potential of a multi-DoF assistive hand orthoses. To date, all of the hand orthoses only showed the number of objects or shape of objects, which can be grasped by the orthoses without performing a standardized test. In Section 6.4, we showed the performance of a hand orthoses in ADL by performing SHFT with and without the exoskeleton. The results show the merits and limits of an active hand orthosis, which are useful for designing an improved version of hand orthoses.

To develop an assistive device that can be practically used by SCI patients,

several technical problems need to be resolved. First, the hand exoskeleton needs to be compact. Although we have observed that the grasping performance of SCI subjects was improved with Maestro, hand function scores were not dramatically improved. The main reason reported in the survey was due to the large size of Maestro. Most subjects pointed out that the biggest challenge in performing tasks in SHFT was due to the interference of Maestro with the workspace for tasks. For example, although subjects could grasp a coin if a researcher passes it, the subjects could not perform the task of picking up a coin from a purse because the size of purse is smaller than the size of Maestro. Second, the compliance of the exoskeleton needs to be selected in a systematic method. If spring stiffness is too low, subjects may not apply a sufficient force to grasp objects. If stiffness is too high, subjects may feel large pressure on their hands and may not delicately manipulate a hand task. Therefore, when selecting adequate compliance of the exoskeleton, which is optimal for a subject and tasks, the subject may efficiently perform tasks. Furthermore, actively controlled variable stiffness may bring additional advantages. Third, a systematic arrangement of the Bowden cable is needed. The Bowden cable-based transmission leads to many advantages for Maestro. However, the Bowden cables also disturbed the motions of hand, arm, and shoulder while performing tasks. Development of a systematic method for arranging the Bowden cables may improve the efficiency of performing hand tasks with a hand assistive device that uses Bowden cable transmission.

The EMG-driven interface can be improved in several ways. First, the training of the EMG classification model needs to be simplified. The EMG signals change depends on many conditions, including locations of sensors and degrees of fatigues.

Thus, the EMG classification program inherently needs frequent training of the model to achieve a robust classification performance. In our experiments, the training usually took about 20 to 30 minutes. If a subject can train the model more often with a simplified method, then the EMG classification model will exhibit higher performance. Second, the selection of locations of sEMG sensors can be improved. The three locations of sEMG sensors were selected based on an anatomy study about the innervation from spinal cord to muscles. Due to this selection, we were able to find the optimal sEMG sensor locations, which are advantageous for general SCI patients. However, because the selection did not consider the symptoms of individual SCI patients, the sensor locations are not optimized for an individual SCI. Every SCI patient has different symptoms resulting in specific availability of muscle signals. For the optimal development of a hand orthosis that uses EMG signals of SCI patients, a developer needs to consider not only the general perspective of SCI but also the individual perspective of SCI. Third, the EMG classification algorithm can be improved by choosing recently devised machine-learning algorithms. Because the development of a machine learning algorithm for EMG classification is not our main research topic, we have implemented one of the most stable and well-known algorithms for EMG classification. Introducing a state-of-art classification algorithm such as a recursive neural network algorithm [127], which outperformed the previous machine learning algorithms, may improve the performance for operating a hand orthoses with sEMG sensors.

The robotics research on the hand function recovery of patients with neurological disorders is still in the early stages, and patients are eagerly waiting for advances

in the technology. Almost every SCI subject who tried Maestro was delighted just by the resulting movements of their hands with their intentions regardless of the scores of SHFT because it was an accomplishment of one of their lifes dreams. While conducting research on rehabilitation and assistive devices, we have met many stroke and SCI subjects who desperately want the recovery of their hand functions. We hope that my research makes a contribution to the progress in the robotics technology for these individuals.

Bibliography

[1] Christer Sollerman and Arvid Ejeskär. Sollerman hand function test: a standardised method and its use in tetraplegic patients. *Scandinavian Journal of Plastic and Reconstructive Surgery and Hand Surgery*, 29(2):167–176, 1995.

[2] John W Garrett. The adult human hand: some anthropometric and biomechanical considerations. *Human Factors: The Journal of the Human Factors and Ergonomics Society*, 13(2):117–131, 1971.

[3] Chad G Rose, Fabrizio Sergi, Youngmok Yun, Kaci Madden, Ashish D Deshpande, and Marcia K O'Malley. Characterization of a hand-wrist exoskeleton, readapt, via kinematic analysis of redundant pointing tasks. In *IEEE International Conference on Rehabilitation Robotics*, pages 205–210. IEEE, 2015.

[4] Youngmok Yun, Sarah Dancausse, Paria Esmatloo, Alfredo Serrato, Curtis A. Merring, and Ashish D. Deshpande. An EMG-Driven assistive hand exoskeleton for spinal cord injury patients: Maestro. In *IEEE International Conference on Robotics and Automation (ICRA)*, 2017.

[5] Dariush Mozaffarian, Emelia J Benjamin, Alan S Go, Donna K Arnett, Michael J Blaha, Mary Cushman, Sandeep R Das, Sarah de Ferranti, Jean-Pierre Després, Heather J Fullerton, et al. Executive summary: Heart disease and

stroke statistics-2016 update: A report from the american heart association. *Circulation*, 133(4):447, 2016.

[6] National Spinal Cord Injury Statistical Center. Spinal cord injury (SCI) facts and figures at a glance. 2016.

[7] Rieko Osu, Ken-ichi Morishige, Jun Nakanishi, Hiroyuki Miyamoto, and Mitsuo Kawato. Practice reduces task relevant variance modulation and forms nominal trajectory. *Scientific reports*, 5, 2015.

[8] Neville Hogan, Hermano Igo Krebs, J Charnnarong, P Srikrishna, and Andre Sharon. MIT-MANUS: a workstation for manual therapy and training. I. In *IEEE International Workshop on Robot and Human Communication*, pages 161–165. IEEE, 1992.

[9] Emanuel Todorov and Michael I Jordan. Optimal feedback control as a theory of motor coordination. *Nature neuroscience*, 5(11):1226–1235, 2002.

[10] Kurt A Thoroughman and Reza Shadmehr. Learning of action through adaptive combination of motor primitives. *Nature*, 407(6805):742–747, 2000.

[11] Robert A Scheidt, Jonathan B Dingwell, and Ferdinando A Mussa-Ivaldi. Learning to move amid uncertainty. *Journal of neurophysiology*, 86(2):971–985, 2001.

[12] Reza Shadmehr and Ferdinando A Mussa-Ivaldi. Adaptive representation of dynamics during learning of a motor task. *The Journal of Neuroscience*, 14(5):3208–3224, 1994.

[13] Francesca Gandolfo, FA Mussa-Ivaldi, and Emilio Bizzi. Motor learning by field approximation. *Proceedings of the National Academy of Sciences*, 93(9):3843–3846, 1996.

[14] Sean P Dukelow, Troy M Herter, Kimberly D Moore, Mary Jo Demers, Janice I Glasgow, Stephen D Bagg, Kathleen E Norman, and Stephen H Scott. Quantitative assessment of limb position sense following stroke. *Neurorehabilitation and neural repair*, 24(2):178–187, 2010.

[15] Daichi Nozaki, Isaac Kurtzer, and Stephen H Scott. Limited transfer of learning between unimanual and bimanual skills within the same limb. *Nature neuroscience*, 9(11):1364–1366, 2006.

[16] MA Urbin, Kimberly J Waddell, and Catherine E Lang. Acceleration metrics are responsive to change in upper extremity function of stroke survivors. *Archives of physical medicine and rehabilitation*, 96(5):854–861, 2015.

[17] MA Urbin, Ryan R Bailey, and Catherine E Lang. Validity of body-worn sensor acceleration metrics to index upper extremity function in hemiparetic stroke. *Journal of neurologic physical therapy: JNPT*, 39(2):111, 2015.

[18] Gustavo Saposnik, Robert Teasell, Muhammad Mamdani, Judith Hall, William McIlroy, Donna Cheung, Kevin E Thorpe, Leonardo G Cohen, Mark Bayley, Stroke Outcome Research Canada (SORCan) Working Group, et al. Effectiveness of virtual reality using wii gaming technology in stroke rehabilitation a pilot randomized clinical trial and proof of principle. *Stroke*, 41(7):1477–1484, 2010.

[19] David Jack, Rares Boian, Alma S Merians, Marilyn Tremaine, Grigore C Burdea, Sergei V Adamovich, Michael Recce, and Howard Poizner. Virtual reality-enhanced stroke rehabilitation. *IEEE transactions on neural systems and rehabilitation engineering*, 9(3):308–318, 2001.

[20] Alma S Merians, David Jack, Rares Boian, Marilyn Tremaine, Grigore C Burdea, Sergei V Adamovich, Michael Recce, and Howard Poizner. Virtual reality–augmented rehabilitation for patients following stroke. *Physical therapy*, 82(9):898–915, 2002.

[21] Mónica S Cameirão, Sergi Bermúdez i Badia, Esther Duarte Oller, and Paul FMJ Verschure. Neurorehabilitation using the virtual reality based rehabilitation gaming system: methodology, design, psychometrics, usability and validation. *Journal of neuroengineering and rehabilitation*, 7(1):1, 2010.

[22] Lance L Cai, Andy J Fong, Chad K Otoshi, Yongqiang Liang, Joel W Burdick, Roland R Roy, and V Reggie Edgerton. Implications of assist-as-needed robotic step training after a complete spinal cord injury on intrinsic strategies of motor learning. *The Journal of neuroscience*, 26(41):10564–10568, 2006.

[23] Damiano Zanotto, Paul Stegall, and Sunil K Agrawal. Adaptive assist-as-needed controller to improve gait symmetry in robot-assisted gait training. In *2014 IEEE International Conference on Robotics and Automation (ICRA)*, pages 724–729. IEEE, 2014.

[24] James L Patton, Mary Ellen Stoykov, Mark Kovic, and Ferdinando A Mussa-Ivaldi. Evaluation of robotic training forces that either enhance or reduce

error in chronic hemiparetic stroke survivors. *Experimental Brain Research*, 168(3):368–383, 2006.

[25] Brenna D Argall. Modular and adaptive wheelchair automation. In *Experimental Robotics*, pages 835–848. Springer, 2016.

[26] Brenna D Argall. Turning assistive machines into assistive robots. In *SPIE OPTO*, pages 93701Y–93701Y. International Society for Optics and Photonics, 2015.

[27] Alberto Esquenazi, Mukul Talaty, Andrew Packel, and Michael Saulino. The rewalk powered exoskeleton to restore ambulatory function to individuals with thoracic-level motor-complete spinal cord injury. *American journal of physical medicine & rehabilitation*, 91(11):911–921, 2012.

[28] Hiroaki Kawamoto and Yoshiyuki Sankai. Comfortable power assist control method for walking aid by hal-3. In *Systems, Man and Cybernetics, 2002 IEEE International Conference on*, volume 4, pages 6–pp. IEEE, 2002.

[29] Christian Fleischer and Günter Hommel. A human–exoskeleton interface utilizing electromyography. *IEEE Transactions on Robotics*, 24(4):872–882, 2008.

[30] Jacob Rosen, Moshe Brand, Moshe B Fuchs, and Mircea Arcan. A myosignal-based powered exoskeleton system. *IEEE Transactions on systems, Man, and Cybernetics-part A: Systems and humans*, 31(3):210–222, 2001.

[31] Kazuo Kiguchi, Shingo Kariya, Keigo Watanabe, Kiyotaka Izumi, and Toshio Fukuda. An exoskeletal robot for human elbow motion support-sensor fusion,

adaptation, and control. *IEEE Transactions on Systems, Man, and Cybernetics, Part B (Cybernetics)*, 31(3):353–361, 2001.

[32] Alessandra Pedrocchi, Simona Ferrante, Emilia Ambrosini, Marta Gandolla, Claudia Casellato, Thomas Schauer, Christian Klauer, Javier Pascual, Carmen Vidaurre, Margit Gföhler, et al. Mundus project: Multimodal neuroprosthesis for daily upper limb support. *Journal of neuroengineering and rehabilitation*, 10(1):1, 2013.

[33] Iñaki Díaz, Jorge Juan Gil, and Emilio Sánchez. Lower-limb robotic rehabilitation: literature review and challenges. *Journal of Robotics*, 2011, 2011.

[34] Paweł Maciejasz, Jörg Eschweiler, Kurt Gerlach-Hahn, Arne Jansen-Troy, and Steffen Leonhardt. A survey on robotic devices for upper limb rehabilitation. *J. Neuroeng. Rehabil*, 11(3):10–1186, 2014.

[35] Ronald A Bos, Claudia JW Haarman, Teun Stortelder, Kostas Nizamis, Just L Herder, Arno HA Stienen, and Dick H Plettenburg. A structured overview of trends and technologies used in dynamic hand orthoses. *Journal of Neuro-Engineering and Rehabilitation*, 13(1):62, 2016.

[36] Pei-hsin Kuo and Ashish D Deshpande. Muscle-tendon units provide limited contributions to the passive stiffness of the index finger metacarpophalangeal joint. *Journal of Biomechanics*, 45:2531–2538, 2012.

[37] Lotte NS Andreasen Struijk. An inductive tongue computer interface for control of computers and assistive devices. *IEEE Trans. Biomed. Engineering*,

53(12):2594–2597, 2006.

[38] Vijay Kumar, Tariq Rahman, and Venkat Krovi. Assistive devices for motor disabilities. *Wiley Encyclopedia of Electrical and Electronics Engineering*, 1997.

[39] Hyunki In, Brian Byunghyun Kang, MinKi Sin, and Kyu-Jin Cho. Exo-Glove: a wearable robot for the hand with a soft tendon routing system. *IEEE Robotics & Automation Magazine*, 22(1):97–105, 2015.

[40] Nisim Benjuya and Steven B Kenney. Myoelectric hand orthosis. *Journal of Prosthetics and Orthotics*, 2(2):149–154, 1990.

[41] Matthew DiCicco, Lenny Lucas, and Yoky Matsuoka. Comparison of control strategies for an EMG controlled orthotic exoskeleton for the hand. In *IEEE International Conference on Robotics and Automation*, volume 2, pages 1622–1627, 2004.

[42] Huichan Zhao, Jonathan Jalving, Rukang Huang, Ross Knepper, Andy Ruina, and Robert Shepherd. A helping hand: Soft orthosis with integrated optical strain sensors and emg control. *IEEE Robotics & Automation Magazine*, 23(3):55–64, 2016.

[43] Priyanshu Agarwal, Youngmok Yun, Jonas Fox, Kaci Madden, and Ashish D Deshpande. Design, control and testing of a thumb exoskeleton with series elastic actuation. *The International Journal of Robotics Research*, 2017.

[44] Pilwon Heo, Gwang Min Gu, Soo-jin Lee, Kyehan Rhee, and Jung Kim. Current hand exoskeleton technologies for rehabilitation and assistive engineering. *International Journal of Precision Engineering and Manufacturing*, 13(5):807–824, 2012.

[45] Ludovic Dovat, Olivier Lambercy, Roger Gassert, Thomas Maeder, Ted Milner, Teo Chee Leong, and Etienne Burdet. Handcare: a cable-actuated rehabilitation system to train hand function after stroke. *Neural Systems and Rehabilitation Engineering, IEEE Transactions on*, 16(6):582–591, 2008.

[46] Christopher N Schabowsky, Sasha B Godfrey, Rahsaan J Holley, Peter S Lum, et al. Development and pilot testing of hexorr: hand exoskeleton rehabilitation robot. *Journal of NeuroEngineering and Rehabilitation*, 7(1):36, 2010.

[47] Craig D Takahashi, Lucy Der-Yeghiaian, Vu Le, Rehan R Motiwala, and Steven C Cramer. Robot-based hand motor therapy after stroke. *Brain*, 131(2):425–437, 2008.

[48] Julius Klein, Steven J Spencer, and David J Reinkensmeyer. Breaking it down is better: haptic decomposition of complex movements aids in robot-assisted motor learning. *IEEE Transactions on Neural Systems and Rehabilitation Engineering*, 20(3):268–275, 2012.

[49] Marie-Hélène Milot, Steven J Spencer, Vicky Chan, James P Allington, Julius Klein, Cathy Chou, James E Bobrow, Steven C Cramer, David J Reinkensmeyer, et al. A crossover pilot study evaluating the functional outcomes of

two different types of robotic movement training in chronic stroke survivors using the arm exoskeleton BONES. *Journal NeuroEngineering Rehabilitation*, 10(112):0003–10, 2013.

[50] Shraddha Srivastava, Pei-Chun Kao, Seok Hun Kim, Paul Stegall, Damiano Zanotto, Jill S Higginson, Sunil K Agrawal, and John P Scholz. Assist-as-needed robot-aided gait training improves walking function in individuals following stroke. *IEEE Transactions on Neural Systems and Rehabilitation Engineering*, 23(6):956–963, 2015.

[51] Eric T Wolbrecht, Vicky Chan, David J Reinkensmeyer, and James E Bobrow. Optimizing compliant, model-based robotic assistance to promote neurorehabilitation. *IEEE Transactions on Neural Systems and Rehabilitation Engineering*, 16(3):286–297, 2008.

[52] Gert Kwakkel, Boudewijn J Kollen, and Hermano I Krebs. Effects of robot-assisted therapy on upper limb recovery after stroke: a systematic review. *Neurorehabilitation and Neural Repair*, 2007.

[53] A. D. Deshpande and Y. Matsuoka. Development of an anatomically correct testbed (ACT) hand. *The Human Hand: A Source of Inspiration for Robotic Hands, Springer Tracts in Advanced Robotics (STAR) series*, 95:453–475, 2014.

[54] Restorative Care of America. Online catalog of hand and wrist orthosis. `http://www.rcai.com/hand_and_wrist_orthoses.html`, 2016. [Online; accessed 12-Aug-2016].

[55] Sasha Blue Godfrey, Rahsaan J Holley, and Peter S Lum. Clinical effects of using hexorr (hand exoskeleton rehabilitation robot) for movement therapy in stroke rehabilitation. *American Journal of Physical Medicine & Rehabilitation*, 92(11):947–958, 2013.

[56] Man Bok Hong, Sin-Jung Kim, Taewoong Um, and Keehoon Kim. Kulex: An adl power-assistance demonstration. In *URAI*, pages 542–544, 2013.

[57] TT Worsnopp, MA Peshkin, JE Colgate, and DG Kamper. An actuated finger exoskeleton for hand rehabilitation following stroke. In *Rehabilitation Robotics, 2007. ICORR 2007. IEEE 10th International Conference on*, pages 896–901. IEEE, 2007.

[58] Ju Wang, Jiting Li, Yuru Zhang, and Shuang Wang. Design of an exoskeleton for index finger rehabilitation. In *Engineering in Medicine and Biology Society, 2009. EMBC 2009. Annual International Conference of the IEEE*, pages 5957–5960. IEEE, 2009.

[59] NSK Ho, KY Tong, XL Hu, KL Fung, XJ Wei, W Rong, and EA Susanto. An emg-driven exoskeleton hand robotic training device on chronic stroke subjects: task training system for stroke rehabilitation. In *Rehabilitation Robotics (ICORR), 2011 IEEE International Conference on*, pages 1–5. IEEE, 2011.

[60] Marco Cempini, Mario Cortese, and Nicola Vitiello. A powered finger–thumb wearable hand exoskeleton with self-aligning joint axes. *IEEE/ASME Transactions on Mechatronics*, 20(2):705–716, 2015.

[61] Marco Fontana, Andrea Dettori, Fabio Salsedo, and Massimo Bergamasco. Mechanical design of a novel hand exoskeleton for accurate force displaying. In *Robotics and Automation, 2009. ICRA'09. IEEE International Conference on*, pages 1704–1709. IEEE, 2009.

[62] Sergei V Adamovich, Gerard G Fluet, Abraham Mathai, Qinyin Qiu, Jeffrey Lewis, and Alma S Merians. Design of a complex virtual reality simulation to train finger motion for persons with hemiparesis: a proof of concept study. *Journal of neuroengineering and rehabilitation*, 6(1):1, 2009.

[63] Satoshi Ueki, Haruhisa Kawasaki, Satoshi Ito, Yutaka Nishimoto, Motoyuki Abe, Takaaki Aoki, Yasuhiko Ishigure, Takeo Ojika, and Tetsuya Mouri. Development of a hand-assist robot with multi-degrees-of-freedom for rehabilitation therapy. *IEEE/ASME Transactions on Mechatronics*, 17(1):136–146, 2012.

[64] Useok Jeong, Hyun-Ki In, and Kyu-Jin Cho. Implementation of various control algorithms for hand rehabilitation exercise using wearable robotic hand. *Intelligent Service Robotics*, 6(4):181–189, 2013.

[65] Panagiotis Polygerinos, Zheng Wang, Kevin C Galloway, Robert J Wood, and Conor J Walsh. Soft robotic glove for combined assistance and at-home rehabilitation. *Robotics and Autonomous Systems*, 2014.

[66] Laura Marchal-Crespo and David J Reinkensmeyer. Review of control strategies for robotic movement training after neurologic injury. *Journal of Neuroengineering and Rehabilitation*, 6(1):20, 2009.

[67] Satoshi Ueki, Haruhisa Kawasaki, Satoshi Ito, Yutaka Nishimoto, Motoyuki Abe, Takaaki Aoki, Yasuhiko Ishigure, Takeo Ojika, and Tetsuya Mouri. Development of a hand-assist robot with multi-degrees-of-freedom for rehabilitation therapy. *IEEE/ASME Transactions on Mechatronics*, 17(1):136–146, 2012.

[68] Marco Fontana, Salsedo Fabio, Simone Marcheschi, and Massimo Bergamasco. Haptic hand exoskeleton for precision grasp simulation. *Journal of Mechanisms and Robotics*, 5(4):041014, 2013.

[69] Olivier Lambercy, David Schröder, Sven Zwicker, and Roger Gassert. Design of a thumb exoskeleton for hand rehabilitation. In *Proceedings of the 7th International Convention on Rehabilitation Engineering and Assistive Technology*, page 41. Singapore Therapeutic, Assistive & Rehabilitative Technologies (START) Centre, 2013.

[70] Carlo Alberto Avizzano, F Bargagli, Antonio Frisoli, and Massimo Bergamasco. The hand force feedback: analysis and control of a haptic device for the human-hand. In *IEEE International Conference on Systems, Man, and Cybernetics*, volume 2, pages 989–994, 2000.

[71] Yasuhisa Hasegawa, Yasuyuki Mikami, Kosuke Watanabe, and Yoshiyuki Sankai. Five-fingered assistive hand with mechanical compliance of human finger. In *IEEE International Conference on Robotics and Automation*, pages 718–724, 2008.

[72] Ioannis Sarakoglou, Nikolaos G Tsagarakis, and Darwin G Caldwell. Occupational and physical therapy using a hand exoskeleton based exerciser. In *IEEE/RSJ International Conference on Intelligent Robots and Systems*, volume 3, pages 2973–2978, 2004.

[73] Jiting Li, Ruoyin Zheng, Yuru Zhang, and Jianchu Yao. iHandRehab: An interactive hand exoskeleton for active and passive rehabilitation. In *IEEE International Conference on Rehabilitation Robotics*, pages 1–6, 2011.

[74] Manuel Aiple and Andre Schiele. Pushing the limits of the cybergrasp for haptic rendering. In *IEEE International Conference on Robotics and Automation*, pages 3541–3546, 2013.

[75] Dr Guilherme N. DeSouza, Patrick Aubin, Kelsey Petersen, Hani Sallum, Conor Walsh, Annette Correia, and Leia Stirling. A pediatric robotic thumb exoskeleton for at-home rehabilitation: The isolated orthosis for thumb actuation (IOTA). *International Journal of Intelligent Computing and Cybernetics*, 7(3):233–252, 2014.

[76] Furui Wang, Milind Shastri, Christopher L Jones, Vikash Gupta, Christian Osswald, Xuan Kang, Derek G Kamper, and Nilanjan Sarkar. Design and control of an actuated thumb exoskeleton for hand rehabilitation following stroke. In *IEEE International Conference on Robotics and Automation*, pages 3688–3693, 2011.

[77] Mourad Bouzit, Grigore Burdea, George Popescu, and Rares Boian. The

Rutgers Master II-new design force-feedback glove. *IEEE/ASME Transactions on Mechatronics*, 7(2):256–263, 2002.

[78] Motoki Takagi, Kie Iwata, Yoshiyuki Takahashi, S-i Yamamoto, Hiroyuki Koyama, and Takashi Komeda. Development of a grip aid system using air cylinders. In *IEEE International Conference on Robotics and Automation*, pages 2312–2317, 2009.

[79] Inseong Jo and Joonbum Bae. Design and control of a wearable hand exoskeleton with force-controllable and compact actuator modules. In *IEEE International Conference on Robotics and Automation*, pages 5596–5601, 2015.

[80] Stephen H Scott. Apparatus for measuring and perturbing shoulder and elbow joint positions and torques during reaching. *Journal of neuroscience methods*, 89(2):119–127, 1999.

[81] Verena Klamroth-Marganska, Javier Blanco, Katrin Campen, Armin Curt, Volker Dietz, Thierry Ettlin, Morena Felder, Bernd Fellinghauer, Marco Guidali, Anja Kollmar, Andreas Luft, Tobias Nef, Corina Schuster-Amft, Werner Stahel, and Robert Riener. Three-dimensional, task-specific robot therapy of the arm after stroke: a multicentre, parallel-group randomised trial. *The Lancet Neurology*, 13(2):159–166, 2014.

[82] C Colomer, A Baldovi, S Torrome, MD Navarro, B Moliner, J Ferri, and E Noe. Efficacy of armeo® spring during the chronic phase of stroke. study in mild to moderate cases of hemiparesis. *Neurologia (English Edition)*, 28(5):261–267, 2013.

[83] Paxton Maeder-York, Tyler Clites, Emily Boggs, Ryan Neff, Panagiotis Polygerinos, Dónal Holland, Leia Stirling, Kevin Galloway, Catherine Wee, and Conor Walsh. Biologically inspired soft robot for thumb rehabilitation. *Journal of Medical Devices*, 8(2):020933–1–3, 2014.

[84] Nadia Garcia-Hernandez, Ioannis Sarakoglou, Nikos Tsagarakis, and Darwin Caldwell. Under-actuated hand exoskeleton with novel kinematics for potential use in rehabilitation. In *EuroHaptics*, pages 463–465, 2014.

[85] Daniele Leonardis, Michele Barsotti, Claudio Loconsole, Massimiliano Solazzi, Marco Troncossi, Claudio Mazzotti, Vincenzo Parenti Castelli, Caterina Procopio, Giuseppe Lamola, Carmelo Chisari, et al. An EMG-controlled robotic hand exoskeleton for bilateral rehabilitation. *IEEE Transactions on Haptics*, 8(2):140–151, 2015.

[86] Camilla Sköld, Richard Levi, and Åke Seiger. Spasticity after traumatic spinal cord injury: nature, severity, and location. *Archives of physical medicine and rehabilitation*, 80(12):1548–1557, 1999.

[87] Christopher L Jones, Furui Wang, Robert Morrison, Niladri Sarkar, and Derek G Kamper. Design and development of the cable actuated finger exoskeleton for hand rehabilitation following stroke. *IEEE/ASME Transactions on Mechatronicss*, 19(1):131–140, 2014.

[88] Andreas Wege and Günter Hommel. Development and control of a hand exoskeleton for rehabilitation of hand injuries. In *IEEE/RSJ International Conference on Intelligent Robots and Systems*, pages 3046–3051. IEEE, 2005.

[89] Jan F Veneman, Ralf Ekkelenkamp, Rik Kruidhof, Frans CT van der Helm, and Herman van der Kooij. A series elastic-and bowden-cable-based actuation system for use as torque actuator in exoskeleton-type robots. *The International Journal of Robotics Research*, 25(3):261–281, 2006.

[90] James S Sulzer, Michael A Peshkin, and James L Patton. Marionet: An exotendon-driven rotary series elastic actuator for exerting joint torque. In *International Conference on Rehabilitation Robotics*, pages 103–108. IEEE, 2005.

[91] SR Soekadar, M Witkowski, C Gómez, E Opisso, J Medina, M Cortese, M Cempini, MC Carrozza, LG Cohen, N Birbaumer, et al. Hybrid eeg/eog-based brain/neural hand exoskeleton restores fully independent daily living activities after quadriplegia. *Science Robotics*, 1(1):eaag3296, 2016.

[92] P. Agarwal, J. Fox, Y. Yun, M. K. OMalley, and A. D. Deshpande. An index finger exoskeleton with series elastic actuation for rehabilitation: Design, control and performance characterization. *The International Journal of Robotics Research*, 34(14):1747–1772, December 2015.

[93] Priyanshu Agarwal, Benito R Fernandez, and Ashish D Deshpande. Assist-as-needed controllers for index finger module of a hand exoskeleton for rehabilitation. In *ASME 2015 Dynamic Systems and Control Conference*, pages V003T42A002–V003T42A002. American Society of Mechanical Engineers, 2015.

[94] Priyanshu Agarwal and Ashish D Deshpande. Impedance and force-field control of the index finger module of a hand exoskeleton for rehabilitation. In *Re-*

habilitation Robotics (ICORR), 2015 IEEE International Conference on, pages 85–90. IEEE, 2015.

[95] Dongyang Chen, Youngmok Yun, and Ashish D Deshpande. Experimental characterization of bowden cable friction. In *IEEE International Conference on Robotics and Automation*, pages 5927–5933. IEEE, 2014.

[96] Kaci E Madden and Ashish D Deshpande. On integration of additive manufacturing during the design and development of a rehabilitation robot: A case study. *Journal of Mechanical Design*, 137(11):111417, 2015.

[97] Youngmok Yun, Priyanshu Agarwal, and Ashish D. Deshpande. Accurate torque control of finger joints with UT hand exoskeleton through Bowden cable SEA. In *IEEE/RSJ International Conference on Intelligent Robots and Systems*, 2016 (under review).

[98] Kyung-Sun Lee and Myung-Chul Jung. Ergonomic evaluation of biomechanical hand function. *Safety and health at work*, 6(1):9–17, 2015.

[99] Ian M Bullock, Joshua Z Zheng, SDL Rosa, Charlotte Guertler, and Aaron M Dollar. Grasp frequency and usage in daily household and machine shop tasks. *IEEE Transactions on Haptics*, 6(3):296–308, 2013.

[100] JD Arbuckle and DA McGrouther. Measurement of the arc of digital flexion and joint movement ranges. *The Journal of Hand Surgery: British & European Volume*, 20(6):836–840, 1995.

[101] Pamela K Levangie and Cynthia C Norkin. *Joint structure and function: a comprehensive analysis*. FA Davis, 2011.

[102] WILLIAM P Cooney and EY Chao. Biomechanical analysis of static forces in the thumb during hand function. *The Journal of Bone & Joint Surgery*, 59(1):27–36, 1977.

[103] Frédéric Schuind, Marc Garcia-Elias, William P Cooney, and Kai-Nan An. Flexor tendon forces: in vivo measurements. *The Journal of hand surgery*, 17(2):291–298, 1992.

[104] KN An, Y Ueba, EY Chao, WP Cooney, and RL Linscheid. Tendon excursion and moment arm of index finger muscles. *Journal of biomechanics*, 16(6):419–425, 1983.

[105] Derek G Kamper, Heidi C Fischer, and Erik G Cruz. Impact of finger posture on mapping from muscle activation to joint torque. *Clinical Biomechanics*, 21(4):361–369, 2006.

[106] Antonia Tzemanaki, Xinge Gao, T Pipe, Chris Melhuish, and Sanja Dogramadzi. Hand exoskeleton for remote control of minimally invasive surgical anthropomorphic instrumentation. In *Proceedings of the 6th Hamlyn Symposium on Medical Robotics. Imperial College, London: London, UK*, 2013.

[107] Peter Weiss, Lars Heyer, Thomas F Munte, Marcus Heldmann, Achim Schweikard, and Erik Maehle. Towards a parameterizable exoskeleton for training of hand

function after stroke. In *Rehabilitation Robotics (ICORR), 2013 IEEE International Conference on*, pages 1–6. IEEE, 2013.

[108] A. Chiri, M. Cempini, S.M.M. De Rossi, T. Lenzi, F. Giovacchini, N. Vitiello, and M.C. Carrozza. On the design of ergonomic wearable robotic devices for motion assistance and rehabilitation. In *2012 Annual International Conference of the IEEE Engineering in Medicine and Biology Society (EMBC)*, pages 6124–6127, August 2012.

[109] Jamshed Iqbal. *Hand Exoskeleton Robotic Systems: Role and Deriving the Design Requirements*. LAP LAMBERT Academic Publishing, Saarbrcken, November 2012.

[110] M. Bouzit, G. Burdea, G. Popescu, and R. Boian. The Rutgers Master II-new design force-feedback glove. *IEEE/ASME Transactions on Mechatronics*, 7(2):256–263, June 2002.

[111] Kiminori Toya, Toyomi Miyagawa, and Yuji Kubota. Power-Assist Glove Operated by Predicting the Grasping Mode. *Journal of System Design and Dynamics*, 5:94–108, 2011.

[112] M. Mulas, M. Folgheraiter, and G. Gini. An EMG-controlled exoskeleton for hand rehabilitation. In *9th International Conference on Rehabilitation Robotics, 2005. ICORR 2005*, pages 371–374, June 2005.

[113] Azzurra Chiri, Nicola Vitiello, Francesco Giovacchini, Stefano Roccella, Fabrizio Vecchi, and Maria Chiara Carrozza. Mechatronic design and charac-

terization of the index finger module of a hand exoskeleton for post-stroke rehabilitation. *IEEE/ASME Transactions on Mechatronics*, 17(5):884–894, 2012.

[114] Robert L Norton. Design of machinery: an introduction to the synthesis and analysis of mechanisms and machines. 1992.

[115] Youngmok Yun, Priyanshu Agarwal, and Ashish D. Deshpande. Accurate, robust, and real-time pose estimation of finger. *Journal of Dynamic Systems Measurement and Control*, 137(3), 2015.

[116] Varun Agrawal. *Modeling and control of cable actuated surgical robotic systems*. PhD thesis, PURDUE UNIVERSITY, 2011.

[117] TN Do, T Tjahjowidodo, MWS Lau, T Yamamoto, and SJ Phee. Hysteresis modeling and position control of tendon-sheath mechanism in flexible endoscopic systems. *Mechatronics*, 24(1):12–22, 2014.

[118] Gang Tao and Frank L Lewis. *Adaptive control of nonsmooth dynamic systems*. Springer Science & Business Media, 2013.

[119] Antonio Barbalace, A Luchetta, G Manduchi, M Moro, A Soppelsa, and C Taliercio. Performance comparison of vxworks, linux, rtai and xenomai in a hard real-time application. In *Real-Time Conference, 2007 15th IEEE-NPSS*, pages 1–5. IEEE, 2007.

[120] Rísin McNaney, John Vines, Daniel Roggen, Madeline Balaam, Pengfei Zhang, Ivan Poliakov, and Patrick Olivier. Exploring the acceptability of google glass

as an everyday assistive device for people with parkinson's. In *Proceedings of the 32nd annual ACM conference on Human factors in computing systems*, pages 2551–2554. ACM, 2014.

[121] Jason Friedman and Tamar Flash. Task-dependent selection of grasp kinematics and stiffness in human object manipulation. *Cortex*, 43(3):444–460, 2007.

[122] Mark R Cutkosky. On grasp choice, grasp models, and the design of hands for manufacturing tasks. *IEEE Transactions on robotics and automation*, 5(3):269–279, 1989.

[123] Jie Liu and Ping Zhou. A novel myoelectric pattern recognition strategy for hand function restoration after incomplete cervical spinal cord injury. *IEEE Transactions on Neural Systems and Rehabilitation Engineering*, 21(1):96–103, 2013.

[124] Howard Demuth and Mark Beale. Neural network toolbox for use with matlab. 1993.

[125] Sukhvinder Kalsi-Ryan, Armin Curt, Mary C Verrier, and Michael G Fehlings. Development of the graded redefined assessment of strength, sensibility and prehension (grassp): reviewing measurement specific to the upper limb in tetraplegia. *Journal of Neurosurgery: Spine*, 17(Suppl1):65–76, 2012.

[126] Naaz Kapadia, Vera Zivanovic, Molly Verrier, and Milos Popovic. Toronto rehabilitation institute–hand function test: assessment of gross motor function in

individuals with spinal cord injury. *Topics in spinal cord injury rehabilitation*, 18(2):167–186, 2012.

[127] Seonwoo Min, Byunghan Lee, and Sungroh Yoon. Deep learning in bioinformatics. *arXiv preprint arXiv:1603.06430*, 2016.

Vita

Youngmok Yun received his Bachelor of Science (B.S.) and Master of Science (M.S.) degrees in Mechanical Engineering from Pohang University of Science and Technology (POSTECH), Pohang, S. Korea in 2006 and in 2008 respectively. He worked in Renault-Samsung Technical Center, Young-in, S. Korea from 2008 till 2011, and in Korea Institute of Science and Technology, Seoul, S. Korea from 2011 till 2012. Since 2012, he has been pursuing his Ph.D. degree in ReNeu Robotics Lab at The University of Texas at Austin, Austin, Texas.

Permanent address: yunyoungmok@utexas.edu

This dissertation was typeset with LaTeX[†] by the author.

[†]LaTeX is a document preparation system developed by Leslie Lamport as a special version of Donald Knuth's TeX Program.